Nat.Lab. Unclassified Report NL-TN 2004/00085

Date of issue: April 2005

MOS Model 11

Level 1102

R. van Langevelde, A.J. Scholten and D.B.M. Klaassen

Unclassified Report

©Koninklijke Philips Electronics N.V. 2003/2004

Authors' address data: R. van Langevelde WAY41; Ronald.van.Langevelde@philips.com
A.J. Scholten WAY41; Andries.Scholten@philips.com
D.B.M. Klaassen WAY41; D.B.M.Klaassen@philips.com

©Koninklijke Philips Electronics N.V. 2003/2004
All rights are reserved. Reproduction in whole or in part is
prohibited without the written consent of the copyright owner.

Unclassified Report: NL-TN 2004/00085

Title: MOS Model 11
Level 1102

Author(s): R. van Langevelde, A.J. Scholten and D.B.M. Klaassen

Part of project: Compact modelling

Customer: Philips Semiconductors

Keywords: MOS Model 11, compact modelling, MOSFET, CMOS, circuit simulation, integrated circuits

Abstract: MOS Model 11, Level 1102, is an updated version of Level 1101 (see NL-UR 2002/802), it uses slightly different equations than Level 1101. The surface potential is calculated iteratively using a second-order Newton-Raphson procedure, resulting in a more accurate description of surface potential. Owing to the increased accuracy, some of the basic equations used in Level 1101 can be simplified, and as a result Level 1102 is computationally as fast as Level 1101. In addition, a more physical and simpler velocity saturation expression is used, and as a consequence the saturation voltage expression has changed slightly as well. This all results in a more accurate description of transconductance in saturation. Finally, more accurate physics-based equations have been implemented for thermal noise, induced gate noise and their correlation.

A new compact model for MOS transistors has been developed, MOS Model 11 (MM11), the successor of MOS Model 9. MM11 not only gives an accurate description of charges and currents and their first-order derivatives (transconductance, conductance, capacitances), but also of their higher-order derivatives. In other words it gives an accurate description of MOSFET distortion behaviour, and as such MM11 is suitable for digital, analog as well as RF circuit design.

MOS Model 11 is a symmetrical, surface-potential-based model. It includes an accurate description of all physical effects important for modern and future CMOS technologies, such as e.g. gate tunnelling current, gate-induced drain leakage, influence of pocket implants, poly-depletion, quantum-mechanical effects and bias-dependent overlap capacitances.

The goal of this report is to present the full definition of the model, including the parameter set, the geometrical and temperature scaling rules, the model implementation, and all the equations for currents, charges and noise sources. Apart from the definition also an introduction into the physical background is given, and a basic parameter extraction procedure is described. The complete physical background will be documented separately in a forthcoming report.

©Koninklijke Philips Electronics N.V. 2004

Preface and History of Model and Documentation

Preface

A first test version of the compact MOS model, MOS MODEL 11, Level 1102, has been put in the public domain in January 2004. Future changes and additions to the model will be documented by extending or changing the documentation in this Unclassified Report.

History of Model

January 2004 : Release of MOS MODEL 11, level 1102, test version

November 2004 : Release of MOS MODEL 11, level 1102, version 0 (1102.0)

Modifications in model equations:

- Addition of temperature dependence of the thermal resistance, A_{th}, in Sections 2.1.1, 2.2, 3.4.1, 3.4.2 and 8.
- Eqs. (2.32) and (6.15) for variable V_{DS_x} have been rewritten to increase numerical efficiency
- Eq. (6.16) has been changed in order to give a simpler description of V_{DB_t}
- Slightly simpler definition of the inital starting conditions (6.32) and (6.77) for the iterative solution of ψ_s and ψ_{ov}, respectively, is used

April 2005 : Release of MOS MODEL 11, level 1102, version 1 (1102.1)

Errors corrected in code:

- Default value of parameter NT in Sections 8.2.1-8.4.2 has been corrected so that it corresponds to the default value of the reference temperature TR.
- Implementation of eq. (6.123) corrected in code.

History of Documentation

January 2004 : Release of MOS MODEL 11, level 1102, test version

November 2004 : Release of MOS MODEL 11, level 1102, version 0 (1102.0)

Errors and inconsistencies corrected in documentation:

- See remarks above in History of Model, November 2004
- Error in Tab. 3.2.1 corrected: value of A changed from -1600 to -800
- Errors in eqs. (2.48), (2.63), (2.110), (6.10), (6.45) and (6.29) corrected
- Eqs. (6.41), (6.42) and (6.43) added

April 2005 : Release of MOS MODEL 11, level 1102, version 1 (1102.1)

Errors and inconsistencies corrected in documentation:

- See remarks above in History of Model, April 2005.
- Naming of parameter VFB in Section 3.4.1 has been corrected.
- Default values of POBINV and POBACC in Section 8.4.2 have been corrected.

©Koninklijke Philips Electronics N.V. 2004

Contents

1 Introduction 1

1.1 Structural Elements of MOS Model 11 1

1.2 Structure of this Technical Note 3

2 Physics 5

2.1 Comments and Physical Background 5

2.1.1 List of Parameters for an Individual Transistor 5

2.1.2 List of Physical Constants 8

2.1.3 List of Input Variables for an Individual Transistor 8

2.1.4 Comments on Current Equations 9

2.1.5 Comments on Charge Equations 14

2.1.6 Comments on Noise Equations 16

2.2 Calculation of Temperature-Dependent Parameters 18

2.3 Basic Equations 20

2.3.1 Internal Parameters 20

2.3.2 Basic Current Equations 20

2.3.3 Basic Charge Equations 26

2.3.4 Basic Noise Equations 27

3 Nomenclature 29

3.1 General Remarks 29

3.2 List of Input Variables and Quantities 30

3.2.1 List of Numerical Constants 30

3.2.2 List of Circuit Simulator Variables 30

3.3 List of Electrical Quantities and Variables 30

3.3.1 External Electrical Quantities and Variables 30

3.3.2 Internal Electrical Quantities and Variables 32

3.4 List of Reference & Scaling Parameters 33

3.4.1 List of Reference & Scaling Parameters for Physical Geometrical Scaling . . 34

3.4.2 List of Reference & Scaling Parameters for Binning Geometrical Scaling . . 38

4 Embedding 45

4.1 Embedding MOS Model 11 in a Circuit Simulator 45

4.2 Self-Heating 49

5 Preprocessing and Clipping 51

©Koninklijke Philips Electronics N.V. 2004

5.1 Calculation of Transistor Geometry 51
5.2 Calculation of Geometry-Dependent Parameters 51
5.2.1 Calculation of Geometry-Dependent Parameters using the Physical Scaling Rules 54
5.2.2 Calculation of Geometry-Dependent Parameters using the Binning Scaling Rules 57
5.3 Calculation of Temperature-Dependent Parameters 61
5.4 Clipping 63

6 Implemented Model Equations 65

6.1 Numerical Adaptations 65
6.2 Extended Equations 68
6.2.1 Internal Parameters 68
6.2.2 Extended Current Equations 68
6.2.3 Extended Charge Equations 78
6.2.4 Extended Noise Equations 79

7 Parameter Extraction 81

7.1 Measurements 81
7.2 Extraction of Miniset Parameters at Room Temperature 82
7.3 Extraction of Temperature Scaling Parameters 86
7.4 Extraction of Geometry Scaling Parameters 87

8 Parameter Clipping and Default Values 89

8.1 Introduction 89
8.2 Parameter Clipping and Default Values for the Electrical Model 90
8.2.1 Parameter Clipping and Default Values for the Electrical N-channel Model . 90
8.2.2 Parameter Clipping and Default Values for the Electrical P-channel Model. . 93
8.3 Parameter Clipping and Default Values for the Physical Geometrical Scaling Rules . 96
8.3.1 Parameter Clipping and Default Values for Physical Geometrical Scaling Rules of the N-channel Model 96
8.3.2 Parameter Clipping and Default Values for Physical Geometrical Scaling Rules of the P-channel Model 100
8.4 Parameter Clipping and Default Values for the Binning Geometrical Scaling Rules . 104
8.4.1 Parameter Clipping and Default Values for Binning Geometrical Scaling Rules of the N-channel Model 104
8.4.2 Parameter Clipping and Default Values for Binning Geometrical Scaling Rules of the P-channel Model 111

9 Pstar Specific Items 119

 ©Koninklijke Philips Electronics N.V. 2004

9.1 Syntax 119
9.2 DC Operating Point Output 120

References 122

A Auxiliary Equations 125

B Coefficients in the binning rules for geometry scaling 127
B.1 Coefficients for type I scaling 127
B.2 Coefficients for type II scaling 128
B.3 Coefficients for type III scaling 129

©Koninklijke Philips Electronics N.V. 2004

©Koninklijke Philips Electronics N.V. 2004

1 Introduction

MOS Model 11 (MM11) is a new compact MOSFET model, intended for digital, analogue and RF circuit simulation in modern and future CMOS technologies [1]-[3]. MM11 is the successor of MOS Model 9, it was especially developed to give not only an accurate description of currents and charges and their first-order derivatives (i.e. transconductance, conductance, capacitances), but also of the higher-order derivatives, resulting in an accurate description of electrical distortion behaviour [4]. The latter is especially important for analog and RF circuit design. The model furthermore gives an accurate description of the noise behaviour of MOSFETs.
MOS Model 11 gives a complete description of all transistor-action related quantities: nodal currents, nodal charges and noise-power spectral densities. The equations describing these quantities are based on surface-potential formulations, resulting in equations valid over all operation regions (i.e., accumulation, depletion and inversion). Additionally, in order for the model to be valid for modern and future MOS devices, several important physical effects have been included in the model: mobility reduction, bias-dependent series-resistance, velocity saturation, drain-induced barrier lowering, static feedback, channel length modulation, self-heating, weak-avalanche (or impact ionization), gate current due to tunnelling, gate-induced drain leakage, poly-depletion, quantum-mechanical effects on charges and bias-dependent overlap capacitances.

MOS Model 11 only provides a model for the intrinsic transistor and the gate/source- and gate/drain overlap regions. Junction charges, junction leakage currents and interconnect capacitances are not included. They are covered by separate models, which are not part of this documentation.

MOS Model 11, Level 1102, is an updated version of Level 1101 [2]. It uses slightly different equations than Level 1101.
The surface potential generally is implicitly related to the terminal voltages and has to be calculated iteratively. Since the iterative procedure was assumed to be time consuming, the surface potential has been approximated by an explicit expression [5] in previous levels of MM11 [1, 2]. In the Level 1102, the surface potential is calculated iteratively using a second-order Newton-Raphson procedure, resulting in a much more accurate description of surface potential which is obtained within 3 iterations. Owing to the increased accuracy, some of the basic equations used in Level 1101 can be simplified, and as a result Level 1102 is computationally as fast as Level 1101. In addition, a more physical and simpler velocity saturation expression is used, and as a consequence the saturation voltage expression has changed slightly as well. This all results in a more accurate description of transconductance in saturation.
The temperature scaling and geometrical scaling of parameters in MM11, Level 1102 is the same as in Level 1101. This implies that Level 1102 includes two types of geometrical scaling rules: physical rules and binning rules. It should be noted that using the source code of the Modelkit on the Philips' website (which can be found at http://www.semconductors.philips.com/Philips_Models)

1. the physical geometry scaling rules can be selected by using Level 11020, while

2. the binning geometry scaling rules can be selected by using Level 11021.

1.1 Structural Elements of MOS Model 11

The structure of MOS Model 11 is the same as the structure of MOS Model 9 [6]. The model is separable into a number of relatively independent parts, namely:

©Koninklijke Philips Electronics N.V. 2004

- **Model embedding:** It is convenient to use one single model for both n– and p–channel devices. For this reason, any p-channel device and its bias conditions are mapped onto those of an equivalent n-channel transistor. This mapping comprises a number of sign changes. Also, the model describes a symmetrical device, i.e. the source and drain nodes can be interchanged without changing the electrical properties. The assignment of source and drain to the channel nodes is based on the voltages of these nodes: for an n-channel transistor the node at the highest potential is called drain. In a circuit simulator the nodes are denoted by their network numbers, based on the circuit configuration. Again, a transformation is necessary involving a number of sign changes, including the directional noise-current sources.

- **Preprocessing:** The complete set of all the parameters, as they occur in the equations for the various electrical quantities, is denoted as the set of actual parameters, usually called the "miniset". In MM11, Level 1102, the temperature scaling parameters are included in the "miniset". Each of these actual parameters can be determined by purely electrical measurements. Since most of these parameters scale with geometry the process as a whole is characterized by an enlarged set of parameters, which is denoted as the set of scaling parameters, usually called the "maxiset". This set of parameters contains most of the actual parameters for an infinitely long and broad device and a large set of sensitivity coefficients. From this, the actual parameters for an arbitrary transistor are obtained by applying a set of transformation rules. The transformation rules describe the dependencies of the actual parameters on the length, width, and temperature. This procedure is called preprocessing, as it is normally done only once, prior to the actual electrical simulation.
  In MM11, Level 1102, parameter binning has been facilitated by adding a second, separate set of geometry scaling rules. Consequently, besides the *physical* geometrical scaling rules there is also a set of *binning* geometrical scaling rules. The physical geometry scaling rules of Level 1102 have been developed to give a good description over the whole geometry range of CMOS technologies. For processes under development, however, it is sometimes useful to have more flexible scaling relations. In this case one could opt for a binning strategy, where the accuracy with geometry is mostly determined by the number of bins used. The physical scaling rules of Level 1102 are not straightforwardly applicable to binning strategies, since they may result in discontinuities in parameter values at the bin boundaries. Consequently, special geometrical binning scaling relations have been developed, which guarantee continuity in the model parameters at the bin boundaries.

- **Clipping:** For very uncommon geometries or temperatures, the preprocessing rules may generate parameters that are outside a physically realistic range or that may create difficulties in the numerical evaluation of the model, for example division by zero. In order to prevent this, all parameters are limited to a pre-specified range directly after the preprocessing. This procedure is called clipping.

- **Current equations:** These are all expressions needed to obtain the DC nodal currents as a function of the bias conditions. They are segmentable in equations for the channel current, the gate tunnelling current and the avalanche current.

- **Charge equations:** These are all the equations that are used to calculate both the intrinsic and extrinsic charge quantities, which are assigned to the nodes.

- **Noise equations:** The total noise output of a transistor consists of a thermal noise and a flicker noise part, which create fluctuations in the channel current. Owing to the capacitive coupling between gate and channel region, current fluctuations in the gate current are induced as well, which is refered to as induced gate noise.

 ©Koninklijke Philips Electronics N.V. 2004

1.2 Structure of this Technical Note

After this introductory section, the physical background of the current, the charge and the noise equations is discussed to elucidate the model. Next, the temperature dependence and the basic equations are presented. To facilitate an unambiguous discussion of these equations, the nomenclature of the parameter set for an individual transistor (“miniset”) and the model constants is given right at the beginning of this documentation. Next all the information, which is needed for the implementation of the model in a circuit simulator, is presented. After the full nomenclature of all different model parameters (both for the physical and the binning scaling rules), quantities and variables, the different structural elements of the model are discussed in detail. The extended model equations contain all the numerical adaptations necessary to facilitate unproblematic evaluation in a circuit simulator. Next the methodology to extract the model parameters is presented. Finally the default values and clipping limits of all parameters are presented, in addition the operating point output (OPO) parameters are described.

©Koninklijke Philips Electronics N.V. 2004

©Koninklijke Philips Electronics N.V. 2004

2 Physics

2.1 Comments and Physical Background

In this section some physical background on the current, charge and noise description of MOS Model 11, Level 1102, will be given. For the full details the reader is referred to a report on the physical background of MM11, Level 1101 [3] that will be updated to Level 1102 in the near future. Additionally, for details on the derivation of the drain-source channel current, the gate current and the noise equations the reader is referred to [4],[5],[7]-[11]. All equations refered to are to be found in Section 2.3.

2.1.1 List of Parameters for an Individual Transistor

In this table the symbolic representation and the recommended programming names for the different parameters of an individual transistor with a certain channel width and length are given. More information on the nomenclature can be found in Section 3.

No.	Parameter	Program Name	Units	Description
0		LEVEL	–	Must be 1102
1	$T_{\rm R}$	TR	$^{\rm o}$C	Reference temperature
2	$V_{\rm FB}$	VFB	V	Flat-band voltage for the actual transistor at the reference temperature
3	$S_{\rm T;V_{FB}}$	STVFB	VK^{-1}	Coefficient of the temperature dependence of $V_{\rm FB}$
4	k_0	KO	V$^{1/2}$	Body-effect factor for the actual transistor
5	$1/k_{\rm P}$	KPINV	V$^{-1/2}$	Inverse of body-effect factor of the poly-silicon gate for the actual transistor
6	$\phi_{\rm B}$	PHIB	V	Surface potential at the onset of strong inversion for the actual transistor at the reference temperature
7	$S_{\rm T;\phi_B}$	STPHIB	VK^{-1}	Coefficient of the temperature dependence of $\phi_{\rm B}$
8	β	BET	AV^{-2}	Gain factor for the actual transistor at the reference temperature
9	η_β	ETABET	–	Exponent of the temperature dependence of the gain factor
10	$\theta_{\rm sr}$	THESR	V^{-1}	Coefficient of the mobility reduction due to surface roughness scattering for the actual transistor at the reference temperature
11	$\eta_{\rm sr}$	ETASR	–	Exponent of the temperature dependence of $\theta_{\rm sr}$
12	$\theta_{\rm ph}$	THEPH	V^{-1}	Coefficient of the mobility reduction due to phonon scattering for the actual transistor at the reference temperature
13	$\eta_{\rm ph}$	ETAPH	–	Exponent of the temperature dependence of $\theta_{\rm ph}$
14	$\eta_{\rm mob}$	ETAMOB	–	Effective field parameter for dependence on depletion/inversion charge for the actual transistor at the reference temperature
15	$S_{\rm T;\eta_{mob}}$	STETAMOB	K^{-1}	Coefficient of the temperature dependence of $\eta_{\rm mob}$

16	ν	NU	-	Exponent of field dependence of mobility model at the reference temperature
17	ν_{EXP}	NUEXP	–	Exponent of the temperature dependence of ν
18	θ_{R}	THER	V^{-1}	Coefficient of the series resistance for the actual transistor at the reference temperature: $\theta_{\mathrm{R}} = 2 \cdot \beta \cdot R_{\mathrm{S}}$
19	η_{R}	ETAR	–	Exponent of the temperature dependence of θ_{R}
20	θ_{R1}	THER1	V	Numerator of the gate voltage dependent part of series resistance for the actual transistor
21	θ_{R2}	THER2	V	Denominator of the gate voltage dependent part of series resistance for the actual transistor
22	θ_{sat}	THESAT	V^{-1}	Velocity saturation parameter due to optical/acoustic phonon scattering for the actual transistor at the reference temperature
23	η_{sat}	ETASAT	–	Exponent of the temperature dependence of θ_{sat}
24	θ_{Th}	THETH	V^{-3}	Coefficient of self-heating for the actual transistor at the reference temperature
25	σ_{dibl}	SDIBL	$\mathrm{V}^{-1/2}$	Drain-induced barrier-lowering parameter for the actual transistor
26	m_0	MO	–	Parameter for (short-channel) subthreshold slope for the actual transistor
27	σ_{sf}	SSF	$\mathrm{V}^{-1/2}$	Static-feedback parameter for the actual transistor
28	α	ALP	–	Factor of the channel length modulation for the actual transistor
29	V_{P}	VP	V	Characteristic voltage of the channel length modulation
30	m	MEXP	-	Smoothing factor for the actual transistor
31	a_1	A1	–	Factor of the weak–avalanche current for the actual transistor at the reference temperature
32	$S_{\mathrm{T};a_1}$	STA1	K^{-1}	Coefficient of the temperature dependence of a_1
33	a_2	A2	V	Exponent of the weak–avalanche current for the actual transistor
34	a_3	A3	–	Factor of the drain–source voltage above which weak–avalanche occurs for the actual transistor
35	I_{GINV}	IGINV	AV^{-2}	Gain factor for intrinsic gate tunnelling current in inversion for the actual transistor
36	B_{inv}	BINV	V	Probability factor for intrinsic gate tunnelling current in inversion
37	I_{GACC}	IGACC	AV^{-2}	Gain factor for intrinsic gate tunnelling current in accumulation for the actual transistor
38	B_{acc}	BACC	V	Probability factor for intrinsic gate tunnelling current in accumulation
39	V_{FBov}	VFBOV	V	Flat-band voltage for the source/drain overlap extensions
40	k_{ov}	KOV	$\mathrm{V}^{1/2}$	Body-effect factor for the source/drain overlap extensions
41	I_{GOV}	IGOV	AV^{-2}	Gain factor for source/drain overlap gate tunnelling current for the actual transistor

©Koninklijke Philips Electronics N.V. 2004

42	A_{GIDL}	AGIDL	AV^{-3}	Gain factor for gate-induced drain leakage current for the actual transistor
43	B_{GIDL}	BGIDL	V	Probability factor for gate-induced drain leakage current at the reference temperature
44	$S_{\mathrm{T};B_{\mathrm{GIDL}}}$	STBGIDL	VK^{-1}	Coefficient of the temperature dependence of B_{GIDL}
45	C_{GIDL}	CGIDL	-	Factor for the lateral field dependence of the gate-induced drain leakage current
46	C_{OX}	COX	F	Oxide capacitance for the intrinsic channel for the actual transistor
47	C_{GDO}	CGDO	F	Oxide capacitance for the gate–drain overlap for the actual transistor
48	C_{GSO}	CGSO	F	Oxide capacitance for the gate–source overlap for the actual transistor
49	–	GATENOISE		Flag for in/exclusion of induced gate thermal noise
50	N_{T}	NT	J	Coefficient of the thermal noise at the reference temperature
51	N_{FA}	NFA	$\mathrm{V}^{-1}\mathrm{m}^{-4}$	First coefficient of the flicker noise for the actual transistor
52	N_{FB}	NFB	$\mathrm{V}^{-1}\mathrm{m}^{-2}$	Second coefficient of the flicker noise for the actual transistor
53	N_{FC}	NFC	V^{-1}	Third coefficient of the flicker noise for the actual transistor
54	t_{ox}	TOX	m	Thickness of gate oxide layer
55	ΔT_{A}	DTA	K	Temperature offset of the device with respect to ambient circuit temperature T_{A}
56	N_{MULT}	MULT	–	Number of devices in parallel

Note: The parameter t_{ox} is used for calculation of the effective oxide thickness (due to quantum-mechanical effects) and the $1/f$ noise, not for the calculation of β!!!

The additional parameters for the model including self-heating (see Section4.2) are listed in the table below.

No.	Parameter	Program Name	Units	Description
57	R_{Th}	RTH	K/W	Thermal resistance
58	C_{Th}	CTH	J/K	Thermal capacitance
59	A_{Th}	ATH	-	Temperature coefficient of the thermal resistance

©Koninklijke Philips Electronics N.V. 2004

2.1.2 List of Physical Constants

In this table the symbolic representation, the recommended programming names and the value of the various physical constants used in MOS Model 11 are given.

No.	Constant	Program Name	Units	Description
1	T_0	TO	K	Offset for conversion from Celsius to Kelvin temperature scale (273.15)
2	k_B	KB	JK^{-1}	Boltzmann constant $(1.3806226 \cdot 10^{-23})$
3	q	Q	C	Elementary unit charge $(1.6021918 \cdot 10^{-19})$
4	ϵ_{ox}	EPSOX	Fm^{-1}	Absolute permittivity of the oxide layer $(3.453143800 \cdot 10^{-11})$
5	QM_N	QMN	$V\,m^{\frac{4}{3}}C^{-\frac{2}{3}}$	Constant of quantum-mechanical behaviour of electrons $(5.951993000 \cdot 10^{+00})$
6	QM_P	QMP	$V\,m^{\frac{4}{3}}C^{-\frac{2}{3}}$	Constant of quantum-mechanical behaviour of holes $(7.448711000 \cdot 10^{+00})$
7	χ_{B_N}	CHIBN	V	Tunnelling barrier height for electrons for Si/SiO_2-structure $(3.100000000 \cdot 10^{+00})$
8	χ_{B_P}	CHIBP	V	Tunnelling barrier height for holes for Si/SiO_2-structure $(4.500000000 \cdot 10^{+00})$

2.1.3 List of Input Variables for an Individual Transistor

In this table the symbolic representation and the recommended programming names for the input variables of the electrical model are given.

No.	Symbol	Program Name	Units	Description
1	T_A	TA	°C	Ambient circuit temperature
2	f	F	s^{-1}	Operation frequency

©Koninklijke Philips Electronics N.V. 2004

2.1.4 Comments on Current Equations

Conventional MOS models such as MOS Model 9 and BSIM4 are threshold-voltage-based models, which make use of approximate expressions of the drain-source channel current I_{DS} in the weak-inversion region (i.e., subthreshold) and in the strong-inversion region (i.e., well above threshold). These approximate equations are tied together using a mathematical smoothing function, resulting in neither a physical nor an accurate description of I_{DS} in the moderate inversion region (i.e., around threshold). With the constant downscaling of supply voltage the moderate inversion region becomes more and more important, and an accurate description of this region is thus essential.

A more accurate type of model is the surface-potential-based model, where the channel current I_{DS} is split up in a drift (I_{drift}) and a diffusion (I_{diff}) component, which are a function of the gate bias V_{GB} and the surface potential at the source (ψ_{s_0}) and the drain (ψ_{s_L}) side. In this way I_{DS} can be accurately described using one equation for all operating regions (i.e., weak, moderate and strong-inversion). MOS Model 11 is a surface-potential-based model.

Surface Potential: The surface potential ψ_s is defined as the electrostatic potential at the gate oxide/substrate interface with respect to the neutral bulk (due to the band bending, see Fig.2.1 (a)). For an n-MOS transistor with uniform doping concentration it can be calculated from the following implicit relation:

$$\left(\frac{V_{GB} - V_{FB} - \psi_p - \psi_s}{k_0}\right)^2 = \psi_s + \phi_T \cdot \left[\exp\left(-\frac{\psi_s}{\phi_T}\right) - 1\right] + \phi_T \cdot \exp\left(-\frac{\phi_B + V}{m_{\phi_T}}\right) \cdot \left[\exp\left(\frac{\psi_s}{m_{\phi_T}}\right) - \frac{\psi_s}{m_{\phi_T}} - 1\right]$$

where V is the quasi-Fermi potential, which ranges from V_{SB} at the source side to V_{DB} at the drain side, and m_{ϕ_T} is given by $(1 + m_0) \cdot \phi_T$. The parameter m_0 has been added to model the non-ideal subthreshold behaviour of short-channel transistors[1], and ψ_p is the potential drop in the polysilicon gate material due to the poly-depletion effect. The latter is given by[2]:

$$\psi_p = \begin{cases} 0 & \text{for: } V_{GB} \leq V_{FB} \\ \left(\sqrt{V_{GB} - V_{FB} - \psi_s + \frac{k_P{}^2}{4}} - \frac{k_P}{2}\right)^2 & \text{for: } V_{GB} > V_{FB} \end{cases}$$

In Fig. 2.1 (b), the surface potential is shown as a function of gate bias for a typical n-type MOS device. The surface potential ψ_s is implicitly related to the gate bias V_{GB} and the quasi-Fermi potential V, and cannot be calculated analytically. It can only be calculated using an iterative solution, which in general is computation-time consuming. As a consequence, an explicit approximation of the surface potential was used in previous levels of MM11. In order to increase the accuracy of the calculated ψ_s, however, in MM11, Level 1102, the surface potential is calculated using a second-order Newton-Raphson iterative procedure [12], see eqs. (2.33)-(2.37)[3]. In this way, ψ_s is calculated with an accuracy of about $2.5 \cdot 10^{-12}$ and this accuracy is reached within 3 iterations. Owing to the

[1] Parameter $m_0 = 0$ for the ideal long-channel case.

[2] For $V_{GB} < V_{FB}$ an accumulation layer is formed in both the substrate silicon and the gate polysilicon, in this case ψ_p is slightly negative and weakly dependent on V_{GB}. This effect has been neglected.

[3] In Section 2.3 the subscript T denotes a temperature dependent model parameter.

©Koninklijke Philips Electronics N.V. 2004

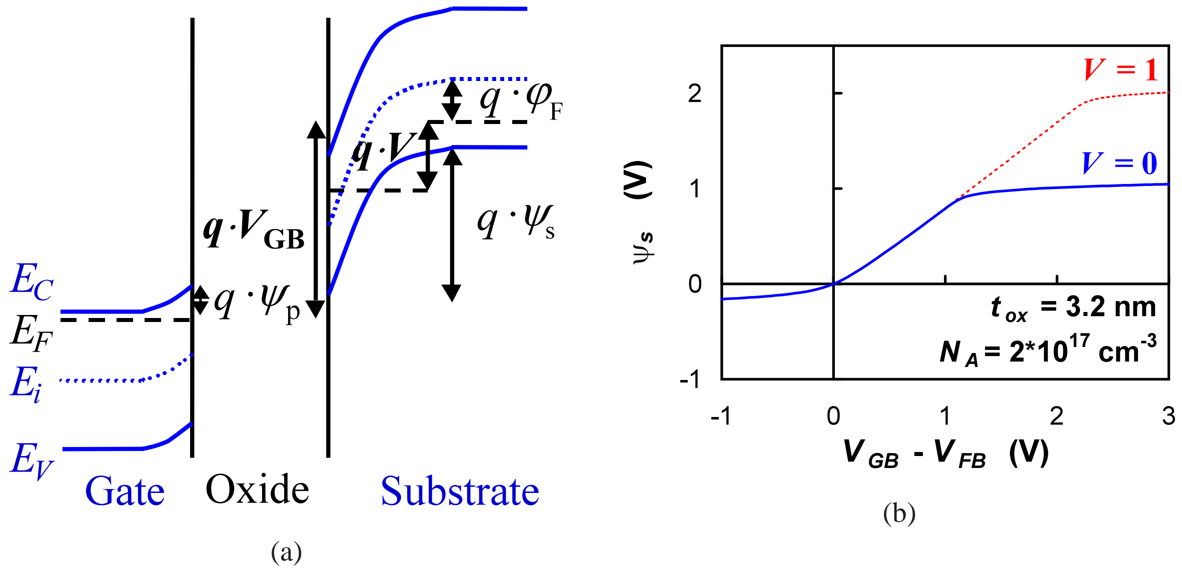

Figure 2.1: (a) The energy band diagram of an n-type MOS transistor in inversion ($V_{GB} > V_{FB}$), where ψ_s is the surface potential, ψ_p is the potential drop in the gate due to the poly-depletion effect, V is the quasi-Fermi potential and ϕ_F is the intrinsic Fermi-potential ($\phi_B = 2 \cdot \phi_F$).
(b) The surface potential as a function of gate bias for different values of quasi-Fermi potential V ($m_0 = 0$).

increased accuracy, some of the basic equations used in Level 1101 can be simplified, and as a result Level 1102 is computationally as fast as Level 1101. A more complete overview of the iterative calculation of ψ_s can be found in Section 6.2 on the implemented model equations.

A surface-potential-based model automatically incorporates the pinch-off condition at the drain side, and as a result it gives a description of both the linear (or ohmic) region and the saturation region for the ideal long-channel case. In this case the saturation voltage V_{DSAT} (i.e., the drain-source voltage above which saturation occurs) corresponds to eq. (2.27). For short-channel devices, however, no real pinch-off occurs and the saturation voltage is affected by velocity saturation and series-resistance. In this case the saturation voltage V_{DSAT} is calculated using eqs. (2.27)-(2.31). The transition from linear to saturation region is no longer automatically described by the surface-potential-based model. This has been solved in the same way as in [13] by introducing an effective drain-source bias V_{DS_x} which changes smoothly from V_{DS} in the linear region to V_{DSAT} in the saturation region, see eq. (2.32).

A surface-potential-based model makes no use of threshold voltage V_T. Circuit designers, however, are used to think in terms of threshold voltage, and as a consequence it would be useful to have a description of V_T in the framework of a surface-potential-model. It has been found that an accurate expression of threshold voltage is simply given by:

$$V_T = V_{FB} + \left(1 + \frac{{k_0}^2}{{k_P}^2}\right) \cdot (V_{SB} + \phi_B + 2 \cdot \phi_T) - V_{SB} + k_0 \cdot \sqrt{V_{SB} + \phi_B + 2 \cdot \phi_T}$$

The threshold voltage and other important parameters for circuit design are part of the operating point output as given in Section 9.2.

 ©Koninklijke Philips Electronics N.V. 2004

Channel Current: Neglecting the influence of gate and bulk current, the channel current can be written as:

$$I_{DS} = I_{drift} + I_{diff}$$

where ideally the drift component I_{drift} can be approximated by (for $V_{GB} > V_{FB}$):

$$I_{drift} = -\beta \cdot \frac{Q_{inv_0} + Q_{inv_L}}{2 \cdot C_{ox}} \cdot \left(\psi_{s_L} - \psi_{s_0}\right)$$

and the diffusion component I_{diff} can be approximated by (for $V_{GB} > V_{FB}$):

$$I_{diff} = \beta \cdot \phi_T \cdot \frac{Q_{inv_L} - Q_{inv_0}}{C_{ox}}$$

Here C_{ox} is given by $\epsilon_{ox} \big/ t_{ox}$, and Q_{inv_0} and Q_{inv_L} denote the inversion-layer charge density at the source and drain side, respectively, which are given by eqs. (2.40)-(2.42) (where $Q_{inv} = -\epsilon_{ox} \big/ t_{ox} \cdot V_{inv}$).

In the non-ideal case the channel current is affected by several physical effects, such as drain-induced barrier lowering, static feedback, mobility reduction, series-resistance, velocity saturation, channel length modulation and self-heating, which have to be taken into account in the channel current expression:

- In threshold-voltage-based models drain-induced barrier lowering and static feedback are traditionally implemented as a decrease in threshold voltage with drain bias. Here these effects have been implemented as an increase in effective gate bias ΔV_G given by eqs. (2.19)-(2.24). An effective drain-source voltage $V_{DS_{eff}}$ has been used to preserve non-singular behaviour in the higher-order derivatives of I_{DS} at $V_{DS} = 0$ V.

- The effects of mobility reduction and series-resistance on channel current have been described in [8], and have consequently been implemented using eqs. (2.51) and (2.55), respectively.

- The effect of velocity saturation has been modelled using the following electron velocity saturation expression [9]:

  $$v = \frac{\mu \cdot E_{\parallel}}{\sqrt{1 + \left(\mu \big/ v_{sat} \cdot E_{\parallel}\right)^2}}$$

  where $E_{\parallel}$ is the lateral electric field $E_{\parallel}$. Using the above expression in the calculation of channel current I_{DS} results in the velocity saturation expression (2.54), where θ_{sat} is theoretically equal to $\mu_0/(v_{sat} \cdot L)$. For holes, the expression is slightly different.

- The effect of channel length modulation and self-heating on channel current have been described in [9], and have consequently been implemented using eqs. (2.52) and (2.56), respectively.

All the above effects can be incorporated into the channel current expression using eq. (2.57) and eq. (2.60).

©Koninklijke Philips Electronics N.V. 2004

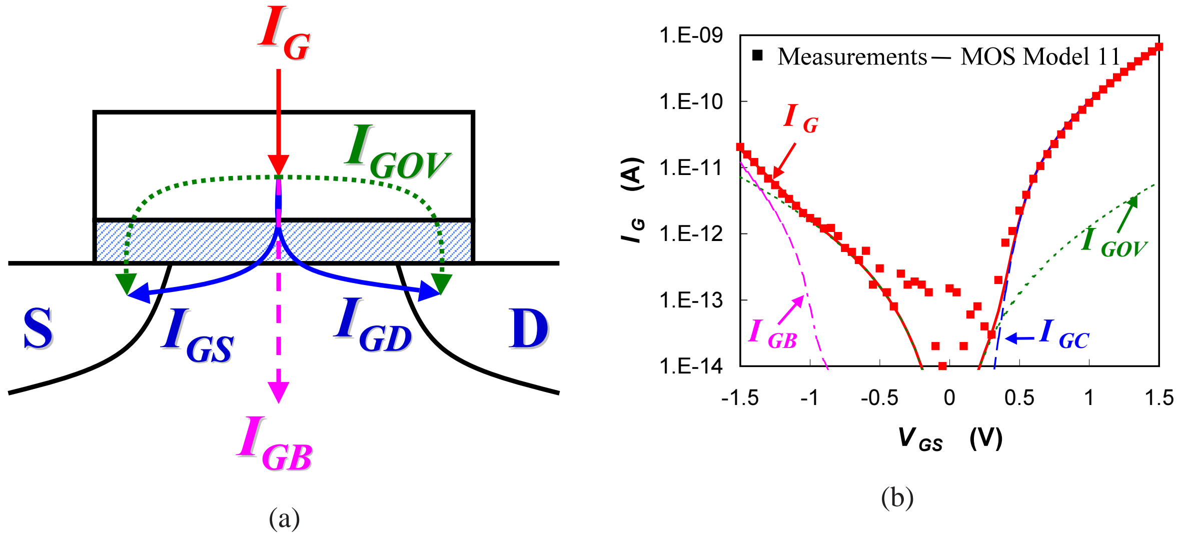

Figure 2.2: (a) The different gate current components in a MOS transistor. One can distinguish the intrinsic components, i.e. the gate-to-channel current I_{GC} ($= I_{\mathrm{GS}} + I_{\mathrm{GD}}$) and the gate-to-bulk current I_{GB}, and the extrinsic, i.e. the gate/source and gate/drain overlap components I_{Gov}. (b) Measured and modelled gate current as a function of gate bias V_{GS} at $V_{\mathrm{DS}} = V_{\mathrm{SB}} = 0$ V, the different gate current components are also shown. NMOS-transistor, $W/L = 10/0.6\mu$m and $t_{\mathrm{ox}} = 2$nm.

Weak-Avalanche Current: At high drain bias, owing to the weak-avalanche effect (or impact ionization), a current I_{avl} will flow between drain and bulk[4]. The description of the weak-avalanche current has been taken from MOS Model 9 [6], and is given by eq. (2.61). With the down-scaling of supply voltage for modern CMOS technologies, weak-avalanche becomes less and less important.

Gate Tunnelling Current: With CMOS technology scaling the gate oxide thickness is reduced and, due to the direct-tunnelling of carriers through the oxide, the gate current is no longer negligible, and has to be taken into account. Several gate current components can be distinguished, three components (I_{GS}, I_{GD} and I_{GB}) due to the intrinsic MOS channel, and two components ($I_{\mathrm{Gov_0}}$ and $I_{\mathrm{Gov_L}}$) due to gate/source and gate/drain overlap region, see Fig. 2.2 (a).

For an n-type MOS transistor operating in inversion, the intrinsic gate current density J_{G} consists of electrons tunnelling from the inversion layer to the gate, the so-called conductance band tunnelling, which in general can be written as [14] (for $V_{\mathrm{GB}} > V_{\mathrm{FB}}$):

$$J_{\mathrm{G}} \propto -V_{\mathrm{ox}} \cdot Q_{\mathrm{inv}} \cdot P_{\mathrm{tun}} \{V_{\mathrm{ox}}, \chi_{\mathrm{B}}, B\}$$

where V_{ox} is the oxide voltage given by $V_{\mathrm{ox}} = V_{\mathrm{GB}} - V_{\mathrm{FB}} - \psi_{\mathrm{p}} - \psi_{\mathrm{s}}$. The carrier tunnelling probability P_{tun} is a function of the oxide voltage V_{ox}, the oxide energy barrier χ_{B} as observed by the inversion-layer carriers, and a parameter B. This probability is given by eq. (2.69), where both direct-tunnelling for $V_{\mathrm{ox}} < \chi_{\mathrm{B}}$ and Fowler-Nordheim tunnelling for $V_{\mathrm{ox}} > \chi_{\mathrm{B}}$ have been taken into account.

Owing to quantum-mechanical energy quantization in the potential well at the SiO_2-surface, the electrons in the inversion layer are not situated at the bottom of the conduction band, but in the lowest

[4] In reality part of the generated avalanche current will also flow from drain to source [4], this has been neglected.

 ©Koninklijke Philips Electronics N.V. 2004

energy subband which lies $\Delta\chi_{B}$ above the conduction band. Assuming that only the lowest energy subband is occupied by electrons, the value of $\Delta\chi_{B}$ can be given by eq. (2.76) [15]. As a result the oxide barrier $\chi_{B_{eff}}$ has to be lowered by an amount of $\Delta\chi_{B}$, see eq. (2.77).
In inversion the total intrinsic gate current consists of electrons tunnelling from inversion layer to gate, the so-called gate-to-channel current I_{GC}. These electrons are supplied by both source (I_{GS}) and drain (I_{GD}). The gate-to-channel current I_{GC} can be calculated from:

$$I_{GC} = W \cdot \int_0^L J_G \cdot dx$$

where x is the coordinate along the channel. Using a first-order perturbation approximation, i.e. assuming the gate current is small enough so that it does not change the distribution of surface potential along the channel, I_{GC} can be calculated by eqs. (2.76)-(2.85). In the same way the partitioning of I_{GC} into I_{GS} and I_{GD} can be calculated using:

$$I_{GS} = W \cdot \int_0^L \left(1 - \frac{x}{L}\right) \cdot J_G \cdot dx$$

$$I_{GD} = W \cdot \int_0^L \frac{x}{L} \cdot J_G \cdot dx$$

which results in expressions for I_{GS} and I_{GD} as given by eqs. (2.86)-(2.88). The gate-to-channel current I_{GC} can be seen in Fig. 2.2 (b) as a function of gate bias for a typical n-MOS transistor at $V_{DS} = 0$ (i.e. $I_{GS} = I_{GD} = 1/2 \cdot I_{GC}$).

For an n-type MOS transistor operating in accumulation, an accumulation layer of holes is formed in the p-type substrate and an accumulation layer of electrons is formed in the n^+-type polysilicon gate. Since the oxide energy barrier for electrons χ_{B_N} is considerably lower than that for holes χ_{B_P}, the gate current will mainly consist of electrons tunnelling from the gate to the bulk silicon, where they are swept to the bulk terminal. In this case the (intrinsic) gate current density J_G can be written as [14] (for $V_{GB} < V_{FB}$):

$$J_G \propto -V_{ox} \cdot Q_{acc} \cdot P_{tun}\{-V_{ox}, \chi_B, B\}$$

where Q_{acc} is the accumulation charge density in the gate given by $\epsilon_{ox}/t_{ox} \cdot V_{ox}$. In order to limit calculation time the quantum-mechanical oxide barrier lowering in this case is neglected, and the resulting expression for I_{GB} is given by eqs. (2.74)-(2.75). The gate-to-bulk current I_{GB} can be seen in Fig. 2.2 (b) as a function of gate bias for a typical n-MOS transistor at $V_{DS} = 0$.

Apart from the intrinsic components I_{GC} and I_{GB}, considerable gate current can be generated in the gate/source- and gate/drain-overlap regions. Concentrating on the gate/source[5]-overlap region, in order to calculate the overlap gate current, the overlap region is treated as an n^+-gate/oxide/n^+-bulk MOS capacitance where the source acts as bulk. Although the impurity doping concentration in the n^+-source extension region is non-uniform in both lateral and transversal direction, it is assumed that an effective flat-band voltage V_{FBov} and body-factor k_{ov} can be defined for this structure. Furthermore

[5] In the following derivation, the same can be done for the gate/drain-overlap region by replacing the source by the drain.

©Koninklijke Philips Electronics N.V. 2004

assuming that only accumulation and depletion occur in the n^+-source region[6], a surface potential ψ_{ov} can be calculated using:

$$\left(\frac{V_{GS} - V_{FBov} - \psi_{p_{ov}} - \psi_{ov}}{k_{ov}}\right)^2 = -\psi_{ov} + \phi_T \cdot \left[\exp\left(\frac{\psi_{s_{ov}}}{\phi_T}\right) - 1\right]$$

where the potential drop in the polysilicon gate material due to the poly-depletion effect $\psi_{p_{ov}}$ is given by:

$$\psi_{p_{ov}} = \begin{cases} 0 & \text{for: } V_{GS} \leq V_{FBov} \\ \left(\sqrt{V_{GS} - V_{FBov} - \psi_{ov} + \frac{k_P{}^2}{4}} - \frac{k_P}{2}\right)^2 & \text{for: } V_{GS} > V_{FBov} \end{cases}$$

Again the surface potential ψ_{ov} is calculated using a second-order Newton-Raphson iterative procedure [12], see eqs. (2.62)-(2.68). A more complete overview of the iterative calculation of ψ_{ov} can be found in Section 6.2 on the implemented model equations.

For $V_{GS} > V_{FBov}$ a negatively charged accumulation layer is formed in the overlapped n^+-source extension and a positively charged depletion layer is formed in the overlapping gate. In this case the overlap gate current will mostly consist of electrons tunnelling from the source accumulation layer to the gate, it is given by:

$$I_{G_{ov}} \propto -V_{ov} \cdot Q_{ov} \cdot P_{tun}\{V_{ov}, \chi_B, B\}$$

where V_{ov} is the oxide voltage for the gate/source-overlap ($= V_{GS} - V_{FBov} - \psi_{p_{ov}} - \psi_{ov}$), given by eqs. (2.63)-(2.68), and Q_{ov} is the total charge density in the n^+-source region ($= -\epsilon_{ox}/t_{ox} \cdot V_{ov}$). For $V_{GS} < V_{FBov}$ the situation is reversed, a positively charged depletion layer is formed in the overlapped n^+-source extension and a negatively charged accumulation layer is formed in the overlapping gate. In this case the overlap gate current will mostly consist of electrons tunnelling from the gate accumulation layer to the source, it is given by:

$$I_{G_{ov}} \propto V_{ov} \cdot Q_{ov} \cdot P_{tun}\{-V_{ov}, \chi_B, B\}$$

The overlap gate current components can now be given by eqs. (2.70)-(2.73). In Fig. 2.2 (b) the gate overlap current $I_{G_{ov}}$ is shown as a function of gate bias for a typical n-MOS transistor at $V_{DS} = 0$ (i.e. $I_{G_{ov_L}} = I_{G_{ov_0}}$).

For n-type and p-type MOS transistors the gate current behaviour is different due to the type of carriers that constitute the different gate current components[7]. The difference is summarized in Tab. 2.1.

2.1.5 Comments on Charge Equations

In a typical MOS structure we can distinguish intrinsic and extrinsic charges. The latter are due to the gate/source and gate/drain overlap regions. The drain/source junctions also contribute to the

[6] Since the source extension has a very high doping concentration, an inversion layer in the gate/source overlap will only be formed at very negative gate-source bias values. This effect has been neglected.

[7] It is assumed here that the gate current is only determined by conductance band tunnelling. For high values of gate bias (i.e. $q \cdot V_{ox} > E_g$) electrons in the bulk valence band may also tunnel through the oxide to the gate conduction band. This mechanism is referred to as valence band tunnelling, and it has not been taken into account in MOS Model 11.

 ©Koninklijke Philips Electronics N.V. 2004

Table 2.1: The type of carriers that contribute to the gate tunnelling current in the various operation regions for the intrinsic MOSFET, the gate/drain- and gate/source-overlap regions. The type of carriers determine the value of oxide energy barrier χ_B that has to be used (χ_{B_N} for electrons, χ_{B_P} for holes). In the last row the direction of gate current is indicated.

Type	Intrinsic MOSFET		Overlap Regions
	Accumulation	Inversion	
NMOS	electrons	electrons	electrons
PMOS	electrons	holes	holes
	I_{GB}	I_{GS} / I_{GD}	I_{GS} / I_{GD}

capacitance behaviour of a MOSFET, but this is not taken into account in MOS Model 11; it is described by a separate junction diode model.

Intrinsic Charges: In the intrinsic MOS transistor charges can be attributed to the four terminals. The gate charge Q_G can be simply calculated from:

$$Q_G = -W \cdot \int_0^L Q_{tot} \cdot dx$$

where Q_{tot} is the total charge density in the silicon bulk ($Q_{tot} = -\epsilon_{ox}/t_{ox} \cdot V_{ox}$). The total inversion-layer charge Q_{inv} is split up in a source Q_S and a drain Q_D charge, they can be calculated using the Ward-Dutton charge partitioning scheme [16]:

$$Q_S = W \cdot \int_0^L \left(1 - \frac{x}{L}\right) \cdot Q_{inv} \cdot dx$$

$$Q_D = W \cdot \int_0^L \frac{x}{L} \cdot Q_{inv} \cdot dx$$

Since charge neutrality holds for the complete transistor, the bulk charge is simply given by:

$$Q_B = -Q_S - Q_D - Q_G$$

The above equations have been solved, and the charges are given by eqs. (2.95)-(2.100). In these equations $C_{ox_{eff}}$ is the effective oxide capacitance, which is smaller than the ideal oxide capacitance C_{OX} due to quantum-mechanical effects: Quantum-mechanically, the inversion/accumulation charge concentration is not maximum at the Si-SiO$_2$-interface (as it would be in the classical case), but reaches a maximum at a distance Δz from the interface [15]. This quantum-mechanical effect can be taken into account by an effective oxide thickness $t_{ox} + \epsilon_{ox} / \epsilon_{Si} \cdot \Delta z$, where Δz is dependent on the effective electric field E_{eff} [15], [17] ($E_{eff} = -\epsilon_{ox} / \epsilon_{Si} \cdot V_{eff} / t_{ox}$). The effective oxide thickness results in an effective oxide capacitance $C_{ox_{eff}}$, see eq. (2.95).

It should be noted that the above charge model is quasi-static. A phase-shift between drain channel current and gate voltage is not taken into account. This implies that for a few applications at high

frequencies approaching the cut-off frequency, errors have to be expected due to non-quasi-static effects. Nevertheless non-quasi-effects can be taken into account using a segmentation model as described in [18].

Extrinsic Charges: The gate/source- and gate/drain-overlap regions act as bias-dependent capacitances. In order to take this bias-dependence into account the overlap regions are treated as an n^+-gate/oxide/n^+-bulk MOS capacitance along the same lines as was done for the overlap gate current, see Section 2.1.4. The charge in the overlap regions can simply be given by eqs. (2.93)-(2.94). The quantum-mechanical effect on oxide thickness has been neglected here in order to reduce calculation time.

2.1.6 Comments on Noise Equations

In a MOS transistor generally three different types of noise can be observed: $1/f$-noise, thermal noise and induced gate noise. The gate tunnel current and the bulk avalanche current will also exhibit noisy behaviour (due to shot noise), however this has been neglected in MOS Model 11.

$1/f$-Noise: At low frequencies flicker (or $1/f$) noise becomes dominant in MOSFETs. In the past this type of noise has been interpreted either in terms of trapping and detrapping of charge carriers in the gate oxide or in terms of mobility fluctuations. Over the past years, a general model for $1/f$-noise which combines both of the above physical origins [19], [20], has found wide acceptance in the field of MOS modelling. The model assumes that the carrier number in the channel fluctuates due to trapping/detrapping in the gate oxide, and that these number fluctuations also affect the carrier mobility resulting in (correlated) mobility fluctuations.

The same model is part of MOS Model 9 [21], and has been used to calculate the $1/f$-noise for MOS Model 11. The calculations have been performed in such a way that the resulting expression for spectral density is valid for all operation regions (i.e. both in subthreshold and above threshold), it is given by eqs. (2.114)-(2.117).

Thermal Noise: Since the MOSFET channel can be considered as a non–linear resistor, the channel current is subject to thermal noise. For an ideal MOSFET where the mobility is position independent, the thermal noise is given by the so-called Klaassen-Prins equation [22]. Let thermal–noise current sources be parallel connected to each infinitesimal short element of the channel, it can be shown that the noise spectral density, which is defined by [22]:

$$< \Delta i_{\mathrm{th}}{}^2 > \quad = \quad \int_0^\infty S_{\mathrm{th}}\,(f)\,\mathrm{d}f$$

is given by a generalized Nyquist relation:

$$S_{\mathrm{th}} \quad = \quad \frac{N_{\mathrm{T}}}{L^2}\int_0^L g\,(x)\,\mathrm{d}x$$

where N_{T} is equal to $4 \cdot k_{\mathrm{B}} \cdot T$ and $g\,(x)$ is the local specific channel conductance:

$$g\,(x) = -\mu \cdot W \cdot Q_{\mathrm{inv}}(x)$$

 ©Koninklijke Philips Electronics N.V. 2004

In reality, however, the mobility $\mu(x)$ is position dependent mainly due to the effect of velocity saturation. In this case, the conventional Klaassen-Prins approach does not hold, and an improved Klaassen-Prins approach has been derived [11]. This improved approach results in the spectral density given by eqs. (2.102)-(2.110). Again continuity of the noise model is assured along all modes of operation. The above thermal noise model has been found to accurately describe experimental results for various CMOS technologies without having to invoke carrier heating effects [11].

Induced Gate Noise: Owing to capacitive coupling between gate and channel, the fluctuating channel current induces noise in the gate terminal at high frequencies. Using the above-mentioned improved Klaassen-Prins approach [11], we can derive eq. (2.111) for the induced gate current noise. In addition, since S_{th} and S_{ig} have the same physical origin, both spectral densities are correlated. Using the above approach, this can be expressed by eq. (2.112).
The induced gate noise S_{ig} is a so-called non-quasi static (NQS) effect. Since the use of the channel current noise description in an NQS segmentation model [18] would automatically result in a correct description of induced gate noise, S_{ig} can be made equal to zero by using parameter GATENOISE, see eq. (2.111).

©Koninklijke Philips Electronics N.V. 2004

2.2 Calculation of Temperature-Dependent Parameters

In this Section the temperature scaling rules for the parameters of the electrical model will be given. In contrast to the geometry scaling rules, as treated in Section 5, the temperature scaling is the same for both Level 11020 and 11021.

Note: Note the addition of the voltage V_{dT} of the thermal node in order to include self-heating, see Section 4.2.

Calculation of Transistor Temperature

$$T_{\mathrm{KR}} = T_0 + T_{\mathrm{R}} \tag{2.1}$$

$$T_{\mathrm{amb}} = T_0 + T_{\mathrm{A}} + \Delta T_{\mathrm{A}} \tag{2.2}$$

$$T_{\mathrm{KD}} = T_0 + T_{\mathrm{A}} + \Delta T_{\mathrm{A}} + V_{\mathrm{dT}} \tag{2.3}$$

Calculation of Threshold–Voltage Parameters

$$\phi_{\mathrm{T}} = \frac{k_{\mathrm{B}} \cdot T_{\mathrm{KD}}}{q} \tag{2.4}$$

$$V_{\mathrm{FB_T}} = V_{\mathrm{FB}} + (T_{\mathrm{KD}} - T_{\mathrm{KR}}) \cdot S_{\mathrm{T;V_{FB}}} \tag{2.5}$$

$$\phi_{\mathrm{B_T}} = \phi_{\mathrm{B}} + (T_{\mathrm{KD}} - T_{\mathrm{KR}}) \cdot S_{\mathrm{T};\phi_{\mathrm{B}}} \tag{2.6}$$

Calculation of Mobility/Series-Resistance Parameters

$$\beta_{\mathrm{T}} = \beta \cdot \left(\frac{T_{\mathrm{KR}}}{T_{\mathrm{KD}}}\right)^{\eta_\beta} \tag{2.7}$$

$$\theta_{\mathrm{sr_T}} = \theta_{\mathrm{sr}} \cdot \left(\frac{T_{\mathrm{KR}}}{T_{\mathrm{KD}}}\right)^{\eta_{\mathrm{sr}}} \tag{2.8}$$

$$\theta_{\mathrm{ph_T}} = \theta_{\mathrm{ph}} \cdot \left(\frac{T_{\mathrm{KD}}}{T_{\mathrm{KR}}}\right)^{\eta_{\mathrm{ph}}} \tag{2.9}$$

$$\eta_{\mathrm{mob_T}} = \eta_{\mathrm{mob}} \cdot \left[1 + (T_{\mathrm{KD}} - T_{\mathrm{KR}}) \cdot S_{\mathrm{T};\eta_{\mathrm{mob}}}\right] \tag{2.10}$$

$$\nu_{\mathrm{T}} = 1 + (\nu - 1) \cdot \left(T_{\mathrm{KR}} / T_{\mathrm{KD}}\right)^{\nu_{\mathrm{exp}}} \tag{2.11}$$

$$\theta_{\mathrm{R_T}} = \theta_{\mathrm{R}} \cdot \left(\frac{T_{\mathrm{KR}}}{T_{\mathrm{KD}}}\right)^{\eta_{\mathrm{R}}} \tag{2.12}$$

$$\theta_{\mathrm{sat_T}} = \theta_{\mathrm{sat}} \cdot \left(\frac{T_{\mathrm{KR}}}{T_{\mathrm{KD}}}\right)^{\eta_{\mathrm{sat}}} \tag{2.13}$$

 ©Koninklijke Philips Electronics N.V. 2004

Calculation of Conductance Parameters

$$\theta_{\mathrm{Th_T}} = \theta_{\mathrm{Th}} \cdot \left(\frac{T_{\mathrm{KR}}}{T_{\mathrm{KD}}}\right)^{\eta_\beta} \tag{2.14}$$

Calculation of Weak–Avalanche Parameters

$$a_{1_\mathrm{T}} = a_1 \cdot \left[1 + (T_{\mathrm{KD}} - T_{\mathrm{KR}}) \cdot S_{\mathrm{T;a_1}}\right] \tag{2.15}$$

Calculation of Gate–Induced Drain Leakage Parameters

$$B_{\mathrm{GIDL_T}} = B_{\mathrm{GIDL}} \cdot \left[1 + (T_{\mathrm{KD}} - T_{\mathrm{KR}}) \cdot S_{\mathrm{T;B_{GIDL}}}\right] \tag{2.16}$$

Calculation of Noise Parameters

$$N_{\mathrm{T_T}} = \frac{T_{\mathrm{KD}}}{T_{\mathrm{KR}}} \cdot N_{\mathrm{T}} \tag{2.17}$$

Calculation of Thermal Resistance

$$R_{\mathrm{Th_T}} = R_{\mathrm{Th}} \cdot \left(\frac{T_{\mathrm{amb}}}{T_{\mathrm{KR}}}\right)^{A_{\mathrm{Th}}} \tag{2.18}$$

©Koninklijke Philips Electronics N.V. 2004

2.3 Basic Equations

The equations listed in the following sections, are the basic equations of MOS Model 11 without any adaptations necessary for numerical reasons. As such they form the bas of parameter extraction. In the following, a function is denoted by $F\{variable, \ldots\}$, where F denotes the function name and the function variables are enclosed by braces {}.

2.3.1 Internal Parameters

$$P_{\mathrm{D}} = 1 + \left(k_0 / k_{\mathrm{P}}\right)^2$$

$$V_{\mathrm{limit}} = 4 \cdot \phi_{\mathrm{T}}$$

$$\theta_{\mathrm{R_{eff}}} = \frac{1}{2} \cdot \theta_{\mathrm{R_T}} \cdot \left(1 + \frac{\theta_{\mathrm{R1}}}{1/2 + \theta_{\mathrm{R2}}}\right)$$

$$m_{\phi_{\mathrm{T}}} = (1 + m_0) \cdot \phi_{\mathrm{T}}$$

$$Acc = \left.\frac{\partial \psi_{\mathrm{s}}}{\partial V_{\mathrm{GB}}}\right|_{V_{\mathrm{GB}}=V_{\mathrm{FB_T}}} = \frac{1}{1 + k_0 / \sqrt{2\phi_{\mathrm{T}}}}$$

$$Acc_{\mathrm{ov}} = \left.\frac{\partial \psi_{\mathrm{sov}}}{\partial V_{\mathrm{GB}}}\right|_{V_{\mathrm{GB}}=V_{\mathrm{FBov}}} = \frac{1}{1 + k_{\mathrm{ov}} / \sqrt{2\phi_{\mathrm{T}}}}$$

$$QM_{\psi} = \begin{cases} QM_{\mathrm{N}} \cdot \left(\epsilon_{\mathrm{ox}} / t_{\mathrm{ox}}\right)^{2/3} & \text{for NMOS} \\ QM_{\mathrm{P}} \cdot \left(\epsilon_{\mathrm{ox}} / t_{\mathrm{ox}}\right)^{2/3} & \text{for PMOS} \end{cases}$$

$$QM_{\mathrm{t_{ox}}} = \frac{2}{5} \cdot QM_{\psi}$$

$$\chi_{\mathrm{B_{inv}}} = \begin{cases} \chi_{\mathrm{B_N}} & \text{for NMOS} \\ \chi_{\mathrm{B_P}} & \text{for PMOS} \end{cases}$$

$$\chi_{\mathrm{B_{acc}}} = \chi_{\mathrm{B_N}}$$

2.3.2 Basic Current Equations

Drain induced barrier lowering and Static Feedback:

$$V_{\mathrm{GB_{eff}}} = \begin{cases} 0 & \text{for: } V_{\mathrm{GS}} + V_{\mathrm{SB}} - V_{\mathrm{FB_T}} \leq 0 \\ V_{\mathrm{GS}} + V_{\mathrm{SB}} - V_{\mathrm{FB_T}} & \text{for: } V_{\mathrm{GS}} + V_{\mathrm{SB}} - V_{\mathrm{FB_T}} > 0 \end{cases} \tag{2.19}$$

$$\psi_{\mathrm{sat_0}} = \left(\frac{\sqrt{P_{\mathrm{D}} \cdot V_{\mathrm{GB_{eff}}} + k_0{}^2/4} - k_0/2}{P_{\mathrm{D}}}\right)^2 \tag{2.20}$$

 ©Koninklijke Philips Electronics N.V. 2004

$$D_{\mathrm{dibl}} = \sigma_{\mathrm{dibl}} \cdot \sqrt{V_{\mathrm{SB}} + \phi_{\mathrm{B_T}}} \tag{2.21}$$

$$D_{\mathrm{sf}} = \begin{cases} 0 & \text{for:} \quad \psi_{\mathrm{sat_0}} - V_{\mathrm{SB}} - \phi_{\mathrm{B_T}} \leq 0 \\ \sigma_{\mathrm{sf}} \cdot \sqrt{\psi_{\mathrm{sat_0}} - V_{\mathrm{SB}} - \phi_{\mathrm{B_T}}} & \text{for:} \quad \psi_{\mathrm{sat_0}} - V_{\mathrm{SB}} - \phi_{\mathrm{B_T}} > 0 \end{cases} \tag{2.22}$$

$$V_{\mathrm{DS_{eff}}} = \frac{{V_{\mathrm{DS}}}^4}{\left({V_{\mathrm{limit}}}^2 + {V_{\mathrm{DS}}}^2\right)^{3/2}} \tag{2.23}$$

$$\Delta V_{\mathrm{G}} = \sqrt{{D_{\mathrm{dibl}}}^2 + {D_{\mathrm{sf}}}^2} \cdot \cdot V_{\mathrm{DS_{eff}}} \tag{2.24}$$

Effective Gate-Bulk Voltage:

$$V_{\mathrm{GB}}^{*} = V_{\mathrm{GS}} + V_{\mathrm{SB}} + \Delta V_{\mathrm{G}} - V_{\mathrm{FB_T}} \tag{2.25}$$

Drain Saturation Voltage:

$$\psi_{\mathrm{sat_1}} = \begin{cases} 0 & \text{for:} \quad V_{\mathrm{GB}}^{*} \leq 0 \\ \left(\left[\sqrt{P_{\mathrm{D}} \cdot V_{\mathrm{GB}}^{*} + {k_0}^2/4} - k_0/2\right] \Big/ P_{\mathrm{D}}\right)^2 & \text{for:} \quad V_{\mathrm{GB}}^{*} > 0 \end{cases} \tag{2.26}$$

$$V_{\mathrm{DSAT_{long}}} = \psi_{\mathrm{sat_1}} - V_{\mathrm{SB}} - \phi_{\mathrm{B_T}} \tag{2.27}$$

$$T_{\mathrm{sat}} = \begin{cases} \theta_{\mathrm{sat_T}} & \text{for NMOS} \\ \frac{\theta_{\mathrm{sat_T}}}{\left(1 + {\theta_{\mathrm{sat_T}}}^2 \cdot {V_{\mathrm{DSAT_{long}}}}^2\right)^{1/4}} & \text{for PMOS} \end{cases} \tag{2.28}$$

$$\Delta_{\mathrm{SAT}} = \frac{\left(T_{\mathrm{sat}} - \theta_{\mathrm{R_{eff}}}\right) \cdot V_{\mathrm{DSAT_{long}}}}{\frac{1}{2} \cdot \left(\sqrt{2} + \sqrt{2 + 2 \cdot {T_{\mathrm{sat}}}^2 \cdot {V_{\mathrm{DSAT_{long}}}}^2}\right) + \theta_{\mathrm{R_{eff}}} \cdot V_{\mathrm{DSAT_{long}}}} \tag{2.29}$$

$$V_{\mathrm{DSAT_{short}}} = V_{\mathrm{DSAT_{long}}} \cdot \left[1 - \frac{44/45 \cdot \Delta_{\mathrm{SAT}}}{1 + \sqrt{1 - \frac{\left(\sqrt{2}-1\right) \cdot T_{\mathrm{sat}} - \theta_{\mathrm{R_{eff}}}}{T_{\mathrm{sat}} - \theta_{\mathrm{R_{eff}}}} \cdot {\Delta_{\mathrm{SAT}}}^2}}\right] \tag{2.30}$$

$$V_{\mathrm{DSAT}} = \begin{cases} V_{\mathrm{limit}} & \text{for:} \quad V_{\mathrm{DSAT_{short}}} \leq V_{\mathrm{limit}} \\ V_{\mathrm{DSAT_{short}}} & \text{for:} \quad V_{\mathrm{DSAT_{short}}} > V_{\mathrm{limit}} \end{cases} \tag{2.31}$$

$$V_{\mathrm{DS_x}} = \frac{V_{\mathrm{DS}}}{\left[1 + (V_{\mathrm{DS}}/V_{\mathrm{DSAT}})^{2 \cdot m}\right]^{\frac{1}{2 \cdot m}}} \tag{2.32}$$

Surface Potential:

The surface potential ψ_s is given by the following implicit relation:

$$F\{\psi_s,\phi\} = -V_{ox}\{\psi_s\}^2 + k_0{}^2\cdot d\{\psi_s,\phi\} = 0 \tag{2.33}$$

where ϕ can be either $V_{SB}+\phi_{B_T}$ or $V_{DS_x}+V_{SB}+\phi_{B_T}$, and:

$$V_{ox}\{\psi_s\} = \begin{cases} V_{GB}^* - \psi_s & \text{for: } V_{GB}^* - \psi_s \leq 0 \\ \frac{2\cdot\left(V_{GB}^*-\psi_s\right)}{1+\sqrt{1+4/k_P{}^2\cdot\left(V_{GB}^*-\psi_s\right)}} & \text{for: } V_{GB}^* - \psi_s > 0 \end{cases} \tag{2.34}$$

$$d\{\psi_s,\phi\} = \psi_s + \phi_T\cdot\left[\exp\left(-\frac{\psi_s}{\phi_T}\right)-1\right] + \phi_T\cdot\exp\left(-\frac{\phi}{m_{\phi_T}}\right)\cdot\left[\exp\left(\frac{\psi_s}{m_{\phi_T}}\right)-\frac{\psi_s}{m_{\phi_T}}-1\right] \tag{2.35}$$

The surface potential is iteratively calculated using a second-order Newton Raphson procedure. The surface potential at the source ψ_{s_0} and at the drain ψ_{s_L} are calculated iteratively using a second-order Newton Raphson procedure from the following implicit relations:

$$F\left\{\psi_{s_0}, V_{SB}+\phi_{B_T}\right\} = 0 \tag{2.36}$$

$$F\left\{\psi_{s_L}, V_{DS_x}+V_{SB}+\phi_{B_T}\right\} = 0 \tag{2.37}$$

Auxiliary Variables:

$$\Delta\psi = \psi_{s_L} - \psi_{s_0} \tag{2.38}$$

$$\bar{\psi} = \frac{\psi_{s_L}+\psi_{s_0}}{2} \tag{2.39}$$

Inversion-Layer Charge ($Q_{inv} = -\epsilon_{ox}/t_{ox}\cdot V_{inv}$):

$$V_{inv}\{\psi_s,\phi\} = \begin{cases} 0 & \text{for: } V_{GB}^* - \psi_s \leq 0 \\ \frac{k_0\cdot\phi_T\cdot\exp\left(-\phi/m_{\phi_T}\right)\cdot\left[\exp\left(\psi_s/m_{\phi_T}\right)-\psi_s/m_{\phi_T}-1\right]}{\sqrt{d\{\phi,\psi_s\}}+\sqrt{\psi_s+\phi_T\cdot\left[\exp\left(-\psi_s/\phi_T\right)-1\right]}} & \text{for: } V_{GB}^* - \psi_s > 0 \end{cases} \tag{2.40}$$

$$V_{inv_0} = V_{inv}\left\{\psi_{s_0}, V_{SB}+\phi_{B_T}\right\} \tag{2.41}$$

$$V_{inv_L} = V_{inv}\left\{\psi_{s_L}, V_{DS_x}+V_{SB}+\phi_{B_T}\right\} \tag{2.42}$$

$$\bar{V}_{inv} = \frac{V_{inv_0}+V_{inv_L}}{2} \tag{2.43}$$

 ©Koninklijke Philips Electronics N.V. 2004

$$\bar{V}_{\text{ox}} = \frac{V_{\text{ox}}\left\{\psi_{\text{s}_0}\right\} + V_{\text{ox}}\left\{\psi_{\text{s}_\text{L}}\right\}}{2} \tag{2.44}$$

$$V_{\text{eff}} = \bar{V}_{\text{inv}} + \eta_{\text{mob}_\text{T}} \cdot \left(\bar{V}_{\text{ox}} - \bar{V}_{\text{inv}}\right) \tag{2.45}$$

$$\xi_{\text{ox}}\left\{\psi_{\text{s}}\right\} = -\phi_{\text{T}} \cdot \frac{\partial V_{\text{ox}}}{\partial \psi_{\text{s}}} = \begin{cases} \phi_{\text{T}} & \text{for: } V^*_{\text{GB}} - \psi_{\text{s}} \leq 0 \\ \frac{\phi_{\text{T}}}{\sqrt{1+4/k_{\text{P}}{}^2 \cdot \left(V^*_{\text{GB}} - \psi_{\text{s}}\right)}} & \text{for: } V^*_{\text{GB}} - \psi_{\text{s}} > 0 \end{cases} \tag{2.46}$$

$$\bar{\xi}_{\text{ox}} = \frac{\xi_{\text{ox}}\left\{\psi_{\text{s}_0}\right\} + \xi_{\text{ox}}\left\{\psi_{\text{s}_\text{L}}\right\}}{2} \tag{2.47}$$

$$\xi\left\{\psi_{\text{s}}\right\} = -\phi_{\text{T}} \cdot \frac{\partial V_{\text{inv}}}{\partial \psi_{\text{s}}} = \begin{cases} \xi_{\text{ox}}\left\{\psi_{\text{s}}\right\} + \phi_{\text{T}} \cdot \left[\frac{1}{Acc} - 1\right] & \text{for: } V^*_{\text{GB}} - \psi_{\text{s}} \leq 0 \\ \xi_{\text{ox}}\left\{\psi_{\text{s}}\right\} + \phi_{\text{T}} \cdot \frac{k_0 \cdot \left[1 - \exp\left(-\psi_{\text{s}}/\phi_{\text{T}}\right)\right]}{2 \cdot \sqrt{\psi_{\text{s}} + \phi_{\text{T}} \cdot \left[\exp\left(-\psi_{\text{s}}/\phi_{\text{T}}\right) - 1\right]}} & \text{for: } V^*_{\text{GB}} - \psi_{\text{s}} > 0 \end{cases} \tag{2.48}$$

$$\bar{\xi} = \frac{\xi\left\{\psi_{\text{s}_0}\right\} + \xi\left\{\psi_{\text{s}_\text{L}}\right\}}{2} \tag{2.49}$$

$$\bar{V}^*_{\text{inv}} = \bar{V}_{\text{inv}} + (1 + m_0) \cdot \bar{\xi} \tag{2.50}$$

Second-Order Effects

Mobility Degradation:

$$G_{\text{mob}} = \frac{\mu_0}{\mu} = \begin{cases} 1 + \left[\left(\theta_{\text{ph}_\text{T}} \cdot V_{\text{eff}}\right)^{\nu_\text{T}/3} + \left(\theta_{\text{sr}_\text{T}} \cdot V_{\text{eff}}\right)^{2 \cdot \nu_\text{T}}\right]^{1/\nu_\text{T}} & \text{for NMOS} \\ \left[1 + \left(\theta_{\text{ph}_\text{T}} \cdot V_{\text{eff}}\right)^{\nu_\text{T}/3} + \left(\theta_{\text{sr}_\text{T}} \cdot V_{\text{eff}}\right)^{\nu_\text{T}}\right]^{1/\nu_\text{T}} & \text{for PMOS} \end{cases} \tag{2.51}$$

Channel Length Modulation:

$$G_{\Delta L} = 1 - \frac{\Delta L}{L} = 1 - \alpha \cdot \ln\left[\frac{V_{\text{DS}} - V_{\text{DS}_\text{x}} + \sqrt{\left(V_{\text{DS}} - V_{\text{DS}_\text{x}}\right)^2 + V_{\text{P}}{}^2}}{V_{\text{P}}}\right] \tag{2.52}$$

Velocity Saturation:

$$x_{\text{sat}} = \begin{cases} \frac{\theta_{\text{sat}_\text{T}} \cdot \Delta\psi}{G_{\text{mob}}} & \text{for NMOS} \\ \frac{\theta_{\text{sat}_\text{T}}}{G_{\text{mob}}} \cdot \frac{\Delta\psi}{\left[1 + \left(\theta_{\text{sat}_\text{T}} \cdot \Delta\psi / G_{\text{mob}}\right)^2\right]^{1/4}} & \text{for PMOS} \end{cases} \tag{2.53}$$

$$G_{\text{vsat}} = \frac{G_{\text{mob}}}{2} \cdot \left[1 + \sqrt{1 + 2 \cdot x_{\text{sat}}{}^2}\right] \tag{2.54}$$

Series Resistance + Self-Heating:

$$G_{\mathrm{R}} = \theta_{\mathrm{R_T}} \cdot \left(1 + \frac{\theta_{\mathrm{R1}}}{\theta_{\mathrm{R2}} + \bar{V}_{\mathrm{inv}}}\right) \cdot \bar{V}^{*}_{\mathrm{inv}} \tag{2.55}$$

$$G_{\mathrm{Th}} = \theta_{\mathrm{Th_T}} \cdot V_{\mathrm{DS}} \cdot \Delta\psi \cdot \bar{V}^{*}_{\mathrm{inv}} \tag{2.56}$$

$$G_{\mathrm{tot}} = G_{\mathrm{Th}} + \frac{G_{\mathrm{vsat}} \cdot G_{\Delta L} + G_{\mathrm{R}}}{2} + \sqrt{\frac{(G_{\mathrm{vsat}} \cdot G_{\Delta L} + G_{\mathrm{R}})^2}{4} - \frac{G_{\mathrm{R}}}{G_{\mathrm{mob}}} \cdot \frac{{x_{\mathrm{sat}}}^2}{\sqrt{1 + 2 \cdot {x_{\mathrm{sat}}}^2}}} \tag{2.57}$$

Drain-Source Channel Current:

$$I_{\mathrm{drift}} = \beta_{\mathrm{T}} \cdot \bar{V}_{\mathrm{inv}} \cdot \Delta\psi \tag{2.58}$$

$$I_{\mathrm{diff}} = \beta_{\mathrm{T}} \cdot m_{\phi_{\mathrm{T}}} \cdot \left(V_{\mathrm{inv_0}} - V_{\mathrm{inv_L}}\right) \tag{2.59}$$

$$I_{\mathrm{DS}} = \frac{I_{\mathrm{drift}} + I_{\mathrm{diff}}}{G_{\mathrm{tot}}} \tag{2.60}$$

Weak-Avalanche:

$$I_{\mathrm{avl}} = \begin{cases} 0 & \text{for:} \quad V_{\mathrm{DS}} \le a_3 \cdot V_{\mathrm{DSAT}} \\ \mathrm{a}_{1_{\mathrm{T}}} \cdot I_{\mathrm{DS}} \cdot \exp\left(-\frac{a_2}{V_{\mathrm{DS}} - a_3 \cdot V_{\mathrm{DSAT}}}\right) & \text{for:} \quad V_{\mathrm{DS}} > a_3 \cdot V_{\mathrm{DSAT}} \end{cases} \tag{2.61}$$

Surface Potential in Gate Overlap Regions:

The surface potential in the overlap region ψ_{ov} is given by the following implicit relation:

$$F_{\mathrm{ov}}\{V_{\mathrm{GX}}, \psi_{\mathrm{ov}}\} = -V_{\mathrm{ov}}\{V_{\mathrm{GX}}, \psi_{\mathrm{ov}}\}^2 + {k_{\mathrm{ov}}}^2 \cdot d_{\mathrm{ov}}\{\psi_{\mathrm{ov}}\} = 0 \tag{2.62}$$

where V_{GX} can be either V_{GS} or V_{GD}, and:

$$V_{\mathrm{ov}}\{V_{\mathrm{GX}}, \psi_{\mathrm{ov}}\} = \begin{cases} V_{\mathrm{GX}} - V_{\mathrm{FBov}} - \psi_{\mathrm{ov}} & \text{for:} \quad V_{\mathrm{GX}} - \psi_{\mathrm{ov}} \le V_{\mathrm{FBov}} \\ \frac{V_{\mathrm{GX}} - V_{\mathrm{FBov}} - \psi_{\mathrm{ov}}}{1 + \sqrt{1 + 4/{k_{\mathrm{P}}}^2 \cdot (V_{\mathrm{GX}} - V_{\mathrm{FBov}} - \psi_{\mathrm{ov}})}} & \text{for:} \quad V_{\mathrm{GX}} - \psi_{\mathrm{ov}} > V_{\mathrm{FBov}} \end{cases} \tag{2.63}$$

$$d_{\mathrm{ov}}\{\psi_{\mathrm{ov}}\} = -\psi_{\mathrm{ov}} + \phi_{\mathrm{T}} \cdot \left[\exp\left(\frac{\psi_{\mathrm{ov}}}{\phi_{\mathrm{T}}}\right) - 1\right] \tag{2.64}$$

The surface potentials in the gate/source overlap $\psi_{\mathrm{ov_0}}$ and in the gate/drain overlap $\psi_{\mathrm{ov_L}}$ are calculated iteratively using a second-order Newton Raphson procedure from the following implicit relations:

$$F_{\mathrm{ov}}\left\{V_{\mathrm{GS}}, \psi_{\mathrm{ov_0}}\right\} = 0 \tag{2.65}$$

$$F_{\mathrm{ov}}\left\{V_{\mathrm{GS}} - V_{\mathrm{DS}}, \psi_{\mathrm{ov_L}}\right\} = 0 \tag{2.66}$$

©Koninklijke Philips Electronics N.V. 2004

The oxide voltages in the gate/source overlap V_{ov_0} and the gate/drain overlap V_{ov_L} are given by:

$$V_{\mathrm{ov}_0} = V_{\mathrm{ov}}\left\{V_{\mathrm{GS}}, \psi_{\mathrm{ov}_0}\right\} \tag{2.67}$$

$$V_{\mathrm{ov}_L} = V_{\mathrm{ov}}\left\{V_{\mathrm{GS}} - V_{\mathrm{DS}}, \psi_{\mathrm{ov}_L}\right\} \tag{2.68}$$

Gate Current Equations:

The tunnelling probability is given by:

$$P_{\mathrm{tun}}\{V_{\mathrm{ox}}, \chi_{\mathrm{B}}, B\} = \begin{cases} \exp\left(-B \cdot \dfrac{\left[1-\left(1-V_{\mathrm{ox}}/\chi_{\mathrm{B}}\right)^{\frac{3}{2}}\right]}{V_{\mathrm{ox}}}\right) & \text{for:} \quad V_{\mathrm{ox}} < \chi_{\mathrm{B}} \\ \exp\left(-\,B\big/V_{\mathrm{ox}}\right) & \text{for:} \quad V_{\mathrm{ox}} \geq \chi_{\mathrm{B}} \end{cases} \tag{2.69}$$

Source/Drain Gate Overlap Current: The gate tunnelling currents in both gate/source and gate/drain overlap are given by:

$$P_{\mathrm{ov}}\{V_{\mathrm{ov}}\} = P_{\mathrm{tun}}\left\{V_{\mathrm{ov}}, \chi_{\mathrm{B_{inv}}}, B_{\mathrm{inv}}\right\} \tag{2.70}$$

$$I_{\mathrm{Gov}}\{V_{\mathrm{GX}}, V_{\mathrm{ov}}\} = I_{\mathrm{GOV}} \cdot V_{\mathrm{GX}} \cdot V_{\mathrm{ov}} \cdot \left[P_{\mathrm{ov}}\{V_{\mathrm{ov}}\} - P_{\mathrm{ov}}\{-V_{\mathrm{ov}}\}\right] \tag{2.71}$$

$$I_{\mathrm{Gov}_0} = I_{\mathrm{Gov}}\left\{V_{\mathrm{GS}}\ ,\ V_{\mathrm{ov}_0}\right\} \tag{2.72}$$

$$I_{\mathrm{Gov}_L} = I_{\mathrm{Gov}}\left\{V_{\mathrm{GS}} - V_{\mathrm{DS}}\ ,\ V_{\mathrm{ov}_L}\right\} \tag{2.73}$$

Intrinsic Gate Current: The gate tunnelling current in accumulation:

$$P_{\mathrm{acc}} = P_{\mathrm{tun}}\left\{-\bar{V}_{\mathrm{ox}}, \chi_{\mathrm{B_{acc}}}, B_{\mathrm{acc}}\right\} \tag{2.74}$$

$$I_{\mathrm{GB}} = \begin{cases} -I_{\mathrm{GACC}} \cdot (V_{\mathrm{GS}} + V_{\mathrm{SB}}) \cdot \bar{V}_{\mathrm{ox}} \cdot P_{\mathrm{acc}} & \text{for:} \quad \bar{V}_{\mathrm{ox}} \leq 0 \\ 0 & \text{for:} \quad \bar{V}_{\mathrm{ox}} > 0 \end{cases} \tag{2.75}$$

The tunnelling current in inversion (i.e., $V^{*}_{\mathrm{GB}} > 0$), including quantum-mechanical barrier lowering $\Delta\chi_{\mathrm{B}}$:

$$\Delta\chi_{\mathrm{B}} = QM_{\psi} \cdot \left(\bar{V}_{\mathrm{inv}}\big/3 + \bar{V}_{\mathrm{ox}} - \bar{V}_{\mathrm{inv}}\right)^{2/3} \tag{2.76}$$

$$\chi_{\mathrm{B_{eff}}} = \chi_{\mathrm{B_{inv}}} - \Delta\chi_{\mathrm{B}} \tag{2.77}$$

$$B_{\mathrm{eff}} = B_{\mathrm{inv}} \cdot \left(\chi_{\mathrm{B_{eff}}}\big/\chi_{\mathrm{B_{inv}}}\right)^{3/2} \tag{2.78}$$

$$P_{\mathrm{inv}} = P_{\mathrm{tun}}\left\{\bar{V}_{\mathrm{ox}}, \chi_{\mathrm{B_{eff}}}, B_{\mathrm{eff}}\right\} \tag{2.79}$$

©Koninklijke Philips Electronics N.V. 2004

$$r_{\mathrm{B}} = \frac{3}{8} \cdot \frac{B_{\mathrm{eff}}}{{\chi_{\mathrm{B_{eff}}}}^2} \cdot \frac{\bar{\xi}_{\mathrm{ox}}}{\phi_{\mathrm{T}}} \tag{2.80}$$

$$r^{*} = \frac{\bar{\xi}}{\phi_{\mathrm{T}} \cdot \bar{V}^{*}_{\mathrm{inv}}} \tag{2.81}$$

$$r_{\mathrm{ox}} = \frac{\bar{\xi}_{\mathrm{ox}}}{\phi_{\mathrm{T}} \cdot \bar{V}_{\mathrm{ox}}} \tag{2.82}$$

$$P_{\mathrm{GC}} = 1 + \frac{{r_{\mathrm{B}}}^2 + 4 \cdot r_{\mathrm{B}} \cdot r^{*} + 2 \cdot r_{\mathrm{B}} \cdot r_{\mathrm{ox}} + 2 \cdot r^{*2} + 4 \cdot r_{\mathrm{ox}} \cdot r^{*}}{24} \cdot \Delta\psi^2 \tag{2.83}$$

$$\bar{I}_{\mathrm{GC}} = I_{\mathrm{GINV}} \cdot G_{\Delta L} \cdot \left(V_{\mathrm{GS}} - \frac{1}{2} V_{\mathrm{DS_x}} \right) \cdot P_{\mathrm{inv}} \tag{2.84}$$

The total intrinsic gate current I_{GC}:

$$I_{\mathrm{GC}} = \bar{I}_{\mathrm{GC}} \cdot \bar{V}_{\mathrm{inv}} \cdot P_{\mathrm{GC}} \tag{2.85}$$

$$P_{\mathrm{GS}} = [r_{\mathrm{B}} + r_{\mathrm{ox}}] \cdot \frac{\Delta\psi}{12} \tag{2.86}$$

$$I_{\mathrm{GS}} = \frac{1}{2} \cdot I_{\mathrm{GC}} + \left(P_{\mathrm{GS}} \cdot \bar{V}_{\mathrm{inv}} + \frac{V_{\mathrm{inv_0}} - V_{\mathrm{inv_L}}}{12} \right) \cdot \bar{I}_{\mathrm{GC}} + I_{\mathrm{Gov_0}} \tag{2.87}$$

$$I_{\mathrm{GD}} = I_{\mathrm{GC}} - I_{\mathrm{GS}} + I_{\mathrm{Gov_0}} + I_{\mathrm{Gov_L}} \tag{2.88}$$

Gate-Induced Drain/Source Leakage Current:

$$V_{\mathrm{tov}} \{V_{\mathrm{ov}}, V\} = \sqrt{{V_{\mathrm{ov}}}^2 + {C_{\mathrm{GIDL}}}^2 \cdot V^2} \tag{2.89}$$

$$I_{\mathrm{gixl}} \{V_{\mathrm{ov}}, V\} = A_{\mathrm{GIDL}} \cdot V \cdot V_{\mathrm{tov}} \{V_{\mathrm{ov}}, V\}^2 \cdot \exp\left(-\frac{B_{\mathrm{GIDL_T}}}{V_{\mathrm{tov}} \{V_{\mathrm{ov}}, V\}} \right) \tag{2.90}$$

$$I_{\mathrm{gisl}} = I_{\mathrm{gixl}} \left\{ V_{\mathrm{ov_0}}, V_{\mathrm{SB}} \right\} \tag{2.91}$$

$$I_{\mathrm{gidl}} = I_{\mathrm{gixl}} \left\{ V_{\mathrm{ov_L}}, V_{\mathrm{DS}} + V_{\mathrm{SB}} \right\} \tag{2.92}$$

2.3.3 Basic Charge Equations

Bias-Dependent Overlap Capacitance:

$$Q_{\mathrm{ov_0}} = C_{\mathrm{GSO}} \cdot V_{\mathrm{ov_0}} \tag{2.93}$$

$$Q_{\mathrm{ov_L}} = C_{\mathrm{GDO}} \cdot V_{\mathrm{ov_L}} \tag{2.94}$$

 ©Koninklijke Philips Electronics N.V. 2004

Intrinsic Charges:

$$C_{OX_{eff}} = \frac{C_{OX}}{1 + QM_{t_{ox}} \cdot \left[\frac{V_{eff}}{\eta_{mob_T}}\right]^{-1/3}} \tag{2.95}$$

$$\Delta V_{inv} = \left(V_{inv_0} - V_{inv_L}\right) \cdot \left(1 - \frac{G_R}{G_{tot}}\right) \tag{2.96}$$

$$F_j = \frac{1}{2} \cdot \frac{\Delta V_{inv}}{\bar{V}^*_{inv}} \tag{2.97}$$

$$Q_S = -\frac{C_{OX_{eff}} \cdot G_{\Delta L}}{2} \cdot \left[\bar{V}_{inv} + \frac{\Delta V_{inv}}{6} \cdot \left(F_j - \frac{{F_j}^2}{5} + 1\right)\right] \tag{2.98}$$

$$Q_D = -\frac{C_{OX_{eff}} \cdot G_{\Delta L}}{2} \cdot \left[\bar{V}_{inv} + \frac{\Delta V_{inv}}{6} \cdot \left(F_j + \frac{{F_j}^2}{5} - 1\right)\right] \tag{2.99}$$

$$Q_G = C_{OX_{eff}} \cdot \left[\bar{V}_{ox} + \frac{\Delta V_{inv}}{6} \cdot F_j \cdot \frac{\bar{\xi}_{ox}}{\bar{\xi}}\right] \tag{2.100}$$

$$Q_B = -\left[Q_S + Q_D + Q_G\right] \tag{2.101}$$

2.3.4 Basic Noise Equations

In these equations f represents the operation frequency of the transistor.

$$G_{eff} = 1 - \frac{G_R}{G_{tot}} \tag{2.102}$$

$$ {x_{sat}}^2 = \begin{cases} {\theta_{sat_T}}^2 \cdot \Delta\psi^2 \cdot {G_{eff}}^2 & \text{for NMOS} \\ \frac{{\theta_{sat_T}}^2 \cdot \Delta\psi^2 \cdot {G_{eff}}^2}{\sqrt{1+{\theta_{sat_T}}^2 \cdot \Delta\psi^2 \cdot {G_{eff}}^2}} & \text{for PMOS} \end{cases} \tag{2.103}$$

$$G_{vsat_R} = \frac{G_{mob} + \sqrt{{G_{mob}}^2 + 2 \cdot {x_{sat}}^2}}{2} \tag{2.104}$$

$$t_1 = \frac{\bar{V}_{inv}}{\bar{V}^*_{inv}} \tag{2.105}$$

$$t_2 = \frac{{F_j}^2}{36} \tag{2.106}$$

$$t_{sat} = \frac{{x_{sat}}^2}{{G_{vsat_R}}^2} \tag{2.107}$$

©Koninklijke Philips Electronics N.V. 2004

$$g_{\text{ideal}} = \frac{\beta_{\text{T}} \cdot \bar{V}^*_{\text{inv}}}{G_{\text{vsat}_\text{R}} \cdot G_{\Delta L}} \tag{2.108}$$

$$B_{\text{G}} = 2 \cdot \pi \cdot f \cdot C_{\text{OX}_{\text{eff}}} \cdot \frac{\bar{\xi}_{\text{ox}}}{\phi_{\text{T}}} \cdot \frac{G_{\text{vsat}_\text{R}} \cdot G_{\Delta L}}{G_{\text{mob}}} \tag{2.109}$$

$$S_{\text{th}} = N_{\text{T}_\text{T}} \cdot {G_{\text{eff}}}^2 \cdot g_{\text{ideal}} \cdot \left[t_1 + 12 \cdot t_2 \cdot \left(1 - 2 \cdot t_{\text{sat}} - 2 \cdot {t_{\text{sat}}}^2\right)\right] \tag{2.110}$$

$$\begin{aligned} S_{\text{ig}} = N_{\text{T}_\text{T}} \cdot \frac{{B_{\text{G}}}^2}{g_{\text{ideal}}} \cdot \Bigg[& \frac{t_1}{12} - t_1 \cdot t_2 - \frac{t_2}{5} + 12 \cdot {t_2}^2 \\ & + t_{\text{sat}} \cdot \left(\frac{t_1}{12} + 3 \cdot t_1 \cdot t_2 - \frac{9 \cdot t_2}{5} - 36 \cdot {t_2}^2\right) \\ & + {t_{\text{sat}}}^2 \cdot \left(\frac{t_1}{12} + 4 \cdot t_1 \cdot t_2 - \frac{17 \cdot t_2}{5} - 24 \cdot {t_2}^2\right)\Bigg] \end{aligned} \tag{2.111}$$

$$\begin{aligned} S_{\text{igth}} = j \cdot N_{\text{T}_\text{T}} \cdot B_{\text{G}} \cdot G_{\text{eff}} \cdot \sqrt{t_2} \cdot \Bigg[& 1 - 12 \cdot t_2 + t_{\text{sat}} \cdot \left(\frac{1}{2} - t_1 + 30 \cdot t_2\right) \\ & + {t_{\text{sat}}}^2 \cdot \left(\frac{3}{8} - \frac{3 \cdot t_1}{2} + \frac{51 \cdot t_2}{2}\right)\Bigg] \end{aligned} \tag{2.112}$$

$$\text{for GATENOISE} = 1: \begin{cases} g_{\text{ideal}} & = \frac{\beta_{\text{T}} \cdot \bar{V}_{\text{inv}}}{G_{\text{mob}} \cdot G_{\Delta L}} \\ S_{\text{th}} & = N_{\text{T}_\text{T}} \cdot {G_{\text{eff}}}^2 \cdot g_{\text{ideal}} \Big/ \sqrt{1 + t_{\text{sat}} + {t_{\text{sat}}}^2} \\ S_{\text{ig}} & = 0 \\ S_{\text{igth}} & = 0 \end{cases} \tag{2.113}$$

$$N_0 = \frac{\epsilon_{ox}}{q \cdot t_{ox}} \cdot \left(\bar{V}_{\text{inv}} + \frac{\Delta V_{\text{inv}}}{2}\right) \tag{2.114}$$

$$N_L = \frac{\epsilon_{ox}}{q \cdot t_{ox}} \cdot \left(\bar{V}_{\text{inv}} - \frac{\Delta V_{\text{inv}}}{2}\right) \tag{2.115}$$

$$N^* = \frac{\epsilon_{ox}}{q \cdot t_{ox}} \cdot \bar{\xi} \tag{2.116}$$

$$\begin{aligned} S_{\text{fl}} = \frac{q \cdot {\phi_{\text{T}}}^2 \cdot t_{ox} \cdot \beta_{\text{T}} \cdot I_{\text{DS}}}{f \cdot \epsilon_{ox} \cdot G_{\text{vsat}} \cdot N^*} \cdot \Bigg[& \left(N_{\text{FA}} - N^* \cdot N_{\text{FB}} + N^{*2} \cdot N_{\text{FC}}\right) \cdot \ln\left(\frac{N_0 + N^*}{N_L + N^*}\right) \\ & + \left(N_{\text{FB}} - N^* \cdot N_{\text{FC}}\right) \cdot (N_0 - N_L) + \frac{N_{\text{FC}}}{2} \cdot \left({N_0}^2 - {N_L}^2\right)\Bigg] \\ & + \frac{\phi_{\text{T}} \cdot {I_{\text{DS}}}^2}{f} \cdot (1 - G_{\Delta L}) \cdot \left[\frac{N_{\text{FA}} + N_{\text{FB}} \cdot N_L + N_{\text{FC}} \cdot {N_L}^2}{(N_L + N^*)^2}\right] \end{aligned} \tag{2.117}$$

 ©Koninklijke Philips Electronics N.V. 2004

3 Nomenclature

3.1 General Remarks

The symbolic representation and the recommended programming names of the quantities listed in the following sections, have been chosen in such a way to express their purpose and relations to other quantities and to preclude ambiguity and inconsistency.

All parameters which refer to the reference transistor and/or the reference temperature have a symbol with the subscript R and a programming name ending with R. All characters 0 (zero) in subscripts of parameters are represented by the capital letter O in the programming name, because often they are distinguishable with great difficulty! Scaling parameters are indicated by S with a subscript where the variables on which the parameter depends, precede a semicolon whereas the parameter succeeds it, e.g. $S_{\mathrm{T};\theta_{\mathrm{Sr}}}$.

Note: Since the list of parameters for an individual transistor (i.e. the so-called miniset parameters) and the list of physical constants can be found in Sections 2.1.1 and 2.1.2, respectively, they will not be repeated here.

©Koninklijke Philips Electronics N.V. 2004

3.2 List of Input Variables and Quantities

3.2.1 List of Numerical Constants

No.	Constant	Program Name	Value
1	A	LN_MINDOUBLE	-800

3.2.2 List of Circuit Simulator Variables

No.	Symbol	Program Name	Units	Description
1	L	L	m	Drawn channel length in the lay-out of the actual transistor
2	W	W	m	Drawn channel width in the lay-out of the actual transistor
3	T_A	TA	°C	Ambient circuit temperature
4	f	F	s^{-1}	Operation frequency

3.3 List of Electrical Quantities and Variables

For the electrical quantities and variables, the distinction is made between external, referring to the nodes of the physical device, and internal, referring to their use in the model equations.

3.3.1 External Electrical Quantities and Variables

The definitions of the external electrical variables are illustrated in fig.3.1.

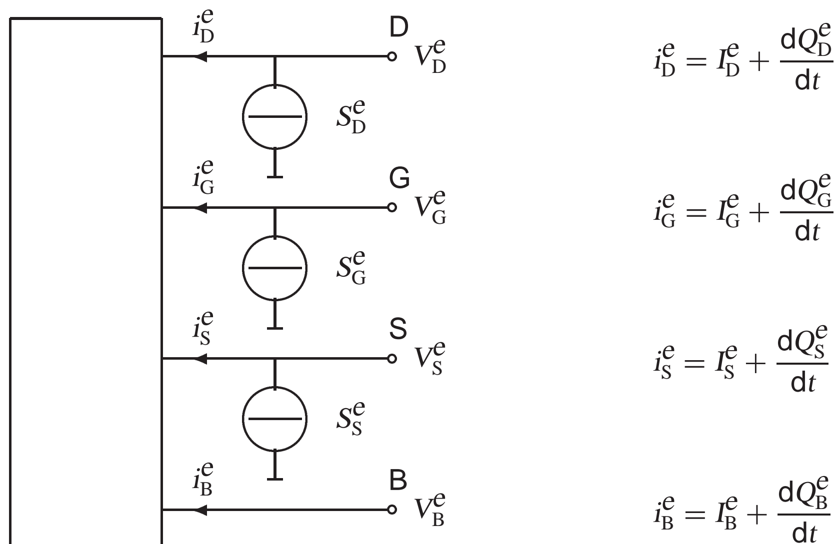

$$i_D^e = I_D^e + \frac{dQ_D^e}{dt}$$

$$i_G^e = I_G^e + \frac{dQ_G^e}{dt}$$

$$i_S^e = I_S^e + \frac{dQ_S^e}{dt}$$

$$i_B^e = I_B^e + \frac{dQ_B^e}{dt}$$

Figure 3.1: Definition of the external electrical quantities and variables

 ©Koninklijke Philips Electronics N.V. 2004

No.	Variable	Program Name	Units	Description
1	$V_{\mathrm{D}}^{\mathrm{e}}$	VDE	V	Potential applied to the drain node
2	$V_{\mathrm{G}}^{\mathrm{e}}$	VGE	V	Potential applied to the gate node
3	$V_{\mathrm{S}}^{\mathrm{e}}$	VSE	V	Potential applied to the source node
4	$V_{\mathrm{B}}^{\mathrm{e}}$	VBE	V	Potential applied to the bulk node
5	$I_{\mathrm{D}}^{\mathrm{e}}$	IDE	A	DC current into the drain
6	$I_{\mathrm{G}}^{\mathrm{e}}$	IGE	A	DC current into the gate
7	$I_{\mathrm{S}}^{\mathrm{e}}$	ISE	A	DC current into the source
8	$I_{\mathrm{B}}^{\mathrm{e}}$	IBE	A	DC current into the bulk
9	$Q_{\mathrm{D}}^{\mathrm{e}}$	QDE	C	Charge in the device attributed to the drain node
10	$Q_{\mathrm{G}}^{\mathrm{e}}$	QGE	C	Charge in the device attributed to the gate node
11	$Q_{\mathrm{S}}^{\mathrm{e}}$	QSE	C	Charge in the device attributed to the source node
12	$Q_{\mathrm{B}}^{\mathrm{e}}$	QBE	C	Charge in the device attributed to the bulk node
13	$S_{\mathrm{D}}^{\mathrm{e}}$	SDE	$\mathrm{A}^2\mathrm{s}$	Spectral density of the noise current into the drain
14	$S_{\mathrm{G}}^{\mathrm{e}}$	SGE	$\mathrm{A}^2\mathrm{s}$	Spectral density of the noise current into the gate
15	$S_{\mathrm{S}}^{\mathrm{e}}$	SSE	$\mathrm{A}^2\mathrm{s}$	Spectral density of the noise current into the source
16	$S_{\mathrm{DG}}^{\mathrm{e}}$	SDGE	$\mathrm{A}^2\mathrm{s}$	Cross spectral density between the drain and the gate noise currents
17	$S_{\mathrm{GS}}^{\mathrm{e}}$	SGSE	$\mathrm{A}^2\mathrm{s}$	Cross spectral density between the gate and the source noise currents
18	$S_{\mathrm{SD}}^{\mathrm{e}}$	SSDE	$\mathrm{A}^2\mathrm{s}$	Cross spectral density between the source and the drain noise currents

©Koninklijke Philips Electronics N.V. 2004

3.3.2 Internal Electrical Quantities and Variables

No.	Variable	Program Name	Units	Description
1	V_{DS}	VDS	V	Drain–to–source voltage applied to the equivalent n–MOST
2	V_{GS}	VGS	V	Gate–to–source voltage applied to the equivalent n–MOST
3	V_{SB}	VSB	V	Source–to–bulk voltage applied to the equivalent n–MOST
4	I_{DS}	IDS	A	DC current through the channel flowing from drain to source
5	I_{AVL}	IAVL	A	DC current flowing from drain to bulk due to the weak–avalanche effect
6	I_{GS}	IGS	A	DC current flowing from gate to source due to the direct tunnelling effect
7	I_{GD}	IGD	A	DC current flowing from gate to drain due to the direct tunnelling effect
8	I_{GB}	IGB	A	DC current flowing from gate to bulk due to the direct tunnelling effect
9	I_{GISL}	IGISL	A	DC current flowing from source to bulk due to the gate–induced source leakage effect
10	I_{GIDL}	IGIDL	A	DC current flowing from drain to bulk due to the gate–induced drain leakage effect
11	Q_{D}	QD	C	Intrinsic charge in the equivalent n–MOST attributed to the drain node
12	Q_{G}	QG	C	Intrinsic charge in the equivalent n–MOST attributed to the gate node
13	Q_{S}	QS	C	Intrinsic charge in the equivalent n–MOST attributed to the source node
14	Q_{B}	QB	C	Intrinsic charge in the equivalent n–MOST attributed to the bulk node
15	Q_{ov_0}	QOVO	C	Extrinsic charge in the equivalent n–MOST attributed to the gate-source overlap
16	Q_{ov_L}	QOVL	C	Extrinsic charge in the equivalent n–MOST attributed to the gate-drain overlap
17	S_{th}	STH	A^2s	Spectral density of the thermal–noise current of the channel
18	S_{fl}	SFL	A^2s	Spectral density of the flicker–noise current of the channel
17	S_{ig}	SIG	A^2s	Spectral density of the noise current induced in the gate
18	S_{igth}	SIGTH	A^2s	Cross spectral density of the noise current induced in the gate and the thermal–noise current of the channel

 ©Koninklijke Philips Electronics N.V. 2004

3.4 List of Reference & Scaling Parameters

In MOS Model 11, Level 1102, parameter binning has been facilitated by adding a second, separate set of geometry scaling rules. Consequently, besides the *physical* geometrical scaling rules there is also a set of *binning* geometrical scaling rules. The physical geometry scaling rules of Level 1102 (see Sections 3.4.1 and 5.2.1) have been developed to give a good description over the whole geometry range of CMOS technologies. For processes under development, however, it is sometimes useful to have more flexible scaling relations. In this case one could opt for a binning strategy, where the accuracy with geometry is mostly determined by the number of bins used. The physical scaling rules of Level 1102 are not straightforwardly applicable to binning strategies, since they may result in discontinuities in parameter values at the bin boundaries. Consequently, special binning geometrical scaling relations have been developed (see Sections 3.4.2 and 5.2.2), which guarantee continuity in the model parameters at the bin boundaries.
It should be noted that using the source code of the Modelkit on the Philips' website (which can be found at http://www.semconductors.philips.com/Philips_Models)

1. the physical geometry scaling rules can be selected by using Level 11020, while
2. the binning geometry scaling rules can be selected by using Level 11021.

3.4.1 List of Reference & Scaling Parameters for Physical Geometrical Scaling

No.	Symbol	Program Name	Units	Description
0		LEVEL	-	Must be 11020
1	ΔL_{PS}	LVAR	m	Difference between the actual and the programmed poly–silicon gate length
2	$\Delta L_{\mathrm{overlap}}$	LAP	m	Effective channel length reduction per side due to the lateral diffusion of the source/drain dopant ions
3	ΔW_{OD}	WVAR	m	Difference between the actual and the programmed field–oxide opening
4	$\Delta W_{\mathrm{narrow}}$	WOT	m	Effective reduction of the channel width per side due to the lateral diffusion of the channel–stop dopant ions
5	T_{R}	TR	$^{\mathrm{o}}\mathrm{C}$	Reference temperature
6	V_{FB}	VFB	V	Flat-band voltage at the reference temperature
7	$S_{\mathrm{T;V_{FB}}}$	STVFB	VK^{-1}	Coefficient of the temperature dependence of V_{FB}
8	$k_{0\mathrm{R}}$	KOR	$\mathrm{V}^{1/2}$	Body-effect factor for an infinite square transistor
9	$S_{\mathrm{L;k_0}}$	SLKO	-	Coefficient of the length dependence of k_0
10	$S_{\mathrm{L2;k_0}}$	SL2KO	-	Second coefficient of the length dependence of k_0
11	$S_{\mathrm{W;k_0}}$	SWKO	-	Coefficient of the width dependence of k_0
12	$1/k_{\mathrm{P}}$	KPINV	$\mathrm{V}^{-1/2}$	Inverse of body-effect factor of the poly-silicon gate
13	ϕ_{BR}	PHIBR	V	Surface potential at the onset of strong inversion at the reference temperature
14	$S_{\mathrm{T};\phi_{\mathrm{B}}}$	STPHIB	VK^{-1}	Coefficient of the temperature dependence of ϕ_{B}
15	$S_{\mathrm{L};\phi_{\mathrm{B}}}$	SLPHIB	-	Coefficient of the length dependence of ϕ_{B}
16	$S_{\mathrm{L2};\phi_{\mathrm{B}}}$	SL2PHIB	-	Second coefficient of the length dependence of ϕ_{B}
17	$S_{\mathrm{W};\phi_{\mathrm{B}}}$	SWPHIB	-	Coefficient of the width dependence of ϕ_{B}
18	β_{sq}	BETSQ	AV^{-2}	Gain factor for an infinite square transistor at the reference temperature
19	$\eta_{\beta\mathrm{R}}$	ETABETR	-	Exponent of the temperature dependence of the gain factor of an infinite square transistor
20	$S_{\mathrm{L};\eta_\beta}$	SLETABET	-	Coefficient of the length dependence of $\eta_{\beta\mathrm{R}}$
21	$f_{\beta,1}$	FBET1	-	Relative mobility decrease due to first lateral profile
22	$L_{\mathrm{P},1}$	LP1	m	Characteristic length of first lateral profile
23	$f_{\beta,2}$	FBET2	-	Relative mobility decrease due to second lateral profile
24	$L_{\mathrm{P},2}$	LP2	m	Characteristic length of second lateral profile
25	θ_{srR}	THESRR	V^{-1}	Coefficient of the mobility reduction due to surface roughness scattering for an infinite square transistor at the reference temperature
26	η_{sr}	ETASR	-	Exponent of the temperature dependence of θ_{sr}

 ©Koninklijke Philips Electronics N.V. 2004

27	$S_{W;\theta_{sr}}$	SWTHESR	-	Coefficient of the width dependence of θ_{sr}
28	θ_{phR}	THEPHR	V^{-1}	Coefficient of the mobility reduction due to phonon scattering for an infinite square transistor at the reference temperature
29	η_{ph}	ETAPH	-	Exponent of the temperature dependence of θ_{ph}
30	$S_{W;\theta_{ph}}$	SWTHEPH	-	Coefficient of the width dependence of θ_{ph}
31	η_{mobR}	ETAMOBR	-	Effective field parameter for dependence on depletion/inversion charge for an infinite square transistor
32	$S_{T;\eta_{mob}}$	STETAMOB	K^{-1}	Coefficient of the temperature dependence of η_{mob}
33	$S_{W;\eta_{mob}}$	SWETAMOB	-	Coefficient of the width dependence of η_{mob}
34	ν	NU	-	Exponent of the field dependence of the mobility model at the reference temperature
35	ν_{EXP}	NUEXP	-	Exponent of the temperature dependence of parameter ν
36	θ_{RR}	THERR	V^{-1}	Coefficient of the series resistance per unit length for an infinitely wide transistor
37	η_{R}	ETAR	-	Exponent of the temperature dependence of θ_{R}
38	$S_{W;\theta_{R}}$	SWTHER	-	Coefficient of the width dependence of θ_{R}
39	θ_{R1}	THER1	V	Numerator of the gate voltage dependent part of series resistance
40	θ_{R2}	THER2	V	Denominator of the gate voltage dependent part of series resistance
41	θ_{satR}	THESATR	V^{-1}	Velocity saturation parameter due to optical/acoustic phonon scattering for an infinite square transistor at the reference temperature
42	η_{sat}	ETASAT	-	Exponent of the temperature dependence of θ_{sat}
43	$S_{L;\theta_{sat}}$	SLTHESAT	-	Coefficient of the length dependence of θ_{sat}
44	θ_{satEXP}	THESATEXP	-	Exponent of the length dependence of θ_{sat}
45	$S_{W;\theta_{sat}}$	SWTHESAT	-	Coefficient of the width dependence of θ_{sat}
46	θ_{ThR}	THETHR	V^{-3}	Coefficient of self-heating per unit length for an infinitely wide transistor at the reference temperature
47	θ_{ThEXP}	THETHEXP	-	Exponent of the length dependence of θ_{Th}
48	$S_{W;\theta_{Th}}$	SWTHETH	-	Coefficient of the width dependence of θ_{Th}
49	σ_{dibl0}	SDIBLO	$V^{-1/2}$	Drain-induced barrier-lowering parameter per unit length
50	$\sigma_{diblEXP}$	SDIBLEXP	-	Exponent of the length dependence of σ_{dibl}
51	m_{00}	MOO	-	Parameter for short-channel subthreshold slope
52	m_{0R}	MOR	-	Parameter for short-channel subthreshold slope per unit length
53	m_{0EXP}	MOEXP	-	Exponent of the length dependence of m_0
54	σ_{sfR}	SSFR	$V^{-1/2}$	Static feedback parameter for an infinite square transistor
55	$S_{L;\sigma_{sf}}$	SLSSF	-	Coefficient of the length dependence of σ_{sf}
56	$S_{W;\sigma_{sf}}$	SWSSF	-	Coefficient of the width dependence of σ_{sf}

©Koninklijke Philips Electronics N.V. 2004

57	α_{R}	ALPR	-	Factor of the channel length modulation for an infinite square transistor
58	$S_{\mathrm{L};\alpha}$	SLALP	-	Coefficient of the length dependence of α
59	α_{EXP}	ALPEXP	-	Exponent of the length dependence of α
60	$S_{\mathrm{W};\alpha}$	SWALP	-	Coefficient of the width dependence of α
61	V_{P}	VP	V	Characteristic voltage of the channel length modulation
62	L_{min}	LMIN	m	Minimum effective channel length in technology, used for calculation of smoothing factor m
63	$a_{1\mathrm{R}}$	A1R	-	Factor of the weak–avalanche current for an infinite square transistor at the reference temperature
64	$S_{\mathrm{T};a_1}$	STA1	K^{-1}	Coefficient of the temperature dependence of a_1
65	$S_{\mathrm{L};a_1}$	SLA1	-	Coefficient of the length dependence of a_1
66	$S_{\mathrm{W};a_1}$	SWA1	-	Coefficient of the width dependence of a_1
67	$a_{2\mathrm{R}}$	A2R	V	Exponent of the weak–avalanche current for an infinite square transistor
68	$S_{\mathrm{L};a_2}$	SLA2	-	Coefficient of the length dependence of a_2
69	$S_{\mathrm{W};a_2}$	SWA2	-	Coefficient of the width dependence of a_2
70	$a_{3\mathrm{R}}$	A3R	-	Factor of the drain–source voltage above which weak–avalanche occurs, an infinite square transistor
71	$S_{\mathrm{L};a_3}$	SLA3	-	Coefficient of the length dependence of a_3
72	$S_{\mathrm{W};a_3}$	SWA3	-	Coefficient of the width dependence of a_3
73	I_{GINVR}	IGINVR	AV^{-2}	Gain factor for intrinsic gate tunnelling current in inversion for a channel area of 1 $\mu\mathrm{m}^2$
74	B_{inv}	BINV	V	Probability factor for intrinsic gate tunnelling current in inversion
75	I_{GACCR}	IGACCR	AV^{-2}	Gain factor for intrinsic gate tunnelling current in accumulation for a channel area of 1 $\mu\mathrm{m}^2$
76	B_{acc}	BACC	V	Probability factor for intrinsic gate tunnelling current in accumulation
77	V_{FBov}	VFBOV	V	Flat-band voltage for the source/drain overlap extensions
78	k_{ov}	KOV	$\mathrm{V}^{1/2}$	Body-effect factor for the source/drain overlap extensions
79	I_{GOVR}	IGOVR	AV^{-2}	Gain factor for source/drain overlap gate tunnelling current for a channel width of 1 μm
80	A_{GIDLR}	AGIDLR	AV^{-3}	Gain factor for gate-induced drain leakage current for a channel width of 1 μm
81	B_{GIDL}	BGIDL	V	Probability factor for gate-induced drain leakage current at the reference temperature
82	$S_{\mathrm{T};B_{\mathrm{GIDL}}}$	STBGIDL	VK^{-1}	Coefficient of the temperature dependence of B_{GIDL}
83	C_{GIDL}	CGIDL	-	Factor for the lateral field dependence of the gate-induced drain leakage current
84	t_{ox}	TOX	m	Thickness of the gate oxide layer

 ©Koninklijke Philips Electronics N.V. 2004

85	C_{ol}	COL	F	Gate overlap capacitance for a channel width of 1 μm
86	–	GATENOISE		Flag for in/exclusion of induced gate thermal noise
87	N_T	NT	J	Coefficient of the thermal noise at the reference temperature
88	N_{FAR}	NFAR	$V^{-1}m^{-4}$	First coefficient of flicker noise for a channel area of 1 μm^2
89	N_{FBR}	NFBR	$V^{-1}m^{-2}$	Second coefficient of flicker noise for a channel area of 1 μm^2
90	N_{FCR}	NFCR	V^{-1}	Third coefficient of flicker noise for a channel area of 1 μm^2
91	L	L	m	Drawn channel length in the lay-out of the actual transistor
92	W	W	m	Drawn channel width in the lay-out of the actual transistor
93	ΔT_A	DTA	K	Temperature offset of the device with respect to T_A
94	N_{MULT}	MULT	-	Number of devices in parallel

Remark: The parameters L, W and DTA are used to calculate the electrical parameters of the actual transistor as specified in the section on parameter preprocessing.

The additional parameters for the model including self-heating (see Section4.2) are listed in the table below.

No.	Symbol	Program Name	Units	Description
95	R_{Th}	RTH	K/W	Thermal resistance
96	C_{Th}	CTH	J/K	Thermal capacitance
97	A_{Th}	ATH	-	Temperature coefficient of the thermal resistance

©Koninklijke Philips Electronics N.V. 2004

3.4.2 List of Reference & Scaling Parameters for Binning Geometrical Scaling

Note that for each bin (W_{min}, W_{max}, L_{min}, L_{max}) there is a separate parameter set, which is valid for (W, L) values with $W_{min} \leq W \leq W_{max}$ and $L_{min} \leq L \leq L_{max}$.

No.	Symbol	Program Name	Units	Description
0		LEVEL	-	Must be 11021
1	ΔL_{PS}	LVAR	m	Difference between the actual and the programmed poly–silicon gate length
2	$\Delta L_{overlap}$	LAP	m	Effective channel length reduction per side due to the lateral diffusion of the source/drain dopant ions
3	ΔW_{OD}	WVAR	m	Difference between the actual and the programmed field–oxide opening
4	ΔW_{narrow}	WOT	m	Effective reduction of the channel width per side due to the lateral diffusion of the channel–stop dopant ions
5	T_R	TR	^oC	Reference temperature
6	V_{FB}	VFB	V	Flat-band voltage for the all transistors in the bin at the reference temperature
7	$P_{0;k_0}$	POKO	$V^{1/2}$	Coefficient for the geometry independent part of k_0
8	$P_{L;k_0}$	PLKO	$V^{1/2}$	Coefficient for the length dependence of k_0
9	$P_{W;k_0}$	PWKO	$V^{1/2}$	Coefficient for the width dependence of k_0
10	$P_{LW;k_0}$	PLWKO	$V^{1/2}$	Coefficient for the length times width dependence of k_0
11	$1/k_P$	KPINV	$V^{-1/2}$	Inverse of body-effect factor of the poly-silicon gate
12	$P_{0;\phi_B}$	POPHIB	V	Coefficient for the geometry independent part of ϕ_B
13	$P_{L;\phi_B}$	PLPHIB	V	Coefficient for the length dependence of ϕ_B
14	$P_{W;\phi_B}$	PWPHIB	V	Coefficient for the width dependence of ϕ_B
15	$P_{LW;\phi_B}$	PLWPHIB	V	Coefficient for the length times width dependence of ϕ_B
16	$P_{0;\beta}$	POBET	AV^{-2}	Coefficient for the geometry independent part of β
17	$P_{L;\beta}$	PLBET	AV^{-2}	Coefficient for the length dependence of β
18	$P_{W;\beta}$	PWBET	AV^{-2}	Coefficient for the width dependence of β
19	$P_{LW;\beta}$	PLWBET	AV^{-2}	Coefficient for the width over length dependence of β
20	$P_{0;\theta_{sr}}$	POTHESR	V^{-1}	Coefficient for the geometry independent part of θ_{sr}
21	$P_{L;\theta_{sr}}$	PLTHESR	V^{-1}	Coefficient for the length dependence of θ_{sr}
22	$P_{W;\theta_{sr}}$	PWTHESR	V^{-1}	Coefficient for the width dependence of θ_{sr}
23	$P_{LW;\theta_{sr}}$	PLWTHESR	V^{-1}	Coefficient for the length times width dependence of θ_{sr}
24	$P_{0;\theta_{ph}}$	POTHEPH	V^{-1}	Coefficient for the geometry independent part of θ_{ph}
25	$P_{L;\theta_{ph}}$	PLTHEPH	V^{-1}	Coefficient for the length dependence of θ_{ph}
26	$P_{W;\theta_{ph}}$	PWTHEPH	V^{-1}	Coefficient for the width dependence of θ_{ph}
27	$P_{LW;\theta_{ph}}$	PLWTHEPH	V^{-1}	Coefficient for the length times width dependence of θ_{ph}

©Koninklijke Philips Electronics N.V. 2004

28	$P_{0;\eta_{mob}}$	POETAMOB	-	Coefficient for the geometry independent part of η_{mob}
29	$P_{L;\eta_{mob}}$	PLETAMOB	-	Coefficient for the length dependence of η_{mob}
30	$P_{W;\eta_{mob}}$	PWETAMOB	-	Coefficient for the width dependence of η_{mob}
31	$P_{LW;\eta_{mob}}$	PLWETAMOB	-	Coefficient for the length times width dependence of η_{mob}
32	$P_{0;\theta_R}$	POTHER	V^{-1}	Coefficient for the geometry independent part of θ_R
33	$P_{L;\theta_R}$	PLTHER	V^{-1}	Coefficient for the length dependence of θ_R
34	$P_{W;\theta_R}$	PWTHER	V^{-1}	Coefficient for the width dependence of θ_R
35	$P_{LW;\theta_R}$	PLWTHER	V^{-1}	Coefficient for the length times width dependence of θ_R
36	θ_{R1}	THER1	V	Numerator of the gate voltage dependent part of series resistance for all the transistors in the bin
37	θ_{R2}	THER2	V	Denominator of the gate voltage dependent part of series resistance for all transistors in the bin
38	$P_{0;\theta_{sat}}$	POTHESAT	V^{-1}	Coefficient for the geometry independent part of θ_{sat}
39	$P_{L;\theta_{sat}}$	PLTHESAT	V^{-1}	Coefficient for the length dependence of θ_{sat}
40	$P_{W;\theta_{sat}}$	PWTHESAT	V^{-1}	Coefficient for the width dependence of θ_{sat}
41	$P_{LW;\theta_{sat}}$	PLWTHESAT	V^{-1}	Coefficient for the length times width dependence of θ_{sat}
42	$P_{0;\theta_{Th}}$	POTHETH	V^{-3}	Coefficient for the geometry independent part of θ_{Th}
43	$P_{L;\theta_{Th}}$	PLTHETH	V^{-3}	Coefficient for the length dependence of θ_{Th}
44	$P_{W;\theta_{Th}}$	PWTHETH	V^{-3}	Coefficient for the width dependence of θ_{Th}
45	$P_{LW;\theta_{Th}}$	PLWTHETH	V^{-3}	Coefficient for the length times width dependence of θ_{Th}
46	$P_{0;\sigma_{dibl}}$	POSDIBL	$V^{-1/2}$	Coefficient for the geometry independent part of σ_{dibl}
47	$P_{L;\sigma_{dibl}}$	PLSDIBL	$V^{-1/2}$	Coefficient for the length dependence of σ_{dibl}
48	$P_{W;\sigma_{dibl}}$	PWSDIBL	$V^{-1/2}$	Coefficient for the width dependence of σ_{dibl}
49	$P_{LW;\sigma_{dibl}}$	PLWSDIBL	$V^{-1/2}$	Coefficient for the length times width dependence of σ_{dibl}
50	$P_{0;m_0}$	POMO	-	Coefficient for the geometry independent part of m_0
51	$P_{L;m_0}$	PLMO	-	Coefficient for the length dependence of m_0
52	$P_{W;m_0}$	PWMO	-	Coefficient for the width dependence of m_0
53	$P_{LW;m_0}$	PLWMO	-	Coefficient for the length times width dependence of m_0
54	$P_{0;\sigma_{sf}}$	POSSF	$V^{-1/2}$	Coefficient for the geometry independent part of σ_{sf}
55	$P_{L;\sigma_{sf}}$	PLSSF	$V^{-1/2}$	Coefficient for the length dependence of σ_{sf}
56	$P_{W;\sigma_{sf}}$	PWSSF	$V^{-1/2}$	Coefficient for the width dependence of σ_{sf}
57	$P_{LW;\sigma_{sf}}$	PLWSSF	$V^{-1/2}$	Coefficient for the length times width dependence of σ_{sf}
58	$P_{0;\alpha}$	POALP	-	Coefficient for the geometry independent part of α
59	$P_{L;\alpha}$	PLALP	-	Coefficient for the length dependence of α
60	$P_{W;\alpha}$	PWALP	-	Coefficient for the width dependence of α
61	$P_{LW;\alpha}$	PLWALP	-	Coefficient for the length times width dependence of α
62	V_P	VP	V	Characteristic voltage of the channel length modulation

©Koninklijke Philips Electronics N.V. 2004

63	$P_{0;m}$	POMEXP	-	Coefficient for the geometry independent part of $1/m$
64	$P_{L;m}$	PLMEXP	-	Coefficient for the length dependence of $1/m$
65	$P_{W;m}$	PWMEXP	-	Coefficient for the width dependence of $1/m$
66	$P_{LW;m}$	PLWMEXP	-	Coefficient for the length times width dependence of $1/m$
67	$P_{0;a_1}$	POA1	-	Coefficient for the geometry independent part of a_1
68	$P_{L;a_1}$	PLA1	-	Coefficient for the length dependence of a_1
69	$P_{W;a_1}$	PWA1	-	Coefficient for the width dependence of a_1
70	$P_{LW;a_1}$	PLWA1	-	Coefficient for the length times width dependence of a_1
71	$P_{0;a_2}$	POA2	V	Coefficient for the geometry independent part of a_2
72	$P_{L;a_2}$	PLA2	V	Coefficient for the length dependence of a_2
73	$P_{W;a_2}$	PWA2	V	Coefficient for the width dependence of a_2
74	$P_{LW;a_2}$	PLWA2	V	Coefficient for the length times width dependence of a_2
75	$P_{0;a_3}$	POA3	-	Coefficient for the geometry independent part of a_3
76	$P_{L;a_3}$	PLA3	-	Coefficient for the length dependence of a_3
77	$P_{W;a_3}$	PWA3	-	Coefficient for the width dependence of a_3
78	$P_{LW;a_3}$	PLWA3	-	Coefficient for the length times width dependence of a_3
79	$P_{0;I_{GINV}}$	POIGINV	AV^{-2}	Coefficient for the geometry independent part of I_{GINV}
80	$P_{L;I_{GINV}}$	PLIGINV	AV^{-2}	Coefficient for the length dependence of I_{GINV}
81	$P_{W;I_{GINV}}$	PWIGINV	AV^{-2}	Coefficient for the width dependence of I_{GINV}
82	$P_{LW;I_{GINV}}$	PLWIGINV	AV^{-2}	Coefficient for the length times width dependence of I_{GINV}
83	$P_{0;B_{inv}}$	POBINV	V	Coefficient for the geometry independent part of B_{inv}
84	$P_{L;B_{inv}}$	PLBINV	V	Coefficient for the length dependence of B_{inv}
85	$P_{W;B_{inv}}$	PWBINV	V	Coefficient for the width dependence of B_{inv}
86	$P_{LW;B_{inv}}$	PLWBINV	V	Coefficient for the length times width dependence of B_{inv}
87	$P_{0;I_{GACC}}$	POIGACC	AV^{-2}	Coefficient for the geometry independent part of I_{GACC}
88	$P_{L;I_{GACC}}$	PLIGACC	AV^{-2}	Coefficient for the length dependence of I_{GACC}
89	$P_{W;I_{GACC}}$	PWIGACC	AV^{-2}	Coefficient for the width dependence of I_{GACC}
90	$P_{LW;I_{GACC}}$	PLWIGACC	AV^{-2}	Coefficient for the length times width dependence of I_{GACC}
91	$P_{0;B_{acc}}$	POBACC	V	Coefficient for the geometry independent part of B_{acc}
92	$P_{L;B_{acc}}$	PLBACC	V	Coefficient for the length dependence of B_{acc}
93	$P_{W;B_{acc}}$	PWBACC	V	Coefficient for the width dependence of B_{acc}
94	$P_{LW;B_{acc}}$	PLWBACC	V	Coefficient for the length times width dependence of B_{acc}
95	V_{FBov}	VFBOV	V	Flat-band voltage for the source/drain overlap extensions
96	k_{ov}	KOV	$V^{1/2}$	Body-effect factor for the source/drain overlap extensions
97	$P_{0;I_{GOV}}$	POIGOV	AV^{-2}	Coefficient for the geometry independent part of I_{GOV}
98	$P_{L;I_{GOV}}$	PLIGOV	AV^{-2}	Coefficient for the length dependence of I_{GOV}

 ©Koninklijke Philips Electronics N.V. 2004

99	$P_{W;I_{GOV}}$	PWIGOV	AV^{-2}	Coefficient for the width dependence of I_{GOV}
100	$P_{LW;I_{GOV}}$	PLWIGOV	AV^{-2}	Coefficient for the width over length dependence of I_{GOV}
101	$P_{0;A_{GIDL}}$	POAGIDL	AV^{-3}	Coefficient for the geometry independent part of A_{GIDL}
102	$P_{L;A_{GIDL}}$	PLAGIDL	AV^{-3}	Coefficient for the length dependence of A_{GIDL}
103	$P_{W;A_{GIDL}}$	PWAGIDL	AV^{-3}	Coefficient for the width dependence of A_{GIDL}
104	$P_{LW;A_{GIDL}}$	PLWAGIDL	AV^{-3}	Coefficient for the width over length dependence of A_{GIDL}
105	$P_{0;B_{GIDL}}$	POBGIDL	V	Coefficient for the geometry independent part of B_{GIDL}
106	$P_{L;B_{GIDL}}$	PLBGIDL	V	Coefficient for the length dependence of B_{GIDL}
107	$P_{W;B_{GIDL}}$	PWBGIDL	V	Coefficient for the width dependence of B_{GIDL}
108	$P_{LW;B_{GIDL}}$	PLWBGIDL	V	Coefficient for the length times width dependence of B_{GIDL}
109	$P_{0;C_{GIDL}}$	POCGIDL	-	Coefficient for the geometry independent part of C_{GIDL}
110	$P_{L;C_{GIDL}}$	PLCGIDL	-	Coefficient for the length dependence of C_{GIDL}
111	$P_{W;C_{GIDL}}$	PWCGIDL	-	Coefficient for the width dependence of C_{GIDL}
112	$P_{LW;C_{GIDL}}$	PLWCGIDL	-	Coefficient for the length times width dependence of C_{GIDL}
113	t_{ox}	TOX	m	Thickness of the gate oxide layer
114	$P_{0;C_{OX}}$	POCOX	F	Coefficient for the geometry independent part of C_{OX}
115	$P_{L;C_{OX}}$	PLCOX	F	Coefficient for the length dependence of C_{OX}
116	$P_{W;C_{OX}}$	PWCOX	F	Coefficient for the width dependence of C_{OX}
117	$P_{LW;C_{OX}}$	PLWCOX	F	Coefficient for the length times width dependence of C_{OX}
118	$P_{0;C_{GDO}}$	POCGDO	F	Coefficient for the geometry independent part of C_{GDO}
119	$P_{L;C_{GDO}}$	PLCGDO	F	Coefficient for the length dependence of C_{GDO}
120	$P_{W;C_{GDO}}$	PWCGDO	F	Coefficient for the width dependence of C_{GDO}
121	$P_{LW;C_{GDO}}$	PLWCGDO	F	Coefficient for the width over length dependence of C_{GDO}
122	$P_{0;C_{GSO}}$	POCGSO	F	Coefficient for the geometry independent part of C_{GSO}
123	$P_{L;C_{GSO}}$	PLCGSO	F	Coefficient for the length dependence of C_{GSO}
124	$P_{W;C_{GSO}}$	PWCGSO	F	Coefficient for the width dependence of C_{GSO}
125	$P_{LW;C_{GSO}}$	PLWCGSO	F	Coefficient for the width over length dependence of C_{GSO}
126	–	GATENOISE		Flag for in/exclusion of induced gate thermal noise
127	N_T	NT	J	Coefficient of the thermal noise at the reference temperature
128	$P_{0;N_{FA}}$	PONFA	$V^{-1}m^{-4}$	Coefficient for the geometry independent part of N_{FA}
129	$P_{L;N_{FA}}$	PLNFA	$V^{-1}m^{-4}$	Coefficient for the length dependence of N_{FA}
130	$P_{W;N_{FA}}$	PWNFA	$V^{-1}m^{-4}$	Coefficient for the width dependence of N_{FA}
131	$P_{LW;N_{FA}}$	PLWNFA	$V^{-1}m^{-4}$	Coefficient for the length times width dependence of N_{FA}
132	$P_{0;N_{FB}}$	PONFB	$V^{-1}m^{-2}$	Coefficient for the geometry independent part of N_{FB}
133	$P_{L;N_{FB}}$	PLNFB	$V^{-1}m^{-2}$	Coefficient for the length dependence of N_{FB}
134	$P_{W;N_{FB}}$	PWNFB	$V^{-1}m^{-2}$	Coefficient for the width dependence of N_{FB}

©Koninklijke Philips Electronics N.V. 2004

135	$P_{\mathrm{LW};N_{\mathrm{FB}}}$	PLWNFB	$\mathrm{V}^{-1}\mathrm{m}^{-2}$	Coefficient for the length times width dependence of N_{FB}
136	$P_{0;N_{\mathrm{FC}}}$	PONFC	V^{-1}	Coefficient for the geometry independent part of N_{FC}
137	$P_{\mathrm{L};N_{\mathrm{FC}}}$	PLNFC	V^{-1}	Coefficient for the length dependence of N_{FC}
138	$P_{\mathrm{W};N_{\mathrm{FC}}}$	PWNFC	V^{-1}	Coefficient for the width dependence of N_{FC}
139	$P_{\mathrm{LW};N_{\mathrm{FC}}}$	PLWNFC	V^{-1}	Coefficient for the length times width dependence of N_{FC}
140	$P_{0;\mathrm{T};V_{\mathrm{FB}}}$	POTVFB	VK^{-1}	Coefficient for the geometry independent part of $S_{\mathrm{T};V_{\mathrm{FB}}}$
141	$P_{\mathrm{L};\mathrm{T};V_{\mathrm{FB}}}$	PLTVFB	VK^{-1}	Coefficient for the length dependence of $S_{\mathrm{T};V_{\mathrm{FB}}}$
142	$P_{\mathrm{W};\mathrm{T};V_{\mathrm{FB}}}$	PWTVFB	VK^{-1}	Coefficient for the width dependence of $S_{\mathrm{T};V_{\mathrm{FB}}}$
143	$P_{\mathrm{LW};\mathrm{T};V_{\mathrm{FB}}}$	PLWTVFB	VK^{-1}	Coefficient for the length times width dependence of $S_{\mathrm{T};V_{\mathrm{FB}}}$
144	$P_{0;\mathrm{T};\phi_{\mathrm{B}}}$	POTPHIB	VK^{-1}	Coefficient for the geometry independent part of $S_{\mathrm{T};\phi_{\mathrm{B}}}$
145	$P_{\mathrm{L};\mathrm{T};\phi_{\mathrm{B}}}$	PLTPHIB	VK^{-1}	Coefficient for the length dependence of $S_{\mathrm{T};\phi_{\mathrm{B}}}$
146	$P_{\mathrm{W};\mathrm{T};\phi_{\mathrm{B}}}$	PWTPHIB	VK^{-1}	Coefficient for the width dependence of $S_{\mathrm{T};\phi_{\mathrm{B}}}$
147	$P_{\mathrm{LW};\mathrm{T};\phi_{\mathrm{B}}}$	PLWTPHIB	VK^{-1}	Coefficient for the length times width dependence of $S_{\mathrm{T};\phi_{\mathrm{B}}}$
148	$P_{0;\mathrm{T};\eta_\beta}$	POTETABET	-	Coefficient for the geometry independent part of η_β
149	$P_{\mathrm{L};\mathrm{T};\eta_\beta}$	PLTETABET	-	Coefficient for the length dependence of η_β
150	$P_{\mathrm{W};\mathrm{T};\eta_\beta}$	PWTETABET	-	Coefficient for the width dependence of η_β
151	$P_{\mathrm{LW};\mathrm{T};\eta_\beta}$	PLWTETABET	-	Coefficient for the length times width dependence of η_β
152	$P_{0;\mathrm{T};\eta_{\mathrm{sr}}}$	POTETASR	-	Coefficient for the geometry independent part of η_{sr}
153	$P_{\mathrm{L};\mathrm{T};\eta_{\mathrm{sr}}}$	PLTETASR	-	Coefficient for the length dependence of η_{sr}
154	$P_{\mathrm{W};\mathrm{T};\eta_{\mathrm{sr}}}$	PWTETASR	-	Coefficient for the width dependence of η_{sr}
155	$P_{\mathrm{LW};\mathrm{T};\eta_{\mathrm{sr}}}$	PLWETASR	-	Coefficient for the length times width dependence of η_{sr}
156	$P_{0;\mathrm{T};\eta_{\mathrm{ph}}}$	POTETAPH	-	Coefficient for the geometry independent part of η_{ph}
157	$P_{\mathrm{L};\mathrm{T};\eta_{\mathrm{ph}}}$	PLTETAPH	-	Coefficient for the length dependence of η_{ph}
158	$P_{\mathrm{W};\mathrm{T};\eta_{\mathrm{ph}}}$	PWTETAPH	-	Coefficient for the width dependence of η_{ph}
159	$P_{\mathrm{LW};\mathrm{T};\eta_{\mathrm{ph}}}$	PLWETAPH	-	Coefficient for the length times width dependence of η_{ph}
160	$P_{0;\mathrm{T};\eta_{\mathrm{mob}}}$	POTETAMOB	K^{-1}	Coefficient for the geometry independent part of $S_{\mathrm{T};\eta_{\mathrm{mob}}}$
161	$P_{\mathrm{L};\mathrm{T};\eta_{\mathrm{mob}}}$	PLTETAMOB	K^{-1}	Coefficient for the length dependence of $S_{\mathrm{T};\eta_{\mathrm{mob}}}$
162	$P_{\mathrm{W};\mathrm{T};\eta_{\mathrm{mob}}}$	PWTETAMOB	K^{-1}	Coefficient for the width dependence of $S_{\mathrm{T};\eta_{\mathrm{mob}}}$
163	$P_{\mathrm{LW};\mathrm{T};\eta_{\mathrm{mob}}}$	PLWTETAMOB	K^{-1}	Coefficient for the length times width dependence of $S_{\mathrm{T};\eta_{\mathrm{mob}}}$
164	ν	NU	-	Exponent of the field dependence of the mobility model at the reference temperature
165	$P_{0;\mathrm{T};\nu_{\mathrm{exp}}}$	POTNUEXP	-	Coefficient for the geometry independent part of ν_{exp}
166	$P_{\mathrm{L};\mathrm{T};\nu_{\mathrm{exp}}}$	PLTNUEXP	-	Coefficient for the length dependence of ν_{exp}
167	$P_{\mathrm{W};\mathrm{T};\nu_{\mathrm{exp}}}$	PWTNUEXP	-	Coefficient for the width dependence of ν_{exp}
168	$P_{\mathrm{LW};\mathrm{T};\nu_{\mathrm{exp}}}$	PLWTNUEXP	-	Coefficient for the length times width dependence of ν_{exp}
169	$P_{0;\mathrm{T};\eta_{\mathrm{R}}}$	POTETAR	-	Coefficient for the geometry independent part of η_{R}

 ©Koninklijke Philips Electronics N.V. 2004

170	$P_{L;T;\eta_R}$	PLTETAR	-	Coefficient for the length dependence of η_R
171	$P_{W;T;\eta_R}$	PWTETAR	-	Coefficient for the width dependence of η_R
172	$P_{LW;T;\eta_R}$	PLWTETAR	-	Coefficient for the length times width dependence of η_R
173	$P_{0;T;\eta_{sat}}$	POTETASAT	-	Coefficient for the geometry independent part of η_{sat}
174	$P_{L;T;\eta_{sat}}$	PLTETASAT	-	Coefficient for the length dependence of η_{sat}
175	$P_{W;T;\eta_{sat}}$	PWTETASAT	-	Coefficient for the width dependence of η_{sat}
176	$P_{LW;T;\eta_{sat}}$	PLWTETASAT	-	Coefficient for the length times width dependence of η_{sat}
177	$P_{0;T;a_1}$	POTA1	K^{-1}	Coefficient for the geometry independent part of $S_{T;a_1}$
178	$P_{L;T;a_1}$	PLTA1	K^{-1}	Coefficient for the length dependence of $S_{T;a_1}$
179	$P_{W;T;a_1}$	PWTA1	K^{-1}	Coefficient for the width dependence of $S_{T;a_1}$
180	$P_{LW;T;a_1}$	PLWTA1	K^{-1}	Coefficient for the length times width dependence of $S_{T;a_1}$
181	$P_{0;T;B_{GIDL}}$	POTBGIDL	VK^{-1}	Coefficient for the geometry independent part of $S_{T;B_{GIDL}}$
182	$P_{L;T;B_{GIDL}}$	PLTBGIDL	VK^{-1}	Coefficient for the length dependence of $S_{T;B_{GIDL}}$
183	$P_{W;T;B_{GIDL}}$	PWTBGIDL	VK^{-1}	Coefficient for the width dependence of $S_{T;B_{GIDL}}$
184	$P_{LW;T;B_{GIDL}}$	PLWTBGIDL	VK^{-1}	Coefficient for the length times width dependence of $S_{T;B_{GIDL}}$
185	L	L	m	Drawn channel length in the lay-out of the actual transistor
186	W	W	m	Drawn channel width in the lay-out of the actual transistor
187	ΔT_A	DTA	K	Temperature offset of the device with respect to T_A
188	N_{MULT}	MULT	-	Number of devices in parallel

Remark: The parameters L, W and DTA are used to calculate the electrical parameters of the actual transistor as specified in the section on parameter preprocessing.

The additional parameters for the model including self-heating (see Section4.2) are listed in the table below.

No.	Symbol	Program Name	Units	Description
189	R_{Th}	RTH	K/W	Thermal resistance
190	C_{Th}	CTH	J/K	Thermal capacitance
191	A_{Th}	ATH	-	Temperature coefficient of the thermal resistance

©Koninklijke Philips Electronics N.V. 2004

4 Embedding

4.1 Embedding MOS Model 11 in a Circuit Simulator

In CMOS technologies both *n*– and *p*–channel MOS transistors are supported. It is convenient to use one model for both type of transistors instead of two separate models. This is accomplished by mapping a *p*–channel device with its bias conditions and parameter set onto an equivalent *n*–channel device with appropriately changed bias conditions (i.e. currents, voltages and charges) and parameters. In this way both type of transistors can be treated as an *n*–channel transistor. Nevertheless, the electrical behaviour of electrons and holes is not exactly the same (e.g. the mobility and tunnelling behaviour), and consequently slightly different equations have to be used in case of *n*– or *p*–type transistors, see Section 2.3.

As said earlier, any circuit simulator internally identifies the terminals of a MOS transistor by a number. However, designers are used to the standard terminology of source, drain, gate and bulk. Therefore, in the context of a circuit simulator it is traditionally possible to address, say, the drain of MOST number 17, even if in reality the corresponding source is at a higher potential (*n*–channel case). More strongly, most circuit simulators provide for model evaluation a so–called V_{DS}, V_{GS}, and V_{SB} based on an a priori assignment of source, drain and bulk that is independent of the actual bias conditions. Since MOS Model 11 assumes saturation occurs at the drain side of the MOSFET, the basic model cannot cope with bias conditions that correspond to $V_{DS} < 0$. Again a transformation of the bias conditions is necessary. In this case, the transformation corresponds to internally reassigning source and drain, applying the standard electrical model, and then reassigning the currents and charges to the original terminals. In MOS Model 11 care has been taken to preserve symmetry with respect to drain and source at $V_{DS} = 0$. In other words no non-singularities will occur in the higher-order derivatives at $V_{DS} = 0$.

In detail, in order to embed MOS Model 11 correctly into a circuit simulator, the following procedure, illustrated in Fig. 4.1 should be followed. We have assumed that indeed the simulator provides the nodal potentials V_D^e, V_G^e, V_S^e and V_B^e based on an a priori assignment of drain, gate, source and bulk.

Step 1 Calculate the voltages $V_{DS}^{''}$, $V_{GS}^{''}$ and $V_{SB}^{''}$, and the additional voltages $V_{DG}^{''}$ and $V_{SG}^{''}$. The latter are used for calculating the charges associated with overlap capacitances.

Step 2 Based on *n*– or *p*–channel devices, calculate the modified voltages $V_{DS}^{'}$, $V_{GS}^{'}$ and $V_{SB}^{'}$. From here onwards only *n*–channel behaviour needs to be considered.

Step 3 Based on a positive or negative $V_{DS}^{'}$, calculate the internal nodal voltages. At this level, the voltages – and the parameters, see below – comply to all the requirements for input quantities of MOS Model 11.

Step 4 Evaluate all the internal output quantities – channel current, weak–avalanche current, gate current, nodal charges, and noise–power spectral densities – using the standard MOS Model 11 equations and the internal voltages.

Step 5 Correct the internal output quantities for a possible source–drain interchange. In fact, this directly establishes the external noise–power spectral densities.

Step 6 Correct for a possible *p*–channel transformation.

Step 7 Change from branch current to nodal currents, establishing the external current output quantities. Calculate the overlap charges that are related to the physical regions and add them to the nodal charges, thus forming the external charge output quantities.

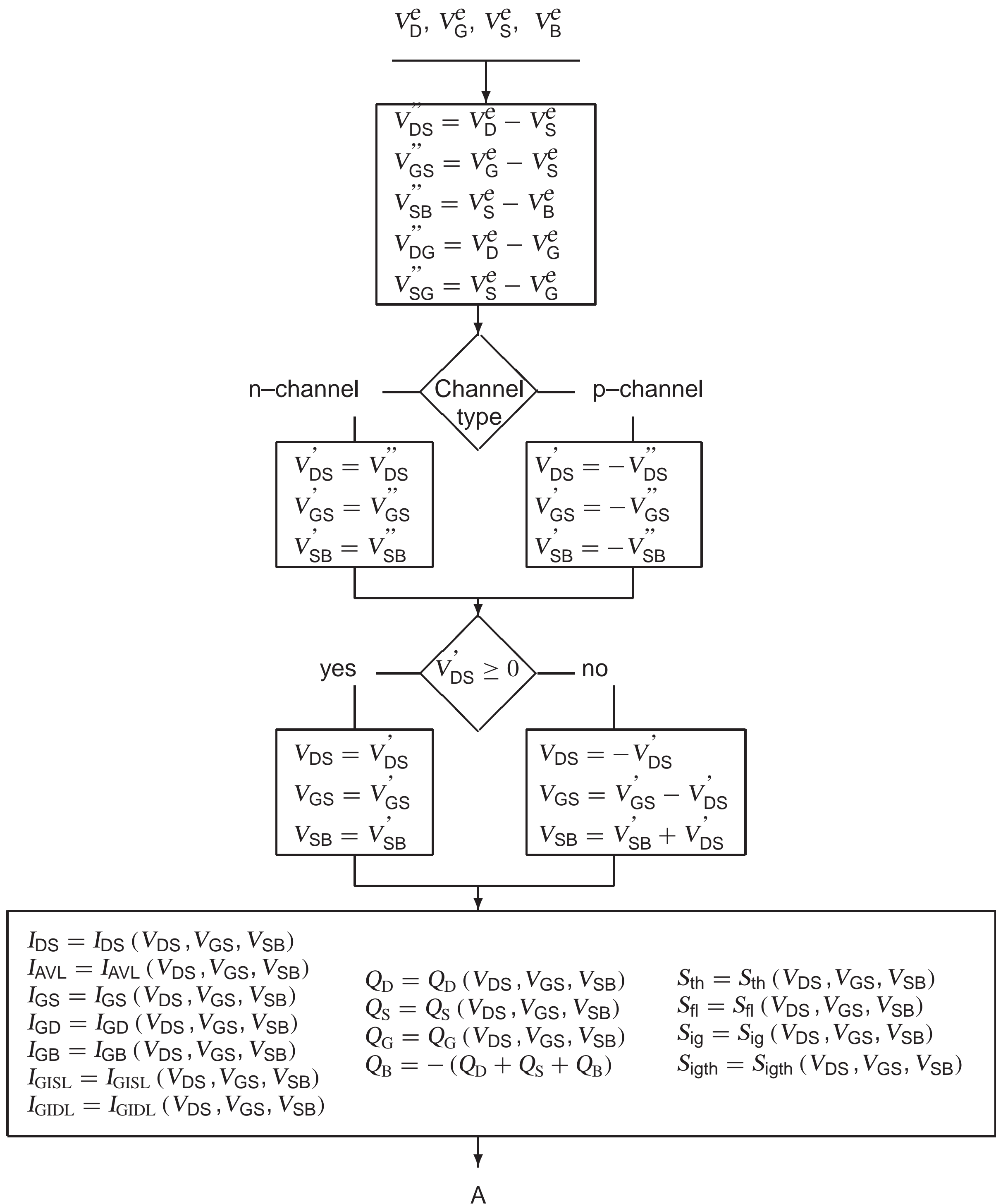

©Koninklijke Philips Electronics N.V. 2004

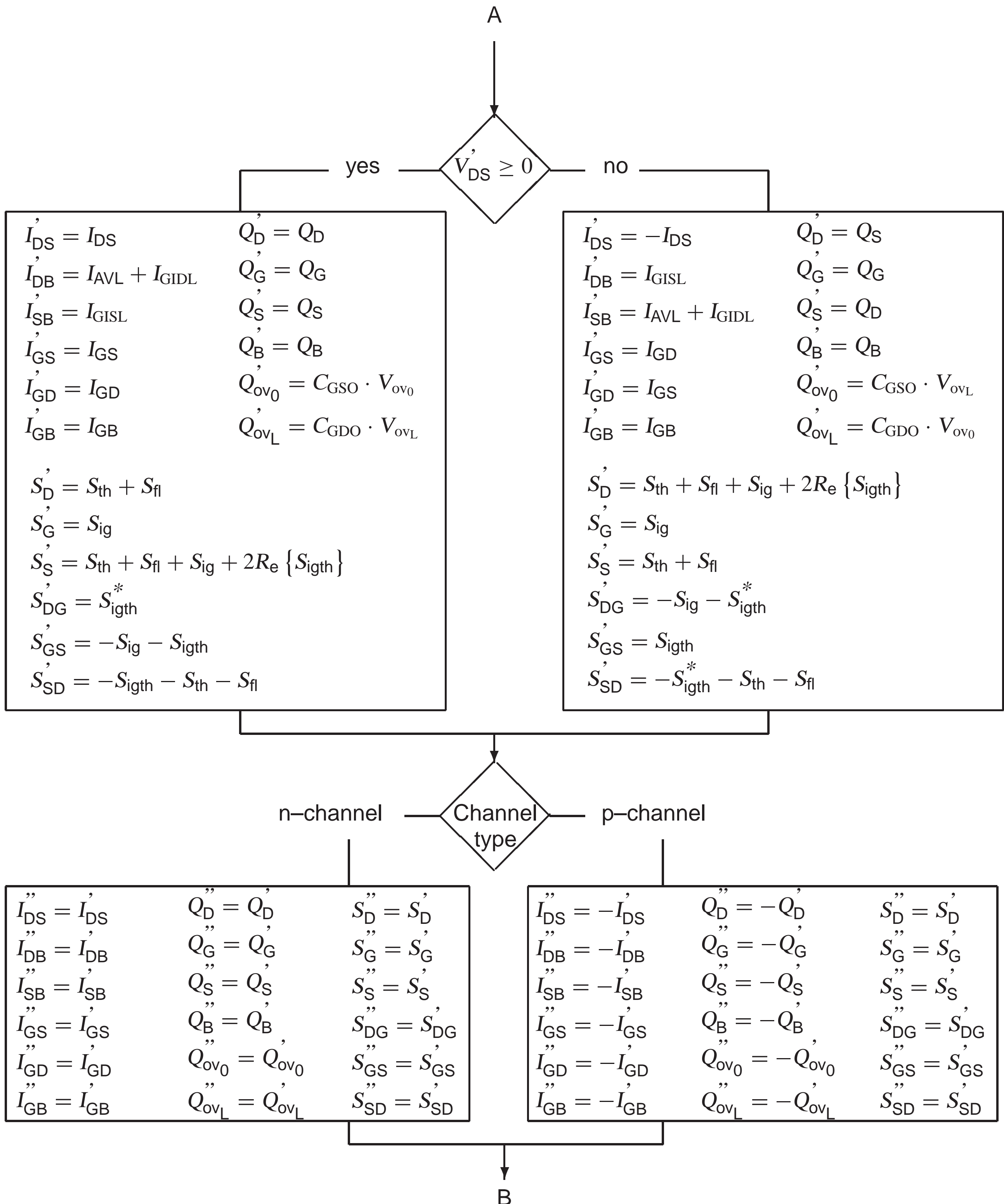

©Koninklijke Philips Electronics N.V. 2004

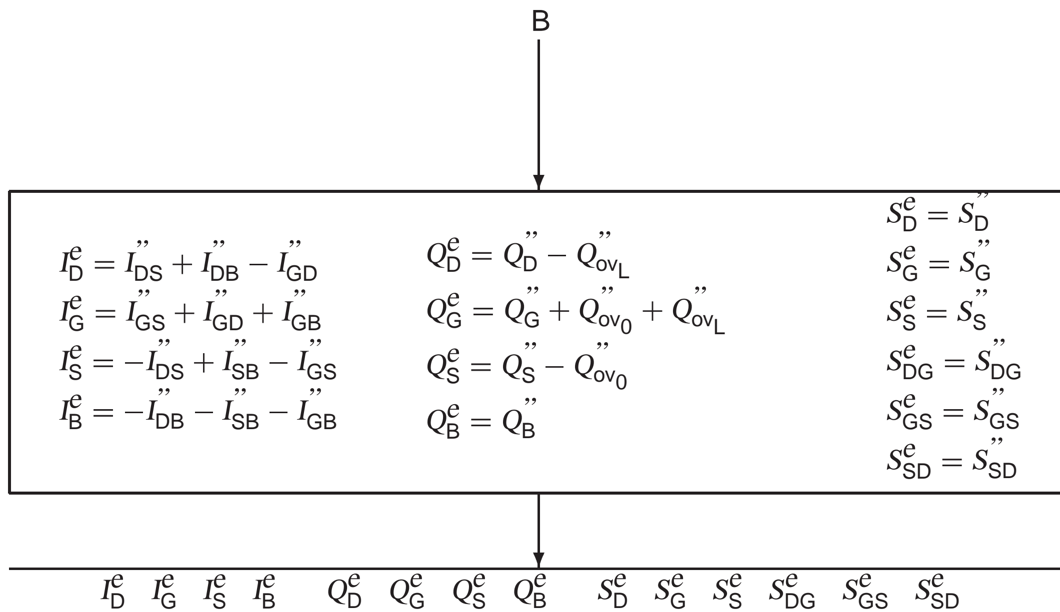

Figure 4.1: Transformation scheme

It is customary to have separate user models in the circuit simulators for n – and p – channel transistors. In that manner it is easy to use a different set of reference and scaling parameters for the two channel types. As a consequence, the changes in the parameter values necessary for a p – channel type transistor are normally already included in the parameter sets on file. The changes should not be included in the simulator.

 ©Koninklijke Philips Electronics N.V. 2004

4.2 Self-Heating

For self-heating, an extra network is introduced, see Fig. 4.2. It contains the temperature-dependent self-heating resistance $R_{\mathrm{Th_T}}$ and capacitance C_{Th}, both connected between ground and the temperature note dT. The value of the nodal voltage V_{dT} at the temperature node gives the increase in local temperature, which is included in the calculation of the temperature scaling relations (2.3) and (5.84), see Sections 2.2 and 5.3. The power dissipation is given by:

$$
\begin{aligned}
P_{\mathrm{diss}} &= I_{\mathrm{D}}^{\mathrm{e}} \cdot V_{\mathrm{D}}^{\mathrm{e}} + I_{\mathrm{G}}^{\mathrm{e}} \cdot V_{\mathrm{G}}^{\mathrm{e}} + I_{\mathrm{S}}^{\mathrm{e}} \cdot V_{\mathrm{S}}^{\mathrm{e}} + I_{\mathrm{B}}^{\mathrm{e}} \cdot V_{\mathrm{B}}^{\mathrm{e}} \qquad (4.1) \\
&= I_{\mathrm{DS}}'' \cdot V_{\mathrm{DS}}'' + I_{\mathrm{DB}}'' \cdot \left(V_{\mathrm{DS}}'' - V_{\mathrm{SB}}''\right) + I_{\mathrm{SB}}'' \cdot V_{\mathrm{SB}}'' + I_{\mathrm{GS}}'' \cdot V_{\mathrm{GS}}'' \\
&\quad + I_{\mathrm{GD}}'' \cdot \left(V_{\mathrm{GS}}'' - V_{\mathrm{DS}}''\right) + I_{\mathrm{GB}}'' \cdot \left(V_{\mathrm{GS}}'' - V_{\mathrm{SB}}''\right)
\end{aligned}
$$

where all variables are given in Fig. 4.1. Note that only the steady-state currents contribute to the dissipated power.

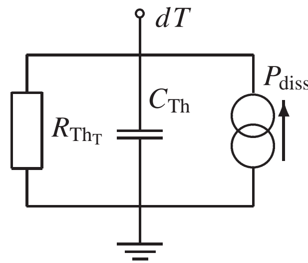

Figure 4.2: The self-heating network, where the node voltage V_{dT} is used in the temperature scaling relations. The thermal resistance $R_{\mathrm{Th_T}}$ is temperature dependent. Note that for increased flexibility the note dT should be available to the user.

©Koninklijke Philips Electronics N.V. 2004

5 Preprocessing and Clipping

In this Chapter the geometry and temperature scaling rules for the model parameters will be given. The temperature scaling rules have already been given in Section 2.2, but they are repeated here for the sake of completeness.

5.1 Calculation of Transistor Geometry

$$L_{\mathrm{E}} = L - \Delta L = L + \Delta L_{\mathrm{PS}} - 2 \cdot \Delta L_{\mathrm{overlap}} \tag{5.1}$$

$$W_{\mathrm{E}} = W - \Delta W = W + \Delta W_{\mathrm{OD}} - 2 \cdot \Delta W_{\mathrm{narrow}} \tag{5.2}$$

WARNING : L_{E} and W_{E} after calculation can not be less than 0 !

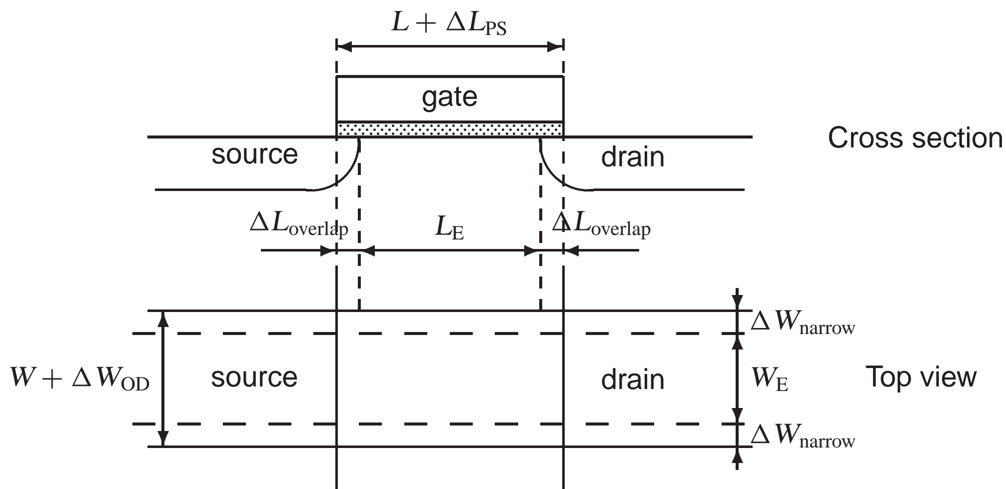

Figure 5.1: Specification of the dimensions of a MOS transistor

5.2 Calculation of Geometry-Dependent Parameters

In MOS Model 11, Level 1102, parameter binning has been facilitated by adding a second, separate set of geometry scaling rules. Consequently, besides the *physical* geometrical scaling rules there is also a set of *binning* geometrical scaling rules. The physical geometry scaling rules of Level 1102 (see Sections 3.4.1 and 5.2.1) have been developed to give a good description over the whole geometry range of CMOS technologies. For processes under development, however, it is sometimes useful to have more flexible scaling relations. In this case one could opt for a binning strategy, where the accuracy with geometry is mostly determined by the number of bins used. The physical scaling rules of Level 1102 are not straightforwardly applicable to binning strategies, since they may result in discontinuities in parameter values at the bin boundaries. Consequently, special binning geometrical scaling relations have been developed (see Sections 3.4.2 and 5.2.2), which guarantee continuity in the model parameters at the bin boundaries.

©Koninklijke Philips Electronics N.V. 2004

It should be noted that using the source code of the Modelkit on the Philips' website (which can be found at http://www.semconductors.philips.com/Philips_Models)

1. the physical geometry scaling rules can be selected by using Level 11020, while
2. the binning geometry scaling rules can be selected by using Level 11021.

Three types of binning geometrical scaling rules can be distinguished:

1. type I

$$P(W_{\mathrm{E}},\ L_{\mathrm{E}}) = P_0 + \frac{L_{\mathrm{EN}}}{L_{\mathrm{E}}} \cdot P_{\mathrm{L}} + \frac{W_{\mathrm{EN}}}{W_{\mathrm{E}}} \cdot P_{\mathrm{W}} + \frac{L_{\mathrm{EN}} \cdot W_{\mathrm{EN}}}{L_{\mathrm{E}} \cdot W_{\mathrm{E}}} \cdot P_{\mathrm{LW}} \tag{5.3}$$

2. type II

$$P(W_{\mathrm{E}},\ L_{\mathrm{E}}) = P_0 + \frac{L_{\mathrm{E}}}{L_{\mathrm{EN}}} \cdot P_{\mathrm{L}} + \frac{W_{\mathrm{E}}}{W_{\mathrm{EN}}} \cdot P_{\mathrm{W}} + \frac{L_{\mathrm{E}} \cdot W_{\mathrm{E}}}{L_{\mathrm{EN}} \cdot W_{\mathrm{EN}}} \cdot P_{\mathrm{LW}} \tag{5.4}$$

3. type III

$$P(W_{\mathrm{E}},\ L_{\mathrm{E}}) = P_0 + \frac{L_{\mathrm{EN}}}{L_{\mathrm{E}}} \cdot P_{\mathrm{L}} + \frac{W_{\mathrm{E}}}{W_{\mathrm{EN}}} \cdot P_{\mathrm{W}} + \frac{W_{\mathrm{E}}}{L_{\mathrm{E}}} \cdot P_{\mathrm{LW}} \tag{5.5}$$

In these equations L_{EN} and W_{EN} are constants (see Sect. 5.2.2). In Table 5.1 a survey of the parameters scaling is given.
When using the above binning rules, the scaling parameters for one bin can be directly calculated from the minisets of the four corner devices of the bin. The binning scheme ensures that the minisets are exactly reproduced in the bin corners, and that no humps occur in parameter values across bin borders. The exact way to calculate binning parameters from minisets is described in AppendixB.

 ©Koninklijke Philips Electronics N.V. 2004

Table 5.1: Survey of parameters scaling. In the third column is indicated if if there is a physical geometrical scaling rule for the parameter; in the fourth column the type of binning geometrical scaling rule for the parameter is indicated.

#	parameter	physical scaling	binning	#	parameter	physical scaling	binning
0	LEVEL	no	no	29	V_{P}	no	no
1	T_{R}	no	no	30	m	yes	type I
2	V_{FB}	no	no	31	a_1	yes	type I
3	$S_{\mathrm{T;V_{FB}}}$	no	type I	32	$S_{\mathrm{T};a_1}$	no	type I
4	k_0	yes	type I	33	a_2	yes	type I
5	$1/k_{\mathrm{P}}$	no	no	34	a_3	yes	type I
6	ϕ_{B}	yes	type I	35	I_{GINV}	yes	type II
7	$S_{\mathrm{T};\phi_{\mathrm{B}}}$	no	type I	36	B_{inv}	no	type I
8	β	yes	type III	37	I_{GACC}	yes	type II
9	η_β	yes	type I	38	B_{acc}	no	type I
10	θ_{sr}	yes	type I	39	V_{FBov}	no	no
11	η_{sr}	no	type I	40	k_{ov}	no	no
12	θ_{ph}	yes	type I	41	I_{GOV}	yes	type III
13	η_{ph}	no	type I	42	A_{GIDL}	yes	type III
14	η_{mob}	yes	type I	43	B_{GIDL}	yes	type I
15	$S_{\mathrm{T};\eta_{\mathrm{mob}}}$	no	type I	44	$S_{\mathrm{T};B_{\mathrm{GIDL}}}$	yes	type I
16	ν	no	no	45	C_{GIDL}	yes	type I
17	ν_{EXP}	no	type I	46	C_{OX}	yes	type II
18	θ_{R}	yes	type I	47	C_{GDO}	yes	type III
19	η_{R}	no	type I	48	C_{GSO}	yes	type III
20	θ_{R1}	no	no	49	GATENOISE	no	no
21	θ_{R2}	no	no	50	N_{T}	no	no
22	θ_{sat}	yes	type I	51	N_{FA}	yes	type I
23	η_{sat}	no	type I	52	N_{FB}	yes	type I
24	θ_{Th}	yes	type I	53	N_{FC}	yes	type I
25	σ_{dibl}	yes	type I	54	t_{ox}	no	no
26	m_0	yes	type I	55	ΔT_{A}	no	no
27	σ_{sf}	yes	type I	56	N_{MULT}	no	no
28	α	yes	type I				

5.2.1 Calculation of Geometry-Dependent Parameters using the Physical Scaling Rules

$$L_{EN} = 10^{-6} \tag{5.6}$$

$$W_{EN} = 10^{-6} \tag{5.7}$$

Calculation of Threshold–Voltage Parameters

$$k_0 = k_{0R} \cdot \left[1 + \frac{L_{EN}}{L_E} \cdot S_{L;k_0} + \left(\frac{L_{EN}}{L_E}\right)^2 \cdot S_{L2;k_0}\right] \cdot \left[1 + \frac{W_{EN}}{W_E} \cdot S_{W;k_0}\right] \tag{5.8}$$

$$\phi_B = \phi_{BR} \cdot \left[1 + \frac{L_{EN}}{L_E} \cdot S_{L;\phi_B} + \left(\frac{L_{EN}}{L_E}\right)^2 \cdot S_{L2;\phi_B}\right] \cdot \left[1 + \frac{W_{EN}}{W_E} \cdot S_{W;\phi_B}\right] \tag{5.9}$$

Calculation of Mobility/Series-Resistance Parameters

$$G_{P,E} = 1 + f_{\beta,1} \cdot \frac{L_{P,1}}{L_E} \cdot \left[1 - \exp\left(-\frac{L_E}{L_{P,1}}\right)\right] + f_{\beta,2} \cdot \frac{L_{P,2}}{L_E} \cdot \left[1 - \exp\left(-\frac{L_E}{L_{P,2}}\right)\right] \tag{5.10}$$

$$\beta = \frac{\beta_{sq}}{G_{P,E}} \cdot \frac{W_E}{L_E} \tag{5.11}$$

$$\theta_{sr} = \theta_{srR} \cdot \left[1 + \frac{W_{EN}}{W_E} \cdot S_{W;\theta_{sr}}\right] \tag{5.12}$$

$$\theta_{ph} = \theta_{phR} \cdot \left[1 + \frac{W_{EN}}{W_E} \cdot S_{W;\theta_{ph}}\right] \tag{5.13}$$

$$\eta_{mob} = \eta_{mobR} \cdot \left[1 + \frac{W_{EN}}{W_E} \cdot S_{W;\eta_{mob}}\right] \tag{5.14}$$

$$\theta_R = \theta_{RR} \cdot \left[1 + \frac{W_{EN}}{W_E} \cdot S_{W;\theta_R}\right] \cdot \frac{L_{EN}}{L_E} \cdot \frac{1}{G_{P,E}} \tag{5.15}$$

$$\theta_{sat} = \theta_{satR} \cdot \left[1 + \frac{W_{EN}}{W_E} \cdot S_{W;\theta_{sat}}\right] \cdot \left[1 + S_{L;\theta_{sat}} \cdot \left\{\left(\frac{L_{EN}}{L_E}\right)^{\theta_{satEXP}} - 1\right\}\right] \tag{5.16}$$

Calculation of Conductance Parameters

$$\theta_{Th} = \theta_{ThR} \cdot \left[1 + \frac{W_{EN}}{W_E} \cdot S_{W;\theta_{Th}}\right] \cdot \left[\frac{L_{EN}}{L_E}\right]^{\theta_{ThEXP}} \tag{5.17}$$

$$\sigma_{sf} = \sigma_{sfR} \cdot \left[1 + \frac{W_{EN}}{W_E} \cdot S_{W;\sigma_{sf}}\right] \cdot \left[1 + \frac{L_{EN}}{L_E} \cdot S_{L;\sigma_{sf}}\right] \tag{5.18}$$

$$\alpha = \alpha_R \cdot \left[1 + \frac{W_{EN}}{W_E} \cdot S_{W;\alpha}\right] \cdot \left[1 + S_{L;\alpha} \cdot \left\{\left(\frac{L_{EN}}{L_E}\right)^{\alpha_{EXP}} - 1\right\}\right] \tag{5.19}$$

 ©Koninklijke Philips Electronics N.V. 2004

Calculation of Sub–Threshold Parameters

$$\sigma_{\rm dibl} = \sigma_{\rm dibl0} \cdot \left(\frac{L_{\rm EN}}{L_{\rm E}}\right)^{\sigma_{\rm diblEXP}} \tag{5.20}$$

$$m_0 = m_{00} + m_{0\rm R} \cdot \left(\frac{L_{\rm EN}}{L_{\rm E}}\right)^{m_{0\rm EXP}} \tag{5.21}$$

Calculation of Smoothing Parameters

$$L_{\rm max} = 10 \cdot 10^{-6} \tag{5.22}$$

$$m = \frac{8 \cdot (L_{\rm max} - L_{\rm min})}{L_{\rm max} - 4 \cdot L_{\rm min} + 3 \cdot \frac{L_{\rm max} \cdot L_{\rm min}}{L_{\rm E}}} \tag{5.23}$$

Calculation of Weak–Avalanche Parameters

$$a_1 = a_{1\rm R} \cdot \left[1 + \frac{L_{\rm EN}}{L_{\rm E}} \cdot S_{\rm L;a_1}\right] \cdot \left[1 + \frac{W_{\rm EN}}{W_{\rm E}} \cdot S_{\rm W;a_1}\right] \tag{5.24}$$

$$a_2 = a_{2\rm R} \cdot \left[1 + \frac{L_{\rm EN}}{L_{\rm E}} \cdot S_{\rm L;a_2}\right] \cdot \left[1 + \frac{W_{\rm EN}}{W_{\rm E}} \cdot S_{\rm W;a_2}\right] \tag{5.25}$$

$$a_3 = a_{3\rm R} \cdot \left[1 + \frac{L_{\rm EN}}{L_{\rm E}} \cdot S_{\rm L;a_3}\right] \cdot \left[1 + \frac{W_{\rm EN}}{W_{\rm E}} \cdot S_{\rm W;a_3}\right] \tag{5.26}$$

Calculation of Gate Current Parameters

$$I_{GINV} = \frac{W_{\rm E} \cdot L_{\rm E}}{W_{\rm EN} \cdot L_{\rm EN}} \cdot I_{\rm GINVR} \tag{5.27}$$

$$I_{GACC} = \frac{W_{\rm E} \cdot L_{\rm E}}{W_{\rm EN} \cdot L_{\rm EN}} \cdot I_{\rm GACCR} \tag{5.28}$$

$$I_{GOV} = \frac{W_{\rm E}}{W_{\rm EN}} \cdot I_{\rm GOVR} \tag{5.29}$$

Calculation of Gate-Induced Drain Leakage Parameters

$$A_{GIDL} = \frac{W_{\rm E}}{W_{\rm EN}} \cdot A_{\rm GIDLR} \tag{5.30}$$

Calculation of Charge Parameters

$$C_{\rm OX} = \epsilon_{\rm ox} \cdot \frac{W_{\rm E} \cdot L_{\rm E}}{t_{\rm ox}} \tag{5.31}$$

$$C_{\rm GDO} = \frac{W_{\rm E}}{W_{\rm EN}} \cdot C_{\rm ol} \tag{5.32}$$

$$C_{\rm GSO} = \frac{W_{\rm E}}{W_{\rm EN}} \cdot C_{\rm ol} \tag{5.33}$$

©Koninklijke Philips Electronics N.V. 2004

Calculation of Noise Parameters

$$N_{\mathrm{FA}} = \frac{W_{\mathrm{EN}} \cdot L_{\mathrm{EN}}}{W_{\mathrm{E}} \cdot L_{\mathrm{E}}} \cdot N_{\mathrm{FAR}} \tag{5.34}$$

$$N_{\mathrm{FB}} = \frac{W_{\mathrm{EN}} \cdot L_{\mathrm{EN}}}{W_{\mathrm{E}} \cdot L_{\mathrm{E}}} \cdot N_{\mathrm{FBR}} \tag{5.35}$$

$$N_{\mathrm{FC}} = \frac{W_{\mathrm{EN}} \cdot L_{\mathrm{EN}}}{W_{\mathrm{E}} \cdot L_{\mathrm{E}}} \cdot N_{\mathrm{FCR}} \tag{5.36}$$

Calculation of Mobility/Series–Resistance Temperature–Scaling Coefficients

$$\eta_{\beta} = \eta_{\beta\mathrm{R}} + S_{\mathrm{L};\eta_{\beta}} \cdot \frac{L_{\mathrm{EN}}}{L_{\mathrm{E}}} \tag{5.37}$$

 ©Koninklijke Philips Electronics N.V. 2004

5.2.2 Calculation of Geometry-Dependent Parameters using the Binning Scaling Rules

Note that for each bin (W_{min}, W_{max}, L_{min}, L_{max}) there is a separate parameter set, which is valid for (W, L) values with $W_{min} \leq W \leq W_{max}$ and $L_{min} \leq L \leq L_{max}$.

$$L_{EN} = 10^{-6} \tag{5.38}$$

$$W_{EN} = 10^{-6} \tag{5.39}$$

Calculation of Threshold–Voltage Parameters

$$k_0 = P_{0;k_0} + \frac{L_{EN}}{L_E} \cdot P_{L;k_0} + \frac{W_{EN}}{W_E} \cdot P_{W;k_0} + \frac{L_{EN} \cdot W_{EN}}{L_E \cdot W_E} \cdot P_{LW;k_0} \tag{5.40}$$

$$\phi_B = P_{0;\phi_B} + \frac{L_{EN}}{L_E} \cdot P_{L;\phi_B} + \frac{W_{EN}}{W_E} \cdot P_{W;\phi_B} + \frac{L_{EN} \cdot W_{EN}}{L_E \cdot W_E} \cdot P_{LW;\phi_B} \tag{5.41}$$

Calculation of Mobility/Series-Resistance Parameters

$$\beta = P_{0;\beta} + \frac{L_{EN}}{L_E} \cdot P_{L;\beta} + \frac{W_E}{W_{EN}} \cdot P_{W;\beta} + \frac{W_E}{L_E} \cdot P_{LW;\beta} \tag{5.42}$$

$$\theta_{sr} = P_{0;\theta_{sr}} + \frac{L_{EN}}{L_E} \cdot P_{L;\theta_{sr}} + \frac{W_{EN}}{W_E} \cdot P_{W;\theta_{sr}} + \frac{L_{EN} \cdot W_{EN}}{L_E \cdot W_E} \cdot P_{LW;\theta_{sr}} \tag{5.43}$$

$$\theta_{ph} = P_{0;\theta_{ph}} + \frac{L_{EN}}{L_E} \cdot P_{L;\theta_{ph}} + \frac{W_{EN}}{W_E} \cdot P_{W;\theta_{ph}} + \frac{L_{EN} \cdot W_{EN}}{L_E \cdot W_E} \cdot P_{LW;\theta_{ph}} \tag{5.44}$$

$$\eta_{mob} = P_{0;\eta_{mob}} + \frac{L_{EN}}{L_E} \cdot P_{L;\eta_{mob}} + \frac{W_{EN}}{W_E} \cdot P_{W;\eta_{mob}} + \frac{L_{EN} \cdot W_{EN}}{L_E \cdot W_E} \cdot P_{LW;\eta_{mob}} \tag{5.45}$$

$$\theta_R = P_{0;\theta_R} + \frac{L_{EN}}{L_E} \cdot P_{L;\theta_R} + \frac{W_{EN}}{W_E} \cdot P_{W;\theta_R} + \frac{L_{EN} \cdot W_{EN}}{L_E \cdot W_E} \cdot P_{LW;\theta_R} \tag{5.46}$$

$$\theta_{sat} = P_{0;\theta_{sat}} + \frac{L_{EN}}{L_E} \cdot P_{L;\theta_{sat}} + \frac{W_{EN}}{W_E} \cdot P_{W;\theta_{sat}} + \frac{L_{EN} \cdot W_{EN}}{L_E \cdot W_E} \cdot P_{LW;\theta_{sat}} \tag{5.47}$$

Calculation of Conductance Parameters

$$\theta_{Th} = P_{0;\theta_{Th}} + \frac{L_{EN}}{L_E} \cdot P_{L;\theta_{Th}} + \frac{W_{EN}}{W_E} \cdot P_{W;\theta_{Th}} + \frac{L_{EN} \cdot W_{EN}}{L_E \cdot W_E} \cdot P_{LW;\theta_{Th}} \tag{5.48}$$

$$\sigma_{sf} = P_{0;\sigma_{sf}} + \frac{L_{EN}}{L_E} \cdot P_{L;\sigma_{sf}} + \frac{W_{EN}}{W_E} \cdot P_{W;\sigma_{sf}} + \frac{L_{EN} \cdot W_{EN}}{L_E \cdot W_E} \cdot P_{LW;\sigma_{sf}} \tag{5.49}$$

$$\alpha = P_{0;\alpha} + \frac{L_{EN}}{L_E} \cdot P_{L;\alpha} + \frac{W_{EN}}{W_E} \cdot P_{W;\alpha} + \frac{L_{EN} \cdot W_{EN}}{L_E \cdot W_E} \cdot P_{LW;\alpha} \tag{5.50}$$

Calculation of Sub–Threshold Parameters

$$\sigma_{dibl} = P_{0;\sigma_{dibl}} + \frac{L_{EN}}{L_E} \cdot P_{L;\sigma_{dibl}} + \frac{W_{EN}}{W_E} \cdot P_{W;\sigma_{dibl}} + \frac{L_{EN} \cdot W_{EN}}{L_E \cdot W_E} \cdot P_{LW;\sigma_{dibl}} \tag{5.51}$$

©Koninklijke Philips Electronics N.V. 2004

$$m_0 = P_{0;m_0} + \frac{L_{EN}}{L_E} \cdot P_{L;m_0} + \frac{W_{EN}}{W_E} \cdot P_{W;m_0} + \frac{L_{EN} \cdot W_{EN}}{L_E \cdot W_E} \cdot P_{LW;m_0} \tag{5.52}$$

Calculation of Smoothing Parameters

$$\frac{1}{m} = P_{0;m} + \frac{L_{EN}}{L_E} \cdot P_{L;m} + \frac{W_{EN}}{W_E} \cdot P_{W;m} + \frac{L_{EN} \cdot W_{EN}}{L_E \cdot W_E} \cdot P_{LW;m} \tag{5.53}$$

Calculation of Weak–Avalanche Parameters

$$a_1 = P_{0;a_1} + \frac{L_{EN}}{L_E} \cdot P_{L;a_1} + \frac{W_{EN}}{W_E} \cdot P_{W;a_1} + \frac{L_{EN} \cdot W_{EN}}{L_E \cdot W_E} \cdot P_{LW;a_1} \tag{5.54}$$

$$a_2 = P_{0;a_2} + \frac{L_{EN}}{L_E} \cdot P_{L;a_2} + \frac{W_{EN}}{W_E} \cdot P_{W;a_2} + \frac{L_{EN} \cdot W_{EN}}{L_E \cdot W_E} \cdot P_{LW;a_2} \tag{5.55}$$

$$a_3 = P_{0;a_3} + \frac{L_{EN}}{L_E} \cdot P_{L;a_3} + \frac{W_{EN}}{W_E} \cdot P_{W;a_3} + \frac{L_{EN} \cdot W_{EN}}{L_E \cdot W_E} \cdot P_{LW;a_3} \tag{5.56}$$

Calculation of Gate Current Parameters

$$I_{GINV} = P_{0;I_{GINV}} + \frac{L_E}{L_{EN}} \cdot P_{L;I_{GINV}} + \frac{W_E}{W_{EN}} \cdot P_{W;I_{GINV}} + \frac{L_E \cdot W_E}{L_{EN} \cdot W_{EN}} \cdot P_{LW;I_{GINV}} \tag{5.57}$$

$$B_{inv} = P_{0;B_{inv}} + \frac{L_{EN}}{L_E} \cdot P_{L;B_{inv}} + \frac{W_{EN}}{W_E} \cdot P_{W;B_{inv}} + \frac{L_{EN} \cdot W_{EN}}{L_E \cdot W_E} \cdot P_{LW;B_{inv}} \tag{5.58}$$

$$I_{GACC} = P_{0;I_{GACC}} + \frac{L_E}{L_{EN}} \cdot P_{L;I_{GACC}} + \frac{W_E}{W_{EN}} \cdot P_{W;I_{GACC}} + \frac{L_E \cdot W_E}{L_{EN} \cdot W_{EN}} \cdot P_{LW;I_{GACC}} \tag{5.59}$$

$$B_{acc} = P_{0;B_{acc}} + \frac{L_{EN}}{L_E} \cdot P_{L;B_{acc}} + \frac{W_{EN}}{W_E} \cdot P_{W;B_{acc}} + \frac{L_{EN} \cdot W_{EN}}{L_E \cdot W_E} \cdot P_{LW;B_{acc}} \tag{5.60}$$

$$I_{GOV} = P_{0;I_{GOV}} + \frac{L_{EN}}{L_E} \cdot P_{L;I_{GOV}} + \frac{W_E}{W_{EN}} \cdot P_{W;I_{GOV}} + \frac{W_E}{L_E} \cdot P_{LW;I_{GOV}} \tag{5.61}$$

Calculation of Gate-Induced Drain Leakage Parameters

$$A_{GIDL} = P_{0;A_{GIDL}} + \frac{L_{EN}}{L_E} \cdot P_{L;A_{GIDL}} + \frac{W_E}{W_{EN}} \cdot P_{W;A_{GIDL}} + \frac{W_E}{L_E} \cdot P_{LW;A_{GIDL}} \tag{5.62}$$

$$B_{GIDL} = P_{0;B_{GIDL}} + \frac{L_{EN}}{L_E} \cdot P_{L;B_{GIDL}} + \frac{W_{EN}}{W_E} \cdot P_{W;B_{GIDL}} + \frac{L_{EN} \cdot W_{EN}}{L_E \cdot W_E} \cdot P_{LW;B_{GIDL}} \tag{5.63}$$

$$C_{GIDL} = P_{0;C_{GIDL}} + \frac{L_{EN}}{L_E} \cdot P_{L;C_{GIDL}} + \frac{W_{EN}}{W_E} \cdot P_{W;C_{GIDL}} + \frac{L_{EN} \cdot W_{EN}}{L_E \cdot W_E} \cdot P_{LW;C_{GIDL}} \tag{5.64}$$

Calculation of Charge Parameters

$$C_{OX} = P_{0;C_{OX}} + \frac{L_E}{L_{EN}} \cdot P_{L;C_{OX}} + \frac{W_E}{W_{EN}} \cdot P_{W;C_{OX}} + \frac{L_E \cdot W_E}{L_{EN} \cdot W_{EN}} \cdot P_{LW;C_{OX}} \tag{5.65}$$

 ©Koninklijke Philips Electronics N.V. 2004

$$C_{\mathrm{GDO}} = P_{0;C_{\mathrm{GDO}}} + \frac{L_{\mathrm{EN}}}{L_{\mathrm{E}}} \cdot P_{\mathrm{L;C_{GDO}}} + \frac{W_{\mathrm{E}}}{W_{\mathrm{EN}}} \cdot P_{\mathrm{W;C_{GDO}}} + \frac{W_{\mathrm{E}}}{L_{\mathrm{E}}} \cdot P_{\mathrm{LW;C_{GDO}}} \quad (5.66)$$

$$C_{\mathrm{GSO}} = P_{0;C_{\mathrm{GSO}}} + \frac{L_{\mathrm{EN}}}{L_{\mathrm{E}}} \cdot P_{\mathrm{L;C_{GSO}}} + \frac{W_{\mathrm{E}}}{W_{\mathrm{EN}}} \cdot P_{\mathrm{W;C_{GSO}}} + \frac{W_{\mathrm{E}}}{L_{\mathrm{E}}} \cdot P_{\mathrm{LW;C_{GSO}}} \quad (5.67)$$

Calculation of Noise Parameters

$$N_{\mathrm{FA}} = P_{0;N_{\mathrm{FA}}} + \frac{L_{\mathrm{EN}}}{L_{\mathrm{E}}} \cdot P_{\mathrm{L;N_{FA}}} + \frac{W_{\mathrm{EN}}}{W_{\mathrm{E}}} \cdot P_{\mathrm{W;N_{FA}}} + \frac{L_{\mathrm{EN}} \cdot W_{\mathrm{EN}}}{L_{\mathrm{E}} \cdot W_{\mathrm{E}}} \cdot P_{\mathrm{LW;N_{FA}}} \quad (5.68)$$

$$N_{\mathrm{FB}} = P_{0;N_{\mathrm{FB}}} + \frac{L_{\mathrm{EN}}}{L_{\mathrm{E}}} \cdot P_{\mathrm{L;N_{FB}}} + \frac{W_{\mathrm{EN}}}{W_{\mathrm{E}}} \cdot P_{\mathrm{W;N_{FB}}} + \frac{L_{\mathrm{EN}} \cdot W_{\mathrm{EN}}}{L_{\mathrm{E}} \cdot W_{\mathrm{E}}} \cdot P_{\mathrm{LW;N_{FB}}} \quad (5.69)$$

$$N_{\mathrm{FC}} = P_{0;N_{\mathrm{FC}}} + \frac{L_{\mathrm{EN}}}{L_{\mathrm{E}}} \cdot P_{\mathrm{L;N_{FC}}} + \frac{W_{\mathrm{EN}}}{W_{\mathrm{E}}} \cdot P_{\mathrm{W;N_{FC}}} + \frac{L_{\mathrm{EN}} \cdot W_{\mathrm{EN}}}{L_{\mathrm{E}} \cdot W_{\mathrm{E}}} \cdot P_{\mathrm{LW;N_{FC}}} \quad (5.70)$$

Calculation of Threshold–Voltage Temperature–Scaling Coefficients

$$S_{\mathrm{T;V_{FB}}} = P_{0;\mathrm{T;V_{FB}}} + \frac{L_{\mathrm{EN}}}{L_{\mathrm{E}}} \cdot P_{\mathrm{L;T;V_{FB}}} + \frac{W_{\mathrm{EN}}}{W_{\mathrm{E}}} \cdot P_{\mathrm{W;T;V_{FB}}} + \frac{L_{\mathrm{EN}} \cdot W_{\mathrm{EN}}}{L_{\mathrm{E}} \cdot W_{\mathrm{E}}} \cdot P_{\mathrm{LW;T;V_{FB}}} \quad (5.71)$$

$$S_{\mathrm{T};\phi_{\mathrm{B}}} = P_{0;\mathrm{T};\phi_{\mathrm{B}}} + \frac{L_{\mathrm{EN}}}{L_{\mathrm{E}}} \cdot P_{\mathrm{L;T};\phi_{\mathrm{B}}} + \frac{W_{\mathrm{EN}}}{W_{\mathrm{E}}} \cdot P_{\mathrm{W;T};\phi_{\mathrm{B}}} + \frac{L_{\mathrm{EN}} \cdot W_{\mathrm{EN}}}{L_{\mathrm{E}} \cdot W_{\mathrm{E}}} \cdot P_{\mathrm{LW;T};\phi_{\mathrm{B}}} \quad (5.72)$$

Calculation of Mobility/Series–Resistance Temperature–Scaling Coefficients

$$\eta_{\beta} = P_{0;\mathrm{T};\eta_{\beta}} + \frac{L_{\mathrm{EN}}}{L_{\mathrm{E}}} \cdot P_{\mathrm{L;T};\eta_{\beta}} + \frac{W_{\mathrm{EN}}}{W_{\mathrm{E}}} \cdot P_{\mathrm{W;T};\eta_{\beta}} + \frac{L_{\mathrm{EN}} \cdot W_{\mathrm{EN}}}{L_{\mathrm{E}} \cdot W_{\mathrm{E}}} \cdot P_{\mathrm{LW;T};\eta_{\beta}} \quad (5.73)$$

$$\eta_{\mathrm{sr}} = P_{0;\mathrm{T};\eta_{\mathrm{sr}}} + \frac{L_{\mathrm{EN}}}{L_{\mathrm{E}}} \cdot P_{\mathrm{L;T};\eta_{\mathrm{sr}}} + \frac{W_{\mathrm{EN}}}{W_{\mathrm{E}}} \cdot P_{\mathrm{W;T};\eta_{\mathrm{sr}}} + \frac{L_{\mathrm{EN}} \cdot W_{\mathrm{EN}}}{L_{\mathrm{E}} \cdot W_{\mathrm{E}}} \cdot P_{\mathrm{LW;T};\eta_{\mathrm{sr}}} \quad (5.74)$$

$$\eta_{\mathrm{ph}} = P_{0;\mathrm{T};\eta_{\mathrm{ph}}} + \frac{L_{\mathrm{EN}}}{L_{\mathrm{E}}} \cdot P_{\mathrm{L;T};\eta_{\mathrm{ph}}} + \frac{W_{\mathrm{EN}}}{W_{\mathrm{E}}} \cdot P_{\mathrm{W;T};\eta_{\mathrm{ph}}} + \frac{L_{\mathrm{EN}} \cdot W_{\mathrm{EN}}}{L_{\mathrm{E}} \cdot W_{\mathrm{E}}} \cdot P_{\mathrm{LW;T};\eta_{\mathrm{ph}}} \quad (5.75)$$

$$S_{\mathrm{T};\eta_{\mathrm{mob}}} = P_{0;\mathrm{T};\eta_{\mathrm{mob}}} + \frac{L_{\mathrm{EN}}}{L_{\mathrm{E}}} \cdot P_{\mathrm{L;T};\eta_{\mathrm{mob}}} + \frac{W_{\mathrm{EN}}}{W_{\mathrm{E}}} \cdot P_{\mathrm{W;T};\eta_{\mathrm{mob}}} + \frac{L_{\mathrm{EN}} \cdot W_{\mathrm{EN}}}{L_{\mathrm{E}} \cdot W_{\mathrm{E}}} \cdot P_{\mathrm{LW;T};\eta_{\mathrm{mob}}} \quad (5.76)$$

$$\nu_{\mathrm{exp}} = P_{0;\mathrm{T};\nu_{\mathrm{exp}}} + \frac{L_{\mathrm{EN}}}{L_{\mathrm{E}}} \cdot P_{\mathrm{L;T};\nu_{\mathrm{exp}}} + \frac{W_{\mathrm{EN}}}{W_{\mathrm{E}}} \cdot P_{\mathrm{W;T};\nu_{\mathrm{exp}}} + \frac{L_{\mathrm{EN}} \cdot W_{\mathrm{EN}}}{L_{\mathrm{E}} \cdot W_{\mathrm{E}}} \cdot P_{\mathrm{LW;T};\nu_{\mathrm{exp}}} \quad (5.77)$$

$$\eta_{\mathrm{R}} = P_{0;\mathrm{T};\eta_{\mathrm{R}}} + \frac{L_{\mathrm{EN}}}{L_{\mathrm{E}}} \cdot P_{\mathrm{L;T};\eta_{\mathrm{R}}} + \frac{W_{\mathrm{EN}}}{W_{\mathrm{E}}} \cdot P_{\mathrm{W;T};\eta_{\mathrm{R}}} + \frac{L_{\mathrm{EN}} \cdot W_{\mathrm{EN}}}{L_{\mathrm{E}} \cdot W_{\mathrm{E}}} \cdot P_{\mathrm{LW;T};\eta_{\mathrm{R}}} \quad (5.78)$$

$$\eta_{\mathrm{sat}} = P_{0;\mathrm{T};\eta_{\mathrm{sat}}} + \frac{L_{\mathrm{EN}}}{L_{\mathrm{E}}} \cdot P_{\mathrm{L;T};\eta_{\mathrm{sat}}} + \frac{W_{\mathrm{EN}}}{W_{\mathrm{E}}} \cdot P_{\mathrm{W;T};\eta_{\mathrm{sat}}} + \frac{L_{\mathrm{EN}} \cdot W_{\mathrm{EN}}}{L_{\mathrm{E}} \cdot W_{\mathrm{E}}} \cdot P_{\mathrm{LW;T};\eta_{\mathrm{sat}}} \quad (5.79)$$

Calculation of Weak–Avalanche Temperature–Scaling Coefficients

$$S_{\mathrm{T;a_1}} = P_{0;\mathrm{T;a_1}} + \frac{L_{\mathrm{EN}}}{L_{\mathrm{E}}} \cdot P_{\mathrm{L;T;a_1}} + \frac{W_{\mathrm{EN}}}{W_{\mathrm{E}}} \cdot P_{\mathrm{W;T;a_1}} + \frac{L_{\mathrm{EN}} \cdot W_{\mathrm{EN}}}{L_{\mathrm{E}} \cdot W_{\mathrm{E}}} \cdot P_{\mathrm{LW;T;a_1}} \quad (5.80)$$

©Koninklijke Philips Electronics N.V. 2004

Calculation of Gate–Induced Drain Leakage Temperature–Scaling Coefficients

$$S_{\mathrm{T;B_{GIDL}}} = P_{\mathrm{0;T;B_{GIDL}}} + \frac{L_{\mathrm{EN}}}{L_{\mathrm{E}}} \cdot P_{\mathrm{L;T;B_{GIDL}}} + \frac{W_{\mathrm{EN}}}{W_{\mathrm{E}}} \cdot P_{\mathrm{W;T;B_{GIDL}}} + \frac{L_{\mathrm{EN}} \cdot W_{\mathrm{EN}}}{L_{\mathrm{E}} \cdot W_{\mathrm{E}}} \cdot P_{\mathrm{LW;T;B_{GIDL}}} \quad (5.81)$$

 ©Koninklijke Philips Electronics N.V. 2004

5.3 Calculation of Temperature-Dependent Parameters

Calculation of Transistor Temperature

Note: Note the addition of the voltage V_{dT} of the thermal node in order to include self-heating, see Section 4.2.

$$T_{KR} = T_0 + T_R \tag{5.82}$$

$$T_{amb} = T_0 + T_A + \Delta T_A \tag{5.83}$$

$$T_{KD} = T_0 + T_A + \Delta T_A + V_{dT} \tag{5.84}$$

Calculation of Threshold–Voltage Parameters

$$\phi_T = \frac{k_B \cdot T_{KD}}{q} \tag{5.85}$$

$$V_{FB_T} = V_{FB} + (T_{KD} - T_{KR}) \cdot S_{T;V_{FB}} \tag{5.86}$$

$$\phi_{B_T} = \phi_B + (T_{KD} - T_{KR}) \cdot S_{T;\phi_B} \tag{5.87}$$

Calculation of Mobility/Series-Resistance Parameters

$$\beta_T = \beta \cdot \left(\frac{T_{KR}}{T_{KD}}\right)^{\eta_\beta} \tag{5.88}$$

$$\theta_{sr_T} = \theta_{sr} \cdot \left(\frac{T_{KR}}{T_{KD}}\right)^{\eta_{sr}} \tag{5.89}$$

$$\theta_{ph_T} = \theta_{ph} \cdot \left(\frac{T_{KD}}{T_{KR}}\right)^{\eta_{ph}} \tag{5.90}$$

$$\eta_{mob_T} = \eta_{mob} \cdot \left[1 + (T_{KD} - T_{KR}) \cdot S_{T;\eta_{mob}}\right] \tag{5.91}$$

$$\nu_T = 1 + (\nu - 1) \cdot \left(T_{KR} / T_{KD}\right)^{\nu_{exp}} \tag{5.92}$$

$$\theta_{R_T} = \theta_R \cdot \left(\frac{T_{KR}}{T_{KD}}\right)^{\eta_R} \tag{5.93}$$

$$\theta_{sat_T} = \theta_{sat} \cdot \left(\frac{T_{KR}}{T_{KD}}\right)^{\eta_{sat}} \tag{5.94}$$

Calculation of Conductance Parameters

$$\theta_{Th_T} = \theta_{Th} \cdot \left(\frac{T_{KR}}{T_{KD}}\right)^{\eta_\beta} \tag{5.95}$$

Calculation of Weak–Avalanche Parameters

$$a_{1_T} = a_1 \cdot \left[1 + (T_{KD} - T_{KR}) \cdot S_{T;a_1}\right] \tag{5.96}$$

©Koninklijke Philips Electronics N.V. 2004

Calculation of Gate–Induced Drain Leakage Parameters

$$B_{\mathrm{GIDL_T}} = B_{\mathrm{GIDL}} \cdot \left[1 + (T_{\mathrm{KD}} - T_{\mathrm{KR}}) \cdot S_{\mathrm{T;B_{GIDL}}}\right] \tag{5.97}$$

Calculation of Noise Parameters

$$N_{\mathrm{T_T}} = \frac{T_{\mathrm{KD}}}{T_{\mathrm{KR}}} \cdot N_{\mathrm{T}} \tag{5.98}$$

Calculation of Thermal Resistance

$$R_{\mathrm{Th_T}} = R_{\mathrm{Th}} \cdot \left(\frac{T_{\mathrm{amb}}}{T_{\mathrm{KR}}}\right)^{A_{\mathrm{Th}}} \tag{5.99}$$

 ©Koninklijke Philips Electronics N.V. 2004

5.4 Clipping

The clipping of parameters is discussed in Section 8.

©Koninklijke Philips Electronics N.V. 2004

 ©Koninklijke Philips Electronics N.V. 2004

6 Implemented Model Equations

The electrical equations of MOS Model 11 to be implemented are essentially the basic equations of Section 2. Since in circuit design equal parallel circuited transistors are frequently applied the specification of one transistor together with a multiplication factor N_{MULT} in the circuit description is convenient and saves computation time. The general and safe method to implement this mechanism into the model is to evaluate the currents, charges, noise spectral densities and their derivatives with respect to the external voltages and, at the end, to multiply them by N_{MULT}. In MOS Model 11 it is allowed to circumvent these multiplications for each model evaluation during circuit simulation by adjusting some parameters. In this case the following rules apply:

$$\begin{aligned}
\beta &= \beta \cdot N_{\mathrm{MULT}} \\
I_{\mathrm{GINV}} &= I_{\mathrm{GINV}} \cdot N_{\mathrm{MULT}} \\
I_{\mathrm{GACC}} &= I_{\mathrm{GACC}} \cdot N_{\mathrm{MULT}} \\
I_{\mathrm{GOV}} &= I_{\mathrm{GOV}} \cdot N_{\mathrm{MULT}} \\
A_{\mathrm{GIDL}} &= A_{\mathrm{GIDL}} \cdot N_{\mathrm{MULT}} \\
C_{\mathrm{OX}} &= C_{\mathrm{OX}} \cdot N_{\mathrm{MULT}} \\
C_{\mathrm{GDO}} &= C_{\mathrm{GDO}} \cdot N_{\mathrm{MULT}} \\
C_{\mathrm{GSO}} &= C_{\mathrm{GSO}} \cdot N_{\mathrm{MULT}} \\
N_{\mathrm{FA}} &= \frac{N_{\mathrm{FA}}}{N_{\mathrm{MULT}}} \\
N_{\mathrm{FB}} &= \frac{N_{\mathrm{FB}}}{N_{\mathrm{MULT}}} \\
N_{\mathrm{FC}} &= \frac{N_{\mathrm{FC}}}{N_{\mathrm{MULT}}} \\
R_{\mathrm{Th}} &= \frac{R_{\mathrm{Th}}}{N_{\mathrm{MULT}}} \\
C_{\mathrm{Th}} &= C_{\mathrm{Th}} \cdot N_{\mathrm{MULT}}
\end{aligned}$$

Although the basic equations, given in Section 2, form a complete set of model equations, they are not yet suited for a circuit simulator. Several equations have to be adapted in order to obtain smooth transitions of the characteristics between adjacent regions of operation and to prevent numerical problems during the iteration process for solving the network equations. In the following section a list of numerical adaptations and elucidations is given, followed by the extended set of model equations.

The definition of the hyp-function, which provides for a smooth C_{∞}-continuous clipping, is to be found in Appendix A.

6.1 Numerical Adaptations

The implemented electrical equations of MOS Model 11 are essentially based on the physical description given in Section 2. The following numerical adaptations have been made in order to obtain

smooth transitions and prevent numerical problems, leading to the equations given in Section6.2:

- The piece-wise eqs. (2.19) for $V_{\mathrm{GB_{eff}}}$, (2.22) for D_{sf}, (2.27) for $V_{\mathrm{DSAT_{long}}}$, (2.31) for V_{DSAT} and (2.75) for I_{GB} have been replaced by smooth C_∞-continuous functions based on hyp-functions.

- Expression (2.21) describing the drain-induced barrier lowering effect has no numerical solution for $V_{\mathrm{SB}} + \phi_{\mathrm{B_T}} < 0$. In order to solve this problem the expression $V_{\mathrm{SB}} + \phi_{\mathrm{B_T}}$ is clipped at a minimum value of $0.1 \cdot \phi_{\mathrm{B_T}}$ using eq. (6.2). At the drain side, eq. (6.16) is used. This equation automatically maintains symmetry.

- In the accumulation region (i.e., $V^*_{\mathrm{GB}} \leq 0$), the inversion-layer charge density is equal to zero (i.e., $V_{\mathrm{inv_0}} = V_{\mathrm{inv_L}} = 0$), as a result the drain-source channel current I_{DS}, the weak-avalanche current I_{avl}, the gate-to-channel current I_{GC}, the total drain charge Q_{D} and source charge Q_{S}, and the noise spectral densities S_{th}, S_{fl} and S_{ig} are all equal to zero. In this case, the model equations can be simplified and only certain equations need to be calculated. The equations that only need to be calculated in the inversion region (i.e., $V^*_{\mathrm{GB}} > 0$) are indicated.

- For very small positive values of ψ_{s} (i.e., $\psi_{\mathrm{s}} < 10^{-9}$ just above $V^*_{\mathrm{GB}} = 0$, the expression (2.40) for V_{inv} may become numerically inaccurate. In this case V_{inv} is very small and can be taken to be equal to zero, see (6.37).

- The theoretical channel length modulation expression (2.52) can become negative for high values of α and V_{DS}. This corresponds to a negative effective channel length, which is not physical. In order to prevent $G_{\Delta L}$ from becoming negative, a second-order Taylor polynomial in $\Delta L/L$ is used in the actual implementation, see eqs. (6.49) and (6.50).

- The term in the square root of eq. (2.57) can become negative for very high values of parameter $\theta_{\mathrm{R_T}}$, which would result in numerical errors. This has been prevented in the actual implementation (6.56) by using a hyp-smoothing function.

- The derivative of the weak-avalanche expression (2.61) with respect to V_{DS} may become numerically unstable for V_{DS} values just above $a_3 \cdot V_{\mathrm{DSAT}}$. This problem has been circumvented by using (6.60), where A is a numerical constant defined in Section 3.2.1.

- The exponent in the tunnelling probability P_{tun}, given by eq. (2.69), results in zero divided by zero for $V_{\mathrm{ox}} = 0$. By simply rewriting the exponent, this problem can be circumvented as has been done in eq. (6.82).

- For very high gate bias values, which could occur during the iteration process of the circuit simulator, the expression of effective oxide barrier $\chi_{\mathrm{B_{eff}}}$, given by eq. (2.77), can become zero or negative resulting in numerical errors. In order to prevent this problem $\chi_{\mathrm{B_{eff}}}$ is clipped at a minimum (arbitrary) value of $0.7 \cdot \chi_{\mathrm{B_{inv}}}$ using a hyp-smoothing function, see eq. (6.91).

- Gate-induced drain (or source) leakage only occurs when the oxide voltage in the drain overlap region is negative, in other words when the overlapped n^+-drain region is depleted. For positive oxide voltage, no GIDL occurs, because, as the overlapped region is in accumulation, the band bending is minimal and as a result band-to-band tunnelling cannot occur. This is, however, not automatically accomplished using (2.90). In order to take this effect into account empirically, we replace V_{ov} in (2.89) by a smoothing function which is equal to V_{ov} for negative values of V_{ov} and equal to 0 for positive values, see (6.103).

 ©Koninklijke Philips Electronics N.V. 2004

- Similar to the weak-avalanche epression (2.61), the derivatives of the gate-induced drain leakage expression (2.90) may become numerically unstable for V_{tov} very close to 0. This problem has been circumvented in the same way as has been done for (6.60), see eq. (6.104)
- The expression of effective oxide capacitance (2.95) due to quantum-mechanical effects gives erroneous results for $V_{eff} = 0$ (i.e., $V^{*}_{GB} = 0$). This can be prevented by replacing V_{eff} / η_{mob} by $\sqrt{\left(V_{eff} / \eta_{mob}\right)^2 + (20 \cdot \phi_T)^2}$, where the value of $20 \cdot \phi_T$ is rather arbitrary but it nevertheless ensures a smooth transition from accumulation to depletion/inversion.
- The thermal noise spectral density S_{th} given by eq. (2.110) can become negative for very high values of parameter θ_{sat}, which is not physical. In order to prevent this, S_{th} is clipped to zero in these cases, see eq. (6.124).

©Koninklijke Philips Electronics N.V. 2004

6.2 Extended Equations

In the following sections a function is denoted by $F\{variable, \ldots\}$, where F denotes the function name and the function variables are enclosed by braces {}. The definitions of the hyp-functions are found in Appendix A.

6.2.1 Internal Parameters

$$\epsilon_1 = 1 \cdot 10^{-2}$$

$$\epsilon_2 = 4 \cdot 10^{-2}$$

$$\epsilon_3 = 1 \cdot 10^{-4}$$

$$P_D = 1 + \left(k_0 / k_P\right)^2$$

$$V_{\text{limit}} = 4 \cdot \phi_T$$

$$\theta_{R_{\text{eff}}} = \frac{1}{2} \cdot \theta_{R_T} \cdot \left(1 + \frac{\theta_{R1}}{1/2 + \theta_{R2}}\right)$$

$$m_{\phi_T} = (1 + m_0) \cdot \phi_T$$

$$Acc = \left.\frac{\partial \psi_s}{\partial V_{GB}}\right|_{V_{GB}=V_{FB_T}} = \frac{1}{1 + k_0 / \sqrt{2\phi_T}}$$

$$Acc_{\text{ov}} = \left.\frac{\partial \psi_{\text{sov}}}{\partial V_{GB}}\right|_{V_{GB}=V_{FBov}} = \frac{1}{1 + k_{\text{ov}} / \sqrt{2\phi_T}}$$

$$QM_\psi = \begin{cases} QM_N \cdot \left(\epsilon_{\text{ox}} / t_{\text{ox}}\right)^{2/3} & \text{for NMOS} \\ QM_P \cdot \left(\epsilon_{\text{ox}} / t_{\text{ox}}\right)^{2/3} & \text{for PMOS} \end{cases}$$

$$QM_{t_{\text{ox}}} = \frac{2}{5} \cdot QM_\psi$$

$$\chi_{B_{\text{inv}}} = \begin{cases} \chi_{B_N} & \text{for NMOS} \\ \chi_{B_P} & \text{for PMOS} \end{cases}$$

$$\chi_{B_{\text{acc}}} = \chi_{B_N}$$

6.2.2 Extended Current Equations

$$V_{GB_{\text{eff}}} = \text{hyp}_1\left\{V_{GS} + V_{SB} - V_{FB_T}, \epsilon_1\right\} \tag{6.1}$$

$$V_{SB_t} = \text{hyp}_1\left\{V_{SB} + 0.9 \cdot \phi_{B_T}, \epsilon_1\right\} + 0.1 \cdot \phi_{B_T} \tag{6.2}$$

$$\psi_{\text{sat}_0} = \left(\frac{\sqrt{P_D \cdot V_{GB_{\text{eff}}} + {k_0}^2/4} - k_0/2}{P_D}\right)^2 \tag{6.3}$$

 ©Koninklijke Philips Electronics N.V. 2004

Drain induced barrier lowering and Static Feedback:

$$D_{\mathrm{dibl}} = \sigma_{\mathrm{dibl}} \cdot \sqrt{V_{\mathrm{SB_t}}} \tag{6.4}$$

$$D_{\mathrm{sf}} = \sigma_{\mathrm{sf}} \cdot \sqrt{\mathrm{hyp}_1\left\{\psi_{\mathrm{sat_0}} - V_{\mathrm{SB_t}}, \epsilon_2\right\}} \tag{6.5}$$

$$V_{\mathrm{DS_{eff}}} = \frac{{V_{\mathrm{DS}}}^4}{\left({V_{\mathrm{limit}}}^2 + {V_{\mathrm{DS}}}^2\right)^{3/2}} \tag{6.6}$$

$$\Delta V_{\mathrm{G}} = \sqrt{{D_{\mathrm{dibl}}}^2 + {D_{\mathrm{sf}}}^2} \cdot V_{\mathrm{DS_{eff}}} \tag{6.7}$$

Effective Gate-Bulk Voltage:

$$V_{\mathrm{GB}}^* = V_{\mathrm{GS}} + V_{\mathrm{SB}} + \Delta V_{\mathrm{G}} - V_{\mathrm{FB_T}} \tag{6.8}$$

Drain Saturation Voltage Eqs. (6.9)-(6.13) are only calculated for $V_{\mathrm{GB}}^* > 0$:

$$\psi_{\mathrm{sat_1}} = \left(\frac{\sqrt{P_{\mathrm{D}} \cdot V_{\mathrm{GB}}^* + {k_0}^2/4} - k_0/2}{P_{\mathrm{D}}}\right)^2 \tag{6.9}$$

$$V_{\mathrm{DSAT_{long}}} = \psi_{\mathrm{sat_1}} - V_{\mathrm{SB_t}} \tag{6.10}$$

$$T_{\mathrm{sat}} = \begin{cases} \theta_{\mathrm{sat_T}} & \text{for NMOS} \\ \dfrac{\theta_{\mathrm{sat_T}}}{\left(1 + {\theta_{\mathrm{sat_T}}}^2 \cdot {V_{\mathrm{DSAT_{long}}}}^2\right)^{1/4}} & \text{for PMOS} \end{cases} \tag{6.11}$$

$$\Delta_{\mathrm{SAT}} = \frac{\left(T_{\mathrm{sat}} - \theta_{\mathrm{R_{eff}}}\right) \cdot V_{\mathrm{DSAT_{long}}}}{\frac{1}{2} \cdot \left(\sqrt{2} + \sqrt{2 + 2 \cdot {T_{\mathrm{sat}}}^2 \cdot {V_{\mathrm{DSAT_{long}}}}^2}\right) + \theta_{\mathrm{R_{eff}}} \cdot V_{\mathrm{DSAT_{long}}}} \tag{6.12}$$

$$V_{\mathrm{DSAT_{short}}} = V_{\mathrm{DSAT_{long}}} \cdot \left[1 - \frac{44/45 \cdot \Delta_{\mathrm{SAT}}}{1 + \sqrt{1 - \frac{\left(\sqrt{2}-1\right) \cdot T_{\mathrm{sat}} - \theta_{\mathrm{R_{eff}}}}{T_{\mathrm{sat}} - \theta_{\mathrm{R_{eff}}}} \cdot {\Delta_{\mathrm{SAT}}}^2}}\right] \tag{6.13}$$

$$V_{\mathrm{DSAT}} = \begin{cases} V_{\mathrm{limit}} & \text{for:} \quad V_{\mathrm{GB}}^* \leq 0 \\ V_{\mathrm{limit}} + \mathrm{hyp}_1\left\{V_{\mathrm{DSAT_{short}}} - V_{\mathrm{limit}}, \epsilon_2\right\} & \text{for:} \quad V_{\mathrm{GB}}^* > 0 \end{cases} \tag{6.14}$$

$$V_{\mathrm{DS_x}} = \frac{V_{\mathrm{DS}}}{\left[1 + \left(V_{\mathrm{DS}}/V_{\mathrm{DSAT}}\right)^{2 \cdot m}\right]^{\frac{1}{2 \cdot m}}} \tag{6.15}$$

$$V_{\mathrm{DB_t}} = V_{\mathrm{DS_x}} + \phi_{\mathrm{B_T}} \tag{6.16}$$

©Koninklijke Philips Electronics N.V. 2004

Surface Potential:

The surface potential ψ_s is given by the following implicit relation:

$$F\{\psi_s, \phi\} = -V_{ox}\{\psi_s\}^2 + k_0{}^2 \cdot d\{\psi_s, \phi\} = 0 \tag{6.17}$$

where ϕ can be either V_{SB_t} or V_{DB_t}, and:

$$V^*_{GC}\{\psi_s\} = V^*_{GB} - \psi_s \tag{6.18}$$

$$c\{\psi_s\} = \frac{1}{2} + \frac{1}{2} \cdot \sqrt{1 + 4/k_P{}^2 \cdot \mathrm{hyp}_1\left\{V^*_{GC}\{\psi_s\}, \epsilon_1\right\}} \tag{6.19}$$

$$V_{ox}\{\psi_s\} = \frac{V^*_{GC}\{\psi_s\}}{c\{\psi_s\}} \tag{6.20}$$

$$\begin{aligned} d\{\psi_s, \phi\} = {} & \psi_s + \phi_T \cdot \left[\exp\left(-\frac{\psi_s}{\phi_T}\right) - 1\right] \\ & + \phi_T \cdot \exp\left(-\frac{\phi}{m_{\phi_T}}\right) \cdot \left[\exp\left(\frac{\psi_s}{m_{\phi_T}}\right) - \frac{\psi_s}{m_{\phi_T}} - 1\right] \end{aligned} \tag{6.21}$$

The surface potential is iteratively calculated using a second-order Newton Raphson procedure, where the surface potential ψ_{i+1} in the $i+1^{th}$ iteration is given in terms of the surface potential ψ_i in the ith iteration by:

$$\psi_{i+1} = \psi_i - \frac{F_i}{F_i^{'} - \frac{1}{2} \cdot F_i \cdot F_i^{''} \big/ F_i^{'}} \tag{6.22}$$

where:

$$F_i = F\{\psi_i, \phi\} = -V_{ox}\{\psi_i\}^2 + k_0{}^2 \cdot d\{\psi_i, \phi\} \tag{6.23}$$

$$F_i^{'} = \left.\frac{\partial F\{\psi_s, \phi\}}{\partial \psi_s}\right|_{\psi_s = \psi_i} = -2 \cdot V_{ox}\{\psi_i\} \cdot V_{ox}^{'}\{\psi_i\} + k_0{}^2 \cdot d^{'}\{\psi_i, \phi\} \tag{6.24}$$

$$F_i^{''} = \left.\frac{\partial^2 F\{\psi_s, \phi\}}{\partial \psi_s{}^2}\right|_{\psi_s = \psi_i} = -2 \cdot V_{ox}^{'}\{\psi_i\}^2 - 2 \cdot V_{ox}\{\psi_i\} \cdot V_{ox}^{''}\{\psi_i\} + k_0{}^2 \cdot d^{''}\{\psi_i, \phi\} \tag{6.25}$$

The first-order and second-order derivatives are given by:

$$c^{'}\{\psi_s\} = \frac{\partial c\{\psi_s\}}{\partial \psi_s} = -\frac{1}{4} \cdot \frac{4/k_P{}^2}{2 \cdot c\{\psi_s\} - 1} \cdot \frac{\partial \mathrm{hyp}_1\left\{V^*_{GC}\{\psi_s\}, \epsilon_1\right\}}{\partial V^*_{GC}} \tag{6.26}$$

$$c^{''}\{\psi_s\} = \frac{\partial^2 c\{\psi_s\}}{\partial \psi_s{}^2} = -\frac{2 \cdot c^{'}\{\psi_s\}^2 - \frac{1}{k_P{}^2} \cdot \frac{\partial^2 \mathrm{hyp}_1\{V^*_{GC}\{\psi_s\}, \epsilon_1\}}{\partial V^{*\,2}_{GC}}}{2 \cdot c\{\psi_s\} - 1} \tag{6.27}$$

$$V_{ox}^{'}\{\psi_s\} = \frac{\partial V_{ox}\{\psi_s\}}{\partial \psi_s} = -\frac{1 + V_{ox}\{\psi_s\} \cdot c^{'}\{\psi_s\}}{c\{\psi_s\}} \tag{6.28}$$

 ©Koninklijke Philips Electronics N.V. 2004

$$V_{\mathrm{ox}}^{''}\{\psi_{\mathrm{s}}\} = \frac{\partial^2 V_{\mathrm{ox}}\{\psi_{\mathrm{s}}\}}{\partial \psi_{\mathrm{s}}^2} = -\frac{2 \cdot c^{'}\{\psi_{\mathrm{s}}\} \cdot V_{\mathrm{ox}}^{'}\{\psi_{\mathrm{s}}\} + V_{\mathrm{ox}}\{\psi_{\mathrm{s}}\} \cdot c^{''}\{\psi_{\mathrm{s}}\}}{c\{\psi_{\mathrm{s}}\}} \tag{6.29}$$

$$\begin{aligned} d^{'}\{\psi_{\mathrm{s}}, \phi\} &= \frac{\partial d\{\psi_{\mathrm{s}}, \phi\}}{\partial \psi_{\mathrm{s}}} \\ &= 1 - \exp\left(-\frac{\psi_{\mathrm{s}}}{\phi_{\mathrm{T}}}\right) + \frac{\phi_{\mathrm{T}}}{m_{\phi_{\mathrm{T}}}} \cdot \exp\left(-\frac{\phi}{m_{\phi_{\mathrm{T}}}}\right) \cdot \left[\exp\left(\frac{\psi_{\mathrm{s}}}{m_{\phi_{\mathrm{T}}}}\right) - 1\right] \end{aligned} \tag{6.30}$$

$$d^{''}\{\psi_{\mathrm{s}}, \phi\} = \frac{\partial^2 d\{\psi_{\mathrm{s}}, \phi\}}{\partial \psi_{\mathrm{s}}^2} = \frac{\exp\left(-\frac{\psi_{\mathrm{s}}}{\phi_{\mathrm{T}}}\right)}{\phi_{\mathrm{T}}} + \frac{\phi_{\mathrm{T}}}{m_{\phi_{\mathrm{T}}}} \cdot \frac{\exp\left(\frac{\psi_{\mathrm{s}} - \phi}{m_{\phi_{\mathrm{T}}}}\right)}{m_{\phi_{\mathrm{T}}}} \tag{6.31}$$

The iterative loop is performed until $|\psi_{\mathrm{i+1}} - \psi_{\mathrm{i}}| < 10^{-10} \cdot \phi_{\mathrm{T}}$, at which point ψ_{s} is taken to be equal to $\psi_{\mathrm{i+1}}$. As a zero-order starting value ψ_0, the following approximation is used:

$$\begin{cases} \text{if } V_{\mathrm{GB}}^{*} \geq \phi_{\mathrm{T}} & \begin{cases} \psi_{\mathrm{sat}} = \left(\frac{\sqrt{P_{\mathrm{D}} \cdot (V_{\mathrm{GB}}^{*} - \phi_{\mathrm{T}}) + k_0^2/4} - k_0/2}{P_{\mathrm{D}}}\right)^2 + \phi_{\mathrm{T}} \\ \text{if } \psi_{\mathrm{sat}} \leq \phi & \begin{cases} \psi_0 = \psi_{\mathrm{sat}} \end{cases} \\ \text{if } \psi_{\mathrm{sat}} > \phi & \begin{cases} V_{\mathrm{ox}} = \frac{2 \cdot [V_{\mathrm{GB}}^{*} - \phi]}{1 + \sqrt{1 + 4/k_{\mathrm{P}}^2 \cdot [V_{\mathrm{GB}}^{*} - \phi]}} \\ x = k_0^2 \cdot \max\left(V_{\mathrm{ox}}^2 / k_0^2 - \phi + \phi_{\mathrm{T}}, \phi_{\mathrm{T}}\right) \\ y = k_0^2 + \frac{2 \cdot V_{\mathrm{ox}}}{\sqrt{1 + 4/k_{\mathrm{P}}^2 \cdot [V_{\mathrm{GB}}^{*} - \phi]}} \\ z = 1 + 4/k_{\mathrm{P}}^2 \cdot \left(V_{\mathrm{GB}}^{*} - \phi\right) \\ \psi_0 = \phi + \frac{2 \cdot m_{\phi_{\mathrm{T}}} \cdot x \cdot \ln\left(\frac{x}{\phi_{\mathrm{T}} \cdot k_0^2}\right)}{x + m_{\phi_{\mathrm{T}}} \cdot y + \sqrt{\left(x + m_{\phi_{\mathrm{T}}} \cdot y\right)^2 - m_{\phi_{\mathrm{T}}}^2 \cdot \left(x/z - y^2/2\right) \cdot \ln\left(\frac{x}{\phi_{\mathrm{T}} \cdot k_0^2}\right)}} \end{cases} \end{cases} \\ \text{if } V_{\mathrm{GB}}^{*} < \phi_{\mathrm{T}} & \begin{cases} \text{if } V_{\mathrm{GB}}^{*} \geq 0 & \begin{cases} \psi_0 = 0 \end{cases} \\ \text{if } V_{\mathrm{GB}}^{*} < 0 & \begin{cases} x = V_{\mathrm{GB}}^{*\,2} + \phi_{\mathrm{T}} \cdot k_0^2 \\ y = k_0^2 + 2 \cdot V_{\mathrm{GB}}^{*} \\ \psi_0 = -\frac{2 \cdot \phi_{\mathrm{T}} \cdot x \cdot \ln\left(\frac{x}{\phi_{\mathrm{T}} \cdot k_0^2}\right)}{x - \phi_{\mathrm{T}} \cdot y + \sqrt{(x - \phi_{\mathrm{T}} \cdot y)^2 - \phi_{\mathrm{T}}^2 \cdot \left(x - y^2/2\right) \cdot \ln\left(\frac{x}{\phi_{\mathrm{T}} \cdot k_0^2}\right)}} \end{cases} \end{cases} \end{cases} \tag{6.32}$$

When $V_{\mathrm{GB}}^{*} = 0$, the starting value ψ_0 is equal to zero. No iterative solution is necessary, and ψ_{s} is automatically taken to be equal to zero. Surface potentials at source and drain are now calculated

©Koninklijke Philips Electronics N.V. 2004

from the following implicit relations:

$$F\left\{\psi_{s_0}, V_{SB_t}\right\} = 0 \tag{6.33}$$

$$F\left\{\psi_{s_L}, V_{DB_t}\right\} = 0 \tag{6.34}$$

Auxiliary Variables:

$$\Delta\psi = \psi_{s_L} - \psi_{s_0} \tag{6.35}$$

$$\bar{\psi} = \frac{\psi_{s_L} + \psi_{s_0}}{2} \tag{6.36}$$

Inversion-Layer Charge ($Q_{inv} = -\epsilon_{ox} / t_{ox} \cdot V_{inv}$):

$$V_{inv}\{\psi_s, \phi\} = \begin{cases} 0 & \text{for: } V_{GB}^* - \psi_s \leq 0 \\ \frac{k_0 \cdot \phi_T \cdot \exp(-\phi/m_{\phi_T}) \cdot [\exp(\psi_s/m_{\phi_T}) - \psi_s/m_{\phi_T} - 1]}{\sqrt{d\{\phi, \psi_s\}} + \sqrt{\psi_s + \phi_T \cdot [\exp(-\psi_s/\phi_T) - 1]}} & \text{for: } V_{GB}^* - \psi_s > 0 \end{cases} \tag{6.37}$$

$$V_{inv_0} = V_{inv}\left\{\psi_{s_0}, V_{SB_t}\right\} \tag{6.38}$$

$$V_{inv_L} = V_{inv}\left\{\psi_{s_L}, V_{DB_t}\right\} \tag{6.39}$$

$$\bar{V}_{inv} = \frac{V_{inv_0} + V_{inv_L}}{2} \tag{6.40}$$

$$\bar{V}_{ox} = \frac{V_{ox}\left\{\psi_{s_0}\right\} + V_{ox}\left\{\psi_{s_L}\right\}}{2} \tag{6.41}$$

$$V_{eff} = \bar{V}_{inv} + \eta_{mob_T} \cdot \left(\bar{V}_{ox} - \bar{V}_{inv}\right) \tag{6.42}$$

$$\xi_{ox}\{\psi_s\} = -\phi_T \cdot V_{ox}^{'}\{\psi_s\} \tag{6.43}$$

$$\bar{\xi}_{ox} = \frac{\xi_{ox}\left\{\psi_{s_0}\right\} + \xi_{ox}\left\{\psi_{s_L}\right\}}{2} \tag{6.44}$$

$$\xi\{\psi_s\} = \begin{cases} \xi_{ox}\{\psi_s\} + \phi_T \cdot \left[\frac{1}{Acc} - 1\right] & \text{for: } V_{GB}^* - \psi_s \leq 0 \\ \xi_{ox}\{\psi_s\} + \phi_T \cdot \frac{k_0 \cdot [1 - \exp(-\psi_s/\phi_T)]}{2 \cdot \sqrt{\psi_s + \phi_T \cdot [\exp(-\psi_s/\phi_T) - 1]}} & \text{for: } V_{GB}^* - \psi_s > 0 \end{cases} \tag{6.45}$$

$$\bar{\xi} = \frac{\xi\left\{\psi_{s_0}\right\} + \xi\left\{\psi_{s_L}\right\}}{2} \tag{6.46}$$

$$\bar{V}_{inv}^* = \bar{V}_{inv} + (1 + m_0) \cdot \bar{\xi} \tag{6.47}$$

 ©Koninklijke Philips Electronics N.V. 2004

Second-Order Effects

The expressions related to the second-order effects (6.48)-(6.56) are only calculated for $V_{\mathrm{GB}}^* > 0$:

Mobility Degradation

$$G_{\mathrm{mob}} = \frac{\mu_0}{\mu} = \begin{cases} 1 + \left[\left(\theta_{\mathrm{ph_T}} \cdot V_{\mathrm{eff}}\right)^{\nu_{\mathrm{T}}/3} + \left(\theta_{\mathrm{sr_T}} \cdot V_{\mathrm{eff}}\right)^{2 \cdot \nu_{\mathrm{T}}} \right]^{1/\nu_{\mathrm{T}}} & \text{for NMOS} \\ \left[1 + \left(\theta_{\mathrm{ph_T}} \cdot V_{\mathrm{eff}}\right)^{\nu_{\mathrm{T}}/3} + \left(\theta_{\mathrm{sr_T}} \cdot V_{\mathrm{eff}}\right)^{\nu_{\mathrm{T}}} \right]^{1/\nu_{\mathrm{T}}} & \text{for PMOS} \end{cases} \tag{6.48}$$

Channel Length Modulation:

$$\frac{\Delta L}{L} = \alpha \cdot \ln \left[\frac{V_{\mathrm{DS}} - V_{\mathrm{DS_x}} + \sqrt{\left(V_{\mathrm{DS}} - V_{\mathrm{DS_x}}\right)^2 + {V_{\mathrm{P}}}^2}}{V_{\mathrm{P}}} \right] \tag{6.49}$$

$$G_{\Delta L} = \frac{1}{1 + (\Delta L / L) + (\Delta L / L)^2} \tag{6.50}$$

Velocity Saturation:

$$x_{\mathrm{sat}} = \begin{cases} \frac{\theta_{\mathrm{sat_T}} \cdot \Delta\psi}{G_{\mathrm{mob}}} & \text{for NMOS} \\ \frac{\theta_{\mathrm{sat_T}}}{G_{\mathrm{mob}}} \cdot \frac{\Delta\psi}{\left[1 + \left(\theta_{\mathrm{sat_T}} \cdot \Delta\psi / G_{\mathrm{mob}}\right)^2\right]^{1/4}} & \text{for PMOS} \end{cases} \tag{6.51}$$

$$G_{\mathrm{vsat}} = \frac{G_{\mathrm{mob}}}{2} \cdot \left[1 + \sqrt{1 + 2 \cdot {x_{\mathrm{sat}}}^2} \right] \tag{6.52}$$

Series Resistance + Self-Heating:

$$G_{\mathrm{R}} = \theta_{\mathrm{R_T}} \cdot \left(1 + \frac{\theta_{\mathrm{R1}}}{\theta_{\mathrm{R2}} + \bar{V}_{\mathrm{inv}}} \right) \cdot \bar{V}_{\mathrm{inv}}^* \tag{6.53}$$

$$G_{\mathrm{Th}} = \theta_{\mathrm{Th_T}} \cdot V_{\mathrm{DS}} \cdot \Delta\psi \cdot \bar{V}_{\mathrm{inv}}^* \tag{6.54}$$

$$G_{\mathrm{tot}}^* = G_{\mathrm{vsat}} \cdot G_{\Delta L} + G_{\mathrm{R}} \tag{6.55}$$

$$G_{\mathrm{tot}} = G_{\mathrm{Th}} + \frac{G_{\mathrm{tot}}^*}{2} + \sqrt{\mathrm{hyp}_1 \left\{ \frac{{G_{\mathrm{tot}}^*}^2}{4} - \frac{G_{\mathrm{R}}}{G_{\mathrm{mob}}} \cdot \frac{{x_{\mathrm{sat}}}^2}{\sqrt{1 + 2 \cdot {x_{\mathrm{sat}}}^2}}, \epsilon_3 \right\}} \tag{6.56}$$

©Koninklijke Philips Electronics N.V. 2004

Drain-Source Channel Current:

Eqs (6.57) and (6.58) are only calculated for $V^*_{\mathrm{GB}} - \bar{\psi} > 0$:

$$I_{\mathrm{drift}} = \beta_{\mathrm{T}} \cdot \bar{V}_{\mathrm{inv}} \cdot \Delta\psi \tag{6.57}$$

$$I_{\mathrm{diff}} = \beta_{\mathrm{T}} \cdot m_{\phi_{\mathrm{T}}} \cdot \left(V_{\mathrm{inv_0}} - V_{\mathrm{inv_L}}\right) \tag{6.58}$$

$$I_{\mathrm{DS}} = \begin{cases} 0 & \text{for:} \quad V^*_{\mathrm{GB}} - \bar{\psi} \le 0 \\ \frac{I_{\mathrm{drift}}+I_{\mathrm{diff}}}{G_{\mathrm{tot}}} & \text{for:} \quad V^*_{\mathrm{GB}} - \bar{\psi} > 0 \end{cases} \tag{6.59}$$

Weak-Avalanche:

$$I_{\mathrm{avl}} = \begin{cases} 0 & \text{for:} \quad V_{\mathrm{DS}} - a_3 \cdot V_{\mathrm{DSAT}} \le -a_2/A \\ a_{1_{\mathrm{T}}} \cdot I_{\mathrm{DS}} \cdot \exp\left(-\frac{a_2}{V_{\mathrm{DS}} - a_3 \cdot V_{\mathrm{DSAT}}}\right) & \text{for:} \quad V_{\mathrm{DS}} - a_3 \cdot V_{\mathrm{DSAT}} > -a_2/A \end{cases} \tag{6.60}$$

Surface Potential in Gate Overlap Regions:

The surface potential in the overlap region ψ_{ov} is given by the following implicit relation:

$$F_{\mathrm{ov}}\{V_{\mathrm{GX}}, \psi_{\mathrm{ov}}\} = -V_{\mathrm{ov}}\{V_{\mathrm{GX}}, \psi_{\mathrm{ov}}\}^2 + k_{\mathrm{ov}}{}^2 \cdot d_{\mathrm{ov}}\{\psi_{\mathrm{ov}}\} = 0 \tag{6.61}$$

where:

$$V^*_{\mathrm{GX}}\{V_{\mathrm{GX}}, \psi_{\mathrm{ov}}\} = V_{\mathrm{GX}} - V_{\mathrm{FBov}} - \psi_{\mathrm{ov}} \tag{6.62}$$

$$c_{\mathrm{ov}}\{V_{\mathrm{GX}}, \psi_{\mathrm{ov}}\} = \frac{1}{2} + \frac{1}{2} \cdot \sqrt{1 + 4/k_{\mathrm{P}}{}^2 \cdot \mathrm{hyp}_1\left\{V^*_{\mathrm{GX}}\{V_{\mathrm{GX}}, \psi_{\mathrm{ov}}\}, \epsilon_1\right\}} \tag{6.63}$$

$$V_{\mathrm{ov}}\{V_{\mathrm{GX}}, \psi_{\mathrm{ov}}\} = \frac{V^*_{\mathrm{GX}}\{V_{\mathrm{GX}}, \psi_{\mathrm{ov}}\}}{c\{V_{\mathrm{GX}}, \psi_{\mathrm{ov}}\}} \tag{6.64}$$

$$d_{\mathrm{ov}}\{\psi_{\mathrm{ov}}\} = -\psi_{\mathrm{ov}} + \phi_{\mathrm{T}} \cdot \left[\exp\left(\frac{\psi_{\mathrm{ov}}}{\phi_{\mathrm{T}}}\right) - 1\right] \tag{6.65}$$

The surface potential is iteratively calculated using a second-order Newton Raphson procedure, where the surface potential $\psi_{\mathrm{i+1}}$ in the $i+1^{\mathrm{th}}$ iteration is given in terms of the surface potential ψ_{i} in the ith iteration by:

$$\psi_{\mathrm{i+1}} = \psi_{\mathrm{i}} - \frac{F_{\mathrm{ov_i}}}{F'_{\mathrm{ov_i}} - \frac{1}{2} \cdot F_{\mathrm{ov_i}} \cdot F''_{\mathrm{ov_i}} \big/ F'_{\mathrm{ov_i}}} \tag{6.66}$$

where:

$$F_{\mathrm{ov_i}} = F_{\mathrm{ov}}\{V_{\mathrm{GX}}, \psi_{\mathrm{i}}\} = -V_{\mathrm{ov}}\{V_{\mathrm{GX}}, \psi_{\mathrm{i}}\}^2 + k_{\mathrm{ov}}{}^2 \cdot d_{\mathrm{ov}}\{\psi_{\mathrm{i}}\} \tag{6.67}$$

$$F'_{\mathrm{ov_i}} = \left.\frac{\partial F_{\mathrm{ov}}\{V_{\mathrm{GX}}, \psi_{\mathrm{ov}}\}}{\partial \psi_{\mathrm{ov}}}\right|_{\psi_{\mathrm{ov}}=\psi_{\mathrm{i}}} = -2 \cdot V_{\mathrm{ov}}\{V_{\mathrm{GX}}, \psi_{\mathrm{i}}\} \cdot V'_{\mathrm{ov}}\{V_{\mathrm{GX}}, \psi_{\mathrm{i}}\} + k_{\mathrm{ov}}{}^2 \cdot d'_{\mathrm{ov}}\{\psi_{\mathrm{i}}\} \tag{6.68}$$

 ©Koninklijke Philips Electronics N.V. 2004

$$F''_{\mathrm{ov_i}} = \left.\frac{\partial^2 F_{\mathrm{ov}}\{V_{\mathrm{GX}}, \psi_{\mathrm{ov}}\}}{\partial \psi_{\mathrm{ov}}{}^2}\right|_{\psi_{\mathrm{ov}}=\psi_{\mathrm{i}}} \quad (6.69)$$

$$= -2 \cdot V'_{\mathrm{ov}}\{V_{\mathrm{GX}}, \psi_{\mathrm{i}}\}^2 - 2 \cdot V_{\mathrm{ov}}\{V_{\mathrm{GX}}, \psi_{\mathrm{i}}\} \cdot V''_{\mathrm{ov}}\{V_{\mathrm{GX}}, \psi_{\mathrm{i}}\} + k_{\mathrm{ov}}{}^2 \cdot d''_{\mathrm{ov}}\{\psi_{\mathrm{i}}\} \quad (6.70)$$

The first-order and second-order derivatives are given by:

$$c'_{\mathrm{ov}}\{V_{\mathrm{GX}}, \psi_{\mathrm{ov}}\} = \frac{\partial c_{\mathrm{ov}}\{V_{\mathrm{GX}}, \psi_{\mathrm{ov}}\}}{\partial \psi_{\mathrm{ov}}} \quad (6.71)$$

$$= -\frac{1}{4} \cdot \frac{4/k_{\mathrm{P}}{}^2}{2 \cdot c_{\mathrm{ov}}\{V_{\mathrm{GX}}, \psi_{\mathrm{ov}}\} - 1} \cdot \frac{\partial \mathrm{hyp}_1\left\{V^*_{\mathrm{GX}}\{V_{\mathrm{GX}}, \psi_{\mathrm{ov}}\}, \epsilon_1\right\}}{\partial V^*_{\mathrm{GX}}}$$

$$c''_{\mathrm{ov}}\{V_{\mathrm{GX}}, \psi_{\mathrm{ov}}\} = \frac{\partial^2 c_{\mathrm{ov}}\{V_{\mathrm{GX}}, \psi_{\mathrm{ov}}\}}{\partial \psi_{\mathrm{ov}}{}^2} \quad (6.72)$$

$$= -\frac{2 \cdot c'_{\mathrm{ov}}\{V_{\mathrm{GX}}, \psi_{\mathrm{ov}}\}^2 - \frac{1}{k_{\mathrm{P}}{}^2} \cdot \frac{\partial^2 \mathrm{hyp}_1\{V^*_{\mathrm{GX}}\{V_{\mathrm{GX}}, \psi_{\mathrm{ov}}\}, \epsilon_1\}}{\partial V^*_{\mathrm{GX}}{}^2}}{2 \cdot c_{\mathrm{ov}}\{V_{\mathrm{GX}}, \psi_{\mathrm{ov}}\} - 1}$$

$$V'_{\mathrm{ov}}\{V_{\mathrm{GX}}, \psi_{\mathrm{ov}}\} = \frac{\partial V_{\mathrm{ov}}\{V_{\mathrm{GX}}, \psi_{\mathrm{ov}}\}}{\partial \psi_{\mathrm{ov}}} = -\frac{1 + V_{\mathrm{ov}}\{V_{\mathrm{GX}}, \psi_{\mathrm{ov}}\} \cdot c'_{\mathrm{ov}}\{V_{\mathrm{GX}}, \psi_{\mathrm{ov}}\}}{c_{\mathrm{ov}}\{V_{\mathrm{GX}}, \psi_{\mathrm{ov}}\}} \quad (6.73)$$

$$V''_{\mathrm{ov}}\{V_{\mathrm{GX}}, \psi_{\mathrm{ov}}\} = \frac{\partial^2 V_{\mathrm{ov}}\{V_{\mathrm{GX}}, \psi_{\mathrm{ov}}\}}{\partial \psi_{\mathrm{ov}}{}^2} \quad (6.74)$$

$$= -\frac{2 \cdot c'_{\mathrm{ov}}\{V_{\mathrm{GX}}, \psi_{\mathrm{ov}}\} \cdot V'_{\mathrm{ov}}\{V_{\mathrm{GX}}, \psi_{\mathrm{ov}}\} + V_{\mathrm{ov}}\{V_{\mathrm{GX}}, \psi_{\mathrm{ov}}\} \cdot c''_{\mathrm{ov}}\{V_{\mathrm{GX}}, \psi_{\mathrm{ov}}\}}{c_{\mathrm{ov}}\{V_{\mathrm{GX}}, \psi_{\mathrm{ov}}\}}$$

$$d'_{\mathrm{ov}}\{\psi_{\mathrm{ov}}\} = \frac{\partial d_{\mathrm{ov}}\{\psi_{\mathrm{ov}}\}}{\partial \psi_{\mathrm{ov}}} = -1 + \exp\left(\frac{\psi_{\mathrm{ov}}}{\phi_{\mathrm{T}}}\right) \quad (6.75)$$

$$d''_{\mathrm{ov}}\{\psi_{\mathrm{ov}}\} = \frac{\partial^2 d_{\mathrm{ov}}\{\psi_{\mathrm{ov}}\}}{\partial \psi_{\mathrm{ov}}{}^2} = \frac{\exp\left(\frac{\psi_{\mathrm{ov}}}{\phi_{\mathrm{T}}}\right)}{\phi_{\mathrm{T}}} \quad (6.76)$$

©Koninklijke Philips Electronics N.V. 2004

The iterative loop is performed until $|\psi_{i+1} - \psi_i| < 10^{-8} \cdot \phi_T$, at which point ψ_{ov} is taken to be equal to ψ_{i+1}. As a zero-order starting value ψ_0, the following approximation is used:

$$\begin{cases} \text{if } V_{GX} \leq V_{FBov} & \begin{cases} x = Acc_{ov} \cdot (V_{GX} - V_{FBov}) \big/ \phi_T \\ \Delta_{acc} = \begin{cases} -\phi_T & \text{for } x \leq -2 \\ \phi_T \cdot \left[\exp(x) - 1\right] & \text{for } x > -2 \end{cases} \\ \psi_0 = -\left(\sqrt{-[V_{GX} - V_{FBov}] + \Delta_{acc} + \frac{{k_{ov}}^2}{4}} - \frac{k_{ov}}{2}\right)^2 + \Delta_{acc} \end{cases} \\ \text{if } V_{GX} > V_{FBov} & \begin{cases} V_{ov} = \frac{2 \cdot [V_{GX} - V_{FBov}]}{1 + \sqrt{1 + 4/{k_P}^2 \cdot [V_{GX} - V_{FBov}]}} \\ x = {V_{ov}}^2 + \phi_T \cdot {k_{ov}}^2 \\ y = -{k_{ov}}^2 + \frac{2 \cdot V_{ov}}{\sqrt{1 + 4/{k_P}^2 \cdot (V_{GX} - V_{FBov})}} \\ z = 1 + 4/{k_P}^2 \cdot (V_{GX} - V_{FBov}) \\ \psi_0 = \frac{2 \cdot \phi_T \cdot x \cdot \ln\left(\frac{x}{\phi_T \cdot {k_{ov}}^2}\right)}{x + \phi_T \cdot y + \sqrt{(x + \phi_T \cdot y)^2 - {\phi_T}^2 \cdot \left(x/z - y^2/2\right) \cdot \ln\left(\frac{x}{\phi_T \cdot {k_{ov}}^2}\right)}} \end{cases} \end{cases} \tag{6.77}$$

When $V_{GX} - V_{FBov} = 0$, the starting value ψ_0 is equal to zero. No iterative solution is necessary, and ψ_{ov} is automatically taken to be equal to zero. Surface potentials in the gate/source overlap ψ_{ov_0} and in the gate/drain overlap ψ_{ov_L} are calculated from the following implicit relations:

$$F_{ov}\left\{V_{GS}, \psi_{ov_0}\right\} = 0 \tag{6.78}$$

$$F_{ov}\left\{V_{GD} - V_{DS}, \psi_{ov_L}\right\} = 0 \tag{6.79}$$

The oxide voltages in the gate/source overlap V_{ov_0} and the gate/drain overlap V_{ov_L} are given by:

$$V_{ov_0} = V_{ov}\left\{V_{GS}, \psi_{ov_0}\right\} \tag{6.80}$$

$$V_{ov_L} = V_{ov}\left\{V_{GD} - V_{DS}, \psi_{ov_L}\right\} \tag{6.81}$$

Gate Current Equations:

The tunnelling probability is given by:

$$P_{tun}\left\{V_{ox}, \chi_B, B\right\} = \begin{cases} \exp\left(-\frac{B}{\chi_B} \cdot \frac{\left[\left(\frac{V_{ox}}{\chi_B}\right)^2 - 3 \cdot \frac{V_{ox}}{\chi_B} + 3\right]}{1 + \left(1 - \frac{V_{ox}}{\chi_B}\right)^{\frac{3}{2}}}\right) & \text{for: } V_{ox} < \chi_B \\ \exp\left(-B \big/ V_{ox}\right) & \text{for: } V_{ox} \geq \chi_B \end{cases} \tag{6.82}$$

 ©Koninklijke Philips Electronics N.V. 2004

Source/Drain Gate Overlap Current: The gate tunnelling currents in both gate/source and gate/drain overlap are given by:

$$P_{\text{ov}}\{V_{\text{ov}}\} = P_{\text{tun}}\left\{V_{\text{ov}}, \chi_{\text{B}_{\text{inv}}}, B_{\text{inv}}\right\} \tag{6.83}$$

$$I_{\text{Gov}}\{V_{\text{GX}}, V_{\text{ov}}\} = I_{\text{GOV}} \cdot V_{\text{GX}} \cdot V_{\text{ov}} \cdot [P_{\text{ov}}\{V_{\text{ov}}\} - P_{\text{ov}}\{-V_{\text{ov}}\}] \tag{6.84}$$

$$I_{\text{Gov}_0} = I_{\text{Gov}}\left\{V_{\text{GS}}\ ,\ V_{\text{ov}_0}\right\} \tag{6.85}$$

$$I_{\text{Gov}_\text{L}} = I_{\text{Gov}}\left\{V_{\text{GS}} - V_{\text{DS}}\ ,\ V_{\text{ov}_\text{L}}\right\} \tag{6.86}$$

Intrinsic Gate-to-Bulk Current: The gate tunnelling current in accumulation:

$$P_{\text{acc}} = P_{\text{tun}}\left\{-\bar{V}_{\text{ox}}, \chi_{\text{B}_{\text{acc}}}, B_{\text{acc}}\right\} \tag{6.87}$$

$$V_{\text{acc}} = \bar{V}_{\text{ox}} - \text{hyp}_1\left\{\bar{V}_{\text{ox}}, \epsilon_3\right\} \tag{6.88}$$

$$I_{\text{GB}} = -I_{\text{GACC}} \cdot (V_{\text{GS}} + V_{\text{SB}}) \cdot V_{\text{acc}} \cdot P_{\text{acc}} \tag{6.89}$$

Intrinsic Gate-to-Channel Current: The tunnelling current in inversion, including quantum-mechanical barrier lowering $\Delta\chi_{\text{B}}$. Eqs. (6.90)-(6.100) are only calculated for $V^*_{\text{GB}} - \bar{\psi} > 0$:

$$\Delta\chi_{\text{B}} = QM_{\psi} \cdot \left(\bar{V}_{\text{inv}}\big/3 + \bar{V}_{\text{ox}} - \bar{V}_{\text{inv}}\right)^{2/3} \tag{6.90}$$

$$\chi_{\text{B}_{\text{eff}}} = 0.7 \cdot \chi_{\text{B}_{\text{inv}}} + \text{hyp}_1\left\{0.3 \cdot \chi_{\text{B}_{\text{inv}}} - \Delta\chi_{\text{B}}, \epsilon_3\right\} \tag{6.91}$$

$$B_{\text{eff}} = B_{\text{inv}} \cdot \left(\chi_{\text{B}_{\text{eff}}}\big/\chi_{\text{B}_{\text{inv}}}\right)^{3/2} \tag{6.92}$$

$$P_{\text{inv}} = P_{\text{tun}}\left\{\bar{V}_{\text{ox}}, \chi_{\text{B}_{\text{eff}}}, B_{\text{eff}}\right\} \tag{6.93}$$

$$r_{\text{B}} = \frac{3}{8} \cdot \frac{B_{\text{eff}}}{\chi_{\text{B}_{\text{eff}}}{}^2} \cdot \frac{\bar{\xi}_{\text{ox}}}{\phi_{\text{T}}} \tag{6.94}$$

$$r^* = \frac{\bar{\xi}}{\phi_{\text{T}} \cdot \bar{V}^*_{\text{inv}}} \tag{6.95}$$

$$r_{\text{ox}} = \frac{\bar{\xi}_{\text{ox}}}{\phi_{\text{T}} \cdot \bar{V}_{\text{ox}}} \tag{6.96}$$

$$P_{\text{GC}} = 1 + \frac{r_{\text{B}}{}^2 + 4 \cdot r_{\text{B}} \cdot r^* + 2 \cdot r_{\text{B}} \cdot r_{\text{ox}} + 2 \cdot r^{*2} + 4 \cdot r_{\text{ox}} \cdot r^*}{24} \cdot \Delta\psi^2 \tag{6.97}$$

$$\bar{I}_{\text{GC}} = I_{\text{GINV}} \cdot G_{\Delta L} \cdot \left(V_{\text{GS}} - \frac{1}{2} V_{\text{DS}_\text{x}}\right) \cdot P_{\text{inv}} \tag{6.98}$$

©Koninklijke Philips Electronics N.V. 2004

The total intrinsic gate current I_{GC}:

$$I_{GC} = \bar{I}_{GC} \cdot \bar{V}_{inv} \cdot P_{GC} \tag{6.99}$$

$$P_{GS} = [r_B + r_{ox}] \cdot \frac{\Delta\psi}{12} \tag{6.100}$$

$$I_{GS} = \begin{cases} I_{Gov_0} & \text{for:} \quad V_{GB}^* - \bar{\psi} \leq 0 \\ \frac{1}{2} \cdot I_{GC} + \left(P_{GS} \cdot \bar{V}_{inv} + \frac{V_{inv_0} - V_{inv_L}}{12}\right) \cdot \bar{I}_{GC} + I_{Gov_0} & \text{for:} \quad V_{GB}^* - \bar{\psi} > 0 \end{cases} \tag{6.101}$$

$$I_{GD} = \begin{cases} I_{Gov_L} & \text{for:} \quad V_{GB}^* - \bar{\psi} \leq 0 \\ I_{GC} - I_{GS} + I_{Gov_0} + I_{Gov_L} & \text{for:} \quad V_{GB}^* - \bar{\psi} > 0 \end{cases} \tag{6.102}$$

Gate-Induced Drain/Source Leakage Current:

$$V_{tov}\{V_{ov}, V\} = \sqrt{\left(V_{ov} - \text{hyp}_1\{V_{ov}, \epsilon_3\}\right)^2 + C_{GIDL}{}^2 \cdot V^2} \tag{6.103}$$

$$I_{gixl}\{V_{ov}, V\} = \begin{cases} A_{GIDL} \cdot V \cdot V_{tov}\{V_{ov}, V\}^2 \cdot e^{-\frac{B_{GIDL_T}}{V_{tov}\{V_{ov}, V\}}} & \text{for:} \quad V_{tov}\{V_{ov}, V\} > -\frac{B_{GIDL_T}}{A} \\ 0 & \text{for:} \quad V_{tov}\{V_{ov}, V\} \leq -\frac{B_{GIDL_T}}{A} \end{cases} \tag{6.104}$$

$$I_{gisl} = I_{gixl}\left\{V_{ov_0}, V_{SB}\right\} \tag{6.105}$$

$$I_{gidl} = I_{gixl}\left\{V_{ov_L}, V_{DS} + V_{SB}\right\} \tag{6.106}$$

6.2.3 Extended Charge Equations

Bias-Dependent Overlap Capacitance:

$$Q_{ov_0} = C_{GSO} \cdot V_{ov_0} \tag{6.107}$$

$$Q_{ov_L} = C_{GDO} \cdot V_{ov_L} \tag{6.108}$$

Intrinsic Charges:

$$C_{OX_{eff}} = \frac{C_{OX}}{1 + QM_{t_{ox}} \cdot \left[\left(\frac{V_{eff}}{\eta_{mob_T}}\right)^2 + (5 \cdot V_{limit})^2\right]^{-1/6}} \tag{6.109}$$

$$\Delta V_{inv} = \left(V_{inv_0} - V_{inv_L}\right) \cdot \left(1 - \frac{G_R}{G_{tot}}\right) \tag{6.110}$$

$$F_j = \frac{1}{2} \cdot \frac{\Delta V_{inv}}{\bar{V}_{inv}^*} \tag{6.111}$$

 ©Koninklijke Philips Electronics N.V. 2004

$$Q_{\mathrm{S}} = -\frac{C_{\mathrm{OX_{eff}}} \cdot G_{\Delta L}}{2} \cdot \left[\bar{V}_{\mathrm{inv}} + \frac{\Delta V_{\mathrm{inv}}}{6} \cdot \left(F_{\mathrm{j}} - \frac{F_{\mathrm{j}}{}^{2}}{5} + 1 \right) \right] \tag{6.112}$$

$$Q_{\mathrm{D}} = -\frac{C_{\mathrm{OX_{eff}}} \cdot G_{\Delta L}}{2} \cdot \left[\bar{V}_{\mathrm{inv}} + \frac{\Delta V_{\mathrm{inv}}}{6} \cdot \left(F_{\mathrm{j}} + \frac{F_{\mathrm{j}}{}^{2}}{5} - 1 \right) \right] \tag{6.113}$$

$$Q_{\mathrm{G}} = C_{\mathrm{OX_{eff}}} \cdot \left[\bar{V}_{\mathrm{ox}} + \frac{\Delta V_{\mathrm{inv}}}{6} \cdot F_{\mathrm{j}} \cdot \frac{\bar{\xi}_{\mathrm{ox}}}{\bar{\xi}} \right] \tag{6.114}$$

$$Q_{\mathrm{B}} = -\left[Q_{\mathrm{S}} + Q_{\mathrm{D}} + Q_{\mathrm{G}} \right] \tag{6.115}$$

6.2.4 Extended Noise Equations

The noise equations (6.116)-(6.131) are only calculated for $V_{\mathrm{GB}}^{*} - \bar{\psi} > 0$. In these equations f represents the operation frequency of the transistor.

$$G_{\mathrm{eff}} = 1 - \frac{G_{\mathrm{R}}}{G_{\mathrm{tot}}} \tag{6.116}$$

$$x_{\mathrm{sat}}{}^{2} = \begin{cases} \theta_{\mathrm{sat_T}}{}^{2} \cdot \Delta\psi^{2} \cdot G_{\mathrm{eff}}{}^{2} & \text{for NMOS} \\ \frac{\theta_{\mathrm{sat_T}}{}^{2} \cdot \Delta\psi^{2} \cdot G_{\mathrm{eff}}{}^{2}}{\sqrt{1+\theta_{\mathrm{sat_T}}{}^{2} \cdot \Delta\psi^{2} \cdot G_{\mathrm{eff}}{}^{2}}} & \text{for PMOS} \end{cases} \tag{6.117}$$

$$G_{\mathrm{vsat_R}} = \frac{G_{\mathrm{mob}} + \sqrt{G_{\mathrm{mob}}{}^{2} + 2 \cdot x_{\mathrm{sat}}{}^{2}}}{2} \tag{6.118}$$

$$t_{1} = \frac{\bar{V}_{\mathrm{inv}}}{\bar{V}_{\mathrm{inv}}^{*}} \tag{6.119}$$

$$t_{2} = \frac{F_{\mathrm{j}}{}^{2}}{36} \tag{6.120}$$

$$t_{\mathrm{sat}} = \frac{x_{\mathrm{sat}}{}^{2}}{G_{\mathrm{vsat_R}}{}^{2}} \tag{6.121}$$

$$g_{\mathrm{ideal}} = \frac{\beta_{\mathrm{T}} \cdot \bar{V}_{\mathrm{inv}}^{*}}{G_{\mathrm{vsat_R}} \cdot G_{\Delta L}} \tag{6.122}$$

$$B_{\mathrm{G}} = 2 \cdot \pi \cdot f \cdot C_{\mathrm{OX_{eff}}} \cdot \frac{\bar{\xi}_{\mathrm{ox}}}{\phi_{\mathrm{T}}} \cdot \frac{G_{\mathrm{vsat_R}} \cdot G_{\Delta L}}{G_{\mathrm{mob}}} \tag{6.123}$$

$$S_{\mathrm{th}} = N_{\mathrm{T_T}} \cdot G_{\mathrm{eff}}{}^{2} \cdot g_{\mathrm{ideal}} \cdot \max\left\{ t_{1} + 12 \cdot t_{2} \cdot \left(1 - 2 \cdot t_{\mathrm{sat}} - 2 \cdot t_{\mathrm{sat}}{}^{2} \right), 0 \right\} \tag{6.124}$$

$$S_{\mathrm{ig}} = N_{\mathrm{T_T}} \cdot \frac{B_{\mathrm{G}}{}^{2}}{g_{\mathrm{ideal}}} \cdot \left[\frac{t_{1}}{12} - t_{1} \cdot t_{2} - \frac{t_{2}}{5} + 12 \cdot t_{2}{}^{2} \right. \tag{6.125}$$

$$+\ t_{\text{sat}} \cdot \left(\frac{t_1}{12} + 3 \cdot t_1 \cdot t_2 - \frac{9 \cdot t_2}{5} - 36 \cdot {t_2}^2 \right)$$

$$+\ {t_{\text{sat}}}^2 \cdot \left(\frac{t_1}{12} + 4 \cdot t_1 \cdot t_2 - \frac{17 \cdot t_2}{5} - 24 \cdot {t_2}^2 \right) \Bigg]$$

$$S_{\text{igth}} = j \cdot N_{\text{T}_\text{T}} \cdot B_{\text{G}} \cdot G_{\text{eff}} \cdot \sqrt{t_2} \cdot \Bigg[1 - 12 \cdot t_2 + t_{\text{sat}} \cdot \left(\frac{1}{2} - t_1 + 30 \cdot t_2 \right) + {t_{\text{sat}}}^2 \cdot \left(\frac{3}{8} - \frac{3 \cdot t_1}{2} + \frac{51 \cdot t_2}{2} \right) \Bigg] \quad (6.126)$$

$$\text{for GATENOISE} = 1 : \begin{cases} g_{\text{ideal}} &= \frac{\beta_{\text{T}} \cdot \bar{V}_{\text{inv}}}{G_{\text{mob}} \cdot G_{\Delta L}} \\ S_{\text{th}} &= N_{\text{T}_\text{T}} \cdot {G_{\text{eff}}}^2 \cdot g_{\text{ideal}} \Big/ \sqrt{1 + t_{\text{sat}} + {t_{\text{sat}}}^2} \\ S_{\text{ig}} &= 0 \\ S_{\text{igth}} &= 0 \end{cases} \quad (6.127)$$

$$N_0 = \frac{\epsilon_{ox}}{q \cdot t_{ox}} \cdot \left(\bar{V}_{\text{inv}} + \frac{\Delta V_{\text{inv}}}{2} \right) \quad (6.128)$$

$$N_L = \frac{\epsilon_{ox}}{q \cdot t_{ox}} \cdot \left(\bar{V}_{\text{inv}} - \frac{\Delta V_{\text{inv}}}{2} \right) \quad (6.129)$$

$$N^* = \frac{\epsilon_{ox}}{q \cdot t_{ox}} \cdot \bar{\xi} \quad (6.130)$$

$$S_{\text{fl}} = \frac{q \cdot {\phi_{\text{T}}}^2 \cdot t_{ox} \cdot \beta_{\text{T}} \cdot I_{\text{DS}}}{f \cdot \epsilon_{ox} \cdot G_{\text{vsat}} \cdot N^*} \cdot \Bigg[\left(N_{\text{FA}} - N^* \cdot N_{\text{FB}} + {N^*}^2 \cdot N_{\text{FC}} \right) \cdot \ln\left(\frac{N_0 + N^*}{N_L + N^*} \right) + \left(N_{\text{FB}} - N^* \cdot N_{\text{FC}} \right) \cdot (N_0 - N_L) + \frac{N_{\text{FC}}}{2} \cdot \left({N_0}^2 - {N_L}^2 \right) \Bigg] \quad (6.131)$$

$$+ \frac{\phi_{\text{T}} \cdot {I_{\text{DS}}}^2}{f} \cdot (1 - G_{\Delta L}) \cdot \left[\frac{N_{\text{FA}} + N_{\text{FB}} \cdot N_L + N_{\text{FC}} \cdot {N_L}^2}{(N_L + N^*)^2} \right]$$

 ©Koninklijke Philips Electronics N.V. 2004

7 Parameter Extraction

The parameter extraction strategy for MOS Model 11 using an **optimization method** consists of four main steps:

1. measurements
2. extraction of miniset parameters at room temperature
3. extraction of temperature scaling parameters
4. extraction of geometry scaling parameters

The above steps will be briefly described in the following sections.

7.1 Measurements

The parameter extraction routine consists of four different dc-measurements and two (optional) capacitance measurements[8]:

• **Measurement I :** $I_D/g_m/I_G$–V_{GS}-characteristics in linear region:
n–channel : $V_{GS} = 0 \ldots V_{sup}$ (with steps of maximum 50 mV).
V_{DS} = 50 mV
$V_{BS} = 0 \ldots -V_{sup}$

p–channel : $V_{GS} = 0 \ldots -V_{sup}$ (with steps of maximum 50 mV).
V_{DS} = -50 mV
$V_{BS} = 0 \ldots V_{sup}$

• **Measurement II :** Subthreshold I_D–V_{GS}-characteristics:
n–channel : $V_{GS} = V_T - 0.6$ V ... $V_T + 0.3$ V
V_{DS} = 3 values starting from 100 mV to V_{sup}
$V_{BS} = 0 \ldots -V_{sup}$

p–channel : $V_{GS} = V_T + 0.6$ V ... $V_T - 0.3$ V
V_{DS} = 3 values starting from -100 mV to $-V_{sup}$
$V_{BS} = 0 \ldots V_{sup}$

• **Measurement III :** $I_D/g_{DS}/I_G$–V_{DS}-characteristics:
n–channel : $V_{DS} = 0 \ldots V_{sup}$ (with steps of maximum 50 mV)
V_{GS} = 4 values starting from $V_T + 0.1$ V, not above V_{sup}
V_{BS} = 3 values starting from 0 V to $-V_{sup}$

p–channel : $V_{DS} = 0 \ldots -V_{sup}$ (with steps of maximum 50 mV)
V_{GS} = 4 values starting from $V_T + 0.1$ V, not below $-V_{sup}$
V_{BS} = 3 values starting from 0 V to V_{sup}

• **Measurement IV :** $I_D/I_S/I_G/I_B$–V_{GS}-characteristics in all operation regions:
n–channel : $V_{GS} = -V_{sup} \ldots V_{sup}$ (with steps of maximum 50 mV).
V_{DS} = 4 values starting from 0 V to V_{sup}
V_{BS} = 0 V

p–channel : $V_{GS} = -V_{sup} \ldots -V_{sup}$ (with steps of maximum 50 mV).
V_{DS} = 4 values starting from 0 V to $-V_{sup}$
V_{BS} = 0 V

[8] The bias conditions to be used for the measurements are dependent on the supply voltage of the process. Of course it is advisable to restrict the range of voltages to this supply voltage V_{sup}. Otherwise physical effects, atypical for normal transistor operation and therefore less well described by MOS Model 11, may dominate the characteristics.

©Koninklijke Philips Electronics N.V. 2004

• **Measurement V :** C_{gg}–V_{GS}-characteristic (optional):
n/p–channel : $V_{GS} = -V_{sup} \ldots V_{sup}$ (with steps of maximum 50 mV).
$V_{DS} = 0$ V
$V_{BS} = 0$ V

• **Measurement VI :** C_{cg}–V_{GS}-characteristic:
n/p–channel : $V_{GS} = -V_{sup} \ldots V_{sup}$
$V_{DS} = 0$ V
$V_{BS} = 0$ V

The values of transconductance g_m and output conductance g_{DS} are extracted from the I–V-curves by calculating in a numerical way the derivative of I_D to V_{GS} and V_{DS}, respectively. In the subthreshold measurements, Measurement II, use is made of threshold voltage V_T, which has to be determined for all the used bulk-source bias values V_{BS}. The determination of V_T is rather arbitrary, and it can be either determined using the linear extrapolation method or the constant current criterion. The channel-to-gate capacitance C_{cg} is the summation of the drain-to-gate capacitance C_{dg} and the source-to-gate capacitance C_{sg} (i.e. source and drain are short-circuited), it is needed to extract overlap capacitance parameters.

For the miniset extraction measurements I through IV have to be performed at room temperature for every device. In addition measurements V and VI need to be performed for a long/broad and a short/broad (i.e. $L = L_{min}$) transistor (at room temperature). Furthermore, for the extraction of temperature scaling parameters measurements I, III and IV have to be performed at different temperatures (at least two, typically -40°C and 125°C) for at least a long/broad and a short/broad transistor.

7.2 Extraction of Miniset Parameters at Room Temperature

The extraction of miniset parameters is performed for every device. In order to ensure that the temperature scaling relations do not affect the behaviour at room temperature, the reference temperature T_R is chosen equal to room temperature. In general the simultaneous determination of all miniset parameters is not advisable, because the value of some parameters can be wrong due to correlation and suboptimization. Therefore it is more practical to split the parameters into several groups, where each parameter group can be determined using specific measurements.

Although the poly-depletion effect affects the dc-behaviour of a MOSFET, the poly-depletion parameter KPINV can only be determined accurately from C-V-measurements. If the (physical) oxide thickness t_{ox} and the polysilicon impurity concentration N_P are known, the parameter KPINV ($= 1/k_P$) can be calculated from[9]:

$$k_P = \frac{t_{ox} \cdot \sqrt{2 \cdot q \cdot \epsilon_{Si} \cdot N_P}}{\epsilon_{ox}} \tag{7.1}$$

If the polysilicon impurity concentration N_P is not known, as a good first-order estimate one can use $N_P = 1 \cdot 10^{26}\mathrm{m}^{-3}$ for n^+-polysilicon gates and $N_P = 5 \cdot 10^{25}\mathrm{m}^{-3}$ for p^+-polysilicon gates. In the latter case a measured C_{GG}-V_{GS}-characteristic for a long-channel transistor is essential for an accurate determination of KPINV.

[9] For metal gates the poly-depletion effect does not occur and in this case KPINV = 0.

 ©Koninklijke Philips Electronics N.V. 2004

Table 7.1: Starting miniset parameter values for DC-parameter extraction at room temperature T_R of a typical MOSFET with channel length L (m), channel width W (m), oxide thickness t_{ox} (m), polysilicon impurity concentration N_P (m^{-3}) and minimum technology feature size L_{min}. If the polysilicon concentration N_P is not known, one can use $N_P = 1 \cdot 10^{26} m^{-3}$ or $5 \cdot 10^{25} m^{-3}$ for n^+- resp. p^+-polysilicon gates. Parameters C_{OX}, C_{GSO} and C_{GDO} are only important for the charge model, and do not affect the dc-model; they have to be extracted from C-V-characteristics. In order to determine the parameter geometry-scaling, the last column indicates for which conditions the parameters have to be extracted: L=long-channel device (fixed for short-channel devices), S=short-channel devices, A=all devices and F=fixed parameter.

Parameter	Program Name	Parameter Value		Extracted for
		NMOS	PMOS	
V_{FB}	VFB	-1.1	-0.95	L
k_0	KO	0.25	0.25	A
$1/k_P$	KPINV	$6.0 \cdot 10^3 / (t_{ox} \cdot \sqrt{N_P})$	$6.0 \cdot 10^3 / (t_{ox} \cdot \sqrt{N_P})$	L
ϕ_B	PHIB	0.95	0.95	A
β	BET	$1.7 \cdot 10^{-12} / t_{ox} \cdot W/L$	$4.5 \cdot 10^{-13} / t_{ox} \cdot W/L$	A
θ_{sr}	THESR	$1.5 \cdot 10^{-9} / t_{ox}$	$2.3 \cdot 10^{-9} / t_{ox}$	L
θ_{ph}	THEPH	$1.3 \cdot 10^{-10} / t_{ox}$	$2.2 \cdot 10^{-10} / t_{ox}$	L
η_{mob}	ETAMOB	1.3	3.0	L
ν	NU	2.0	2.0	A
θ_R	THER	$1.3 \cdot 10^{-7} / L$	$8.0 \cdot 10^{-8} / L$	S
θ_{R1}	THER1	0	0	–
θ_{R2}	THER2	1	1	–
θ_{sat}	THESAT	$4.5 \cdot 10^{-7} / L$	$2.0 \cdot 10^{-7} / L$	A
θ_{Th}	THETH	$1.0 \cdot 10^{-6}$	$1.0 \cdot 10^{-6}$	A
σ_{dibl}	SDIBL	$5.0 \cdot 10^{-2} \cdot (L_{min} / L)^2$	$5.0 \cdot 10^{-2} \cdot (L_{min} / L)^2$	S
m_0	MO	$1.0 \cdot 10^{-3}$	$1.0 \cdot 10^{-3}$	A
σ_{sf}	SSF	$6.0 \cdot 10^{-2} \cdot L_{min} / L$	$6.0 \cdot 10^{-2} \cdot L_{min} / L$	A
α	ALP	$6.0 \cdot 10^{-2} \cdot L_{min} / L$	$6.0 \cdot 10^{-2} \cdot L_{min} / L$	A
V_P	VP	$5.0 \cdot 10^{-2}$	$1.0 \cdot 10^{-1}$	F
m	MEXP	use Eq. (5.23)	use Eq. (5.23)	–
a_1	A1	25	100	A
a_2	A2	25	37	A
a_3	A3	1	1	A
I_{GINV}	IGINV	$1.6 \cdot 10^{-4} \cdot W \cdot L / t_{ox}^2$	$8.0 \cdot 10^{-6} \cdot W \cdot L / t_{ox}^2$	A
B_{INV}	BINV	$2.9 \cdot 10^{+10} \cdot t_{ox}$	$4.3 \cdot 10^{+10} \cdot t_{ox}$	L
I_{GACC}	IGACC	$2.0 \cdot 10^{-4} \cdot W \cdot L / t_{ox}^2$	$6.0 \cdot 10^{-6} \cdot W \cdot L / t_{ox}^2$	A
B_{ACC}	BACC	B_{INV}	$2.9 \cdot 10^{+10} \cdot t_{ox}$	L
V_{FBov}	VFBOV	0.1	0.1	L
k_{ov}	KOV	$9.3 \cdot 10^{+8} \cdot t_{ox}$	$3.8 \cdot 10^{+8} \cdot t_{ox}$	L
I_{GOV}	IGOV	$4.0 \cdot 10^{-12} \cdot W / t_{ox}^2$	$1.0 \cdot 10^{-12} \cdot W / t_{ox}^2$	A
A_{GIDL}	AGIDL	$1.6 \cdot 10^{-13} \cdot W / t_{ox}^2$	$1.2 \cdot 10^{-17} \cdot W / t_{ox}^2$	A
B_{GIDL}	BGIDL	$1.6 \cdot 10^{+10} \cdot t_{ox}$	$1.0 \cdot 10^{+10} \cdot t_{ox}$	L
C_{GIDL}	CGIDL	0	0	L

©Koninklijke Philips Electronics N.V. 2004

Before the optimization is started a parameter set has to be determined which contains a first estimation of the parameters to be extracted and the parameters which remain constant. The value of smoothing factor m is calculated from the device length L and from the minimum feature size of the technology $L_{\rm min}$ using eq. (5.23). The parameter set used as a first-order estimation of the parameters to be extracted is given in Table 7.1. With this parameter set a first optimization following the scheme below, is performed. After this the new parameter set serves as an estimation for the second optimization, which is performed following the same scheme. This method yields a proper set of parameters after the second optimization. Experiments with transistors of different processes show that the parameter set does not change very much after a third optimization. For an accurate extraction

Table 7.2: DC-parameter extraction procedure for a long-channel n-MOSFET, where Steps 2 and 12 are optional. For p-type transistors all voltages and currents have to be multiplied by -1. The optimisation is either performed on the absolute or relative deviation between model and measurements. Parameter $I_{\rm tst}$ is 2.5 μA for NMOS and 0.8 μA for PMOS. For n-MOSFETs $B_{\rm acc} = B_{\rm inv}$, and as a result $B_{\rm acc}$ does not have to be extracted. For p-MOSFETs this is not the case, see Tab. 2.1.

Step	Optimised Parameters	Measurement	Fitted On	Absolute/ Relative	Specific Conditions
1	$\phi_{\rm B}$, k_0 , β , $\theta_{\rm sr}$	I	$I_{\rm D}$	Absolute	–
2	$V_{\rm FB}$, k_0 , $k_{\rm P}$, $C_{\rm OX}$	V	$C_{\rm gg}$	Relative	–
3	$\phi_{\rm B}$, k_0 , m_0	II	$I_{\rm D}$	Relative	–
4	β , $\theta_{\rm sr}$, $\theta_{\rm ph}$	I	$I_{\rm D} / g_{\rm m}$	Relative	$V_{\rm SB} = 0$ V $V_{\rm GS} > V_{\rm T} + 0.3$ V
5	$\eta_{\rm mob}$	I	$I_{\rm D}$	Absolute	$I_{\rm D} > W/L \cdot I_{\rm tst}$
6	$\theta_{\rm sat}$	III	$I_{\rm D}$	Absolute	–
7	$\sigma_{\rm sf}$, α , $\theta_{\rm Th}$	III	$g_{\rm DS}$	Relative	–
8	$\theta_{\rm sat}$	III	$I_{\rm D}$	Absolute	–
9	$I_{\rm GINV}$, $B_{\rm inv}$	I	$I_{\rm G}$	Absolute	–
10	$I_{\rm GOV}$, $(B_{\rm acc})$, $I_{\rm GACC}$, $k_{\rm ov}$	IV	$I_{\rm G}$	Relative	$V_{\rm GS} < 0$ V
11	a_1 , a_2 , a_3	IV	$I_{\rm B}$	Absolute	$V_{\rm GS} \geq 0$ V
12	$A_{\rm GIDL}$, $B_{\rm GIDL}$, $C_{\rm GIDL}$	IV	$I_{\rm B}$	Absolute	$V_{\rm GS} < 0$ V
13	$V_{\rm FB}$, $k_{\rm P}$, $C_{\rm OX}$	V	$C_{\rm gg}$	Relative	–
14	Repeat Steps 3, 4, 5, 6, 7, 8, 9, 10, 11 and 12				

of parameter values, the parameter set for a long-channel transistor has to be determined first. In the long-channel case the poly-depletion parameter $1/k_{\rm P}$, the flat-band voltage $V_{\rm FB}$, the carrier mobility (i.e. $\theta_{\rm sr}$, $\theta_{\rm ph}$ and $\eta_{\rm mob}$) and the gate tunnelling probability factors ($B_{\rm inv}$ and $B_{\rm acc}$) can be determined, and they can subsequently be fixed for the short and narrow-channel devices, see Tab.7.1. In Table 7.2 the extraction procedure for long-channel transistors is given. Since the value of body-factor k_0 may change much over geometry and over technology, the first-order estimate in Tab. 7.1 is very crude and a more accurate, preliminary value is obtained using Step 1. In Step 2 (optional) more accurate values of the poly-depletion parameter $1/k_{\rm P}$ and the flat-band voltage $V_{\rm FB}$ (which determines the onset of accumulation) are extracted. Next the subthreshold parameters $\phi_{\rm B}$, k_0 and m_0 are optimised in Step 3, neglecting short-channel effects such as drain-induced barrier-lowering (DIBL). After that the mobility parameters are optimised using Steps 4 and 5, neglecting the influence of series-resistance. In Step 6 a preliminary value of the velocity saturation parameter is obtained, and subsequently the conductance parameters $\sigma_{\rm sf}$, α and $\theta_{\rm Th}$ are determined in Step 7. A more accurate value of $\theta_{\rm sat}$ can now

 ©Koninklijke Philips Electronics N.V. 2004

be obtained using Step 8 (which is Step 6 repeated). The gate current parameters are determined in Steps 9 and 10, followed by the weak-avalanche parameters in Step 11, and finally, the gate-induced leakage current parameters are optimised in Step 12.

Table 7.3: DC-parameter extraction procedure for a short-channel n-MOSFET. For p-type transistors all voltages and currents have to be multiplied by -1. Parameters $1/k_{\mathrm{P}}$, V_{FB}, θ_{sr}, θ_{ph}, η_{mob}, B_{inv}, B_{acc}, k_{ov}, B_{GIDL} and C_{GIDL} are taken from the long-channel case. The optimisation is either performed on the absolute or relative deviation between model and measurements.

Step	Optimised Parameters	Measure-ment	Fitted On	Absolute/ Relative	Specific Conditions
1	ϕ_{B} , k_0 , β , θ_{R}	I	I_{D}	Absolute	–
2	ϕ_{B} , k_0 , m_0 , σ_{dibl}	II	I_{D}	Relative	–
3	β , θ_{R}	I	$I_{\mathrm{D}} \big/ g_{\mathrm{m}}$	Relative	$V_{\mathrm{SB}} = 0$ V $V_{\mathrm{GS}} > V_{\mathrm{T}} + 0.3$ V
4	θ_{sat}	III	I_{D}	Absolute	–
5	σ_{sf} , α , θ_{Th} , σ_{dibl}	III	g_{DS}	Relative	–
6	θ_{sat}	III	I_{D}	Absolute	–
7	I_{GINV} , I_{GOV} , I_{GACC}	IV	I_{G}	Relative	–
8	a_1 , a_2 , a_3	IV	I_{B}	Absolute	$V_{\mathrm{GS}} \geq 0$ V
9	A_{GIDL}	IV	I_{B}	Absolute	$V_{\mathrm{GS}} < 0$ V
9	Repeat Steps 2, 3, 4, 5, 7, 8 and 9				

For short-channel devices the values of the poly-depletion parameter $1/k_{\mathrm{P}}$, flat-band voltage V_{FB}, the carrier mobility parameters (θ_{sr}, θ_{ph} and η_{mob}) and the gate tunnelling probability factors (B_{inv} and B_{acc}) of the long-channel device are copied, and next the extraction procedure as given in Table7.3 is executed. In contrast to the long-channel case, the extraction procedure for short-channel devices also optimises the parameters for series-resistance[10] and DIBL.

Table 7.4: Starting miniset parameter values for AC-parameter extraction of a typical MOSFET with channel length L (m), channel width W (m) and oxide thickness t_{ox} (m).

Parameter	Program Name	Parameter Value	
		NMOS	PMOS
C_{OX}	COX	$\epsilon_{\mathrm{ox}} \big/ t_{\mathrm{ox}} \cdot W \cdot L$	$\epsilon_{\mathrm{ox}} \big/ t_{\mathrm{ox}} \cdot W \cdot L$
C_{GDO}	CGDO	$3.0 \cdot 10^{-10} \cdot W$	$3.0 \cdot 10^{-10} \cdot W$
C_{GSO}	CGSO	$3.0 \cdot 10^{-10} \cdot W$	$3.0 \cdot 10^{-10} \cdot W$

AC-parameters: In Tab. 7.4, a first-order estimation of the AC-parameters is given. The AC-parameters C_{OX}, C_{GSO}, C_{GDO}, and in addition k_{ov} and V_{FBov} cannot be (accurately) determined from DC-characteristics, and as a consequence they have to be determined from C–V–characteristics[11]. Since normal MOS transistors are symmetrical devices, one can assume that the oxide capacitance

[10] Note that in Table 7.3 parameters θ_{R1} and θ_{R2} are not included, which implies that the series-resistance is assumed to be voltage-independent. This holds true for modern CMOS technologies, where no use is made of LDD-structures.

[11] Although parameter k_{ov} can be determined from overlap gate current, see Tab. 7.2, it is nonetheless more accurately determined from the C_{cg}–V_{GS} characteristic.

©Koninklijke Philips Electronics N.V. 2004

of the source and drain extension are identical, which implies that C_{GSO}=C_{GDO}. The oxide capacitance of the intrisic MOSFET C_{OX} can be extracted from Measurement VI. In Table 7.5 the extraction procedure for the AC-parameters is given.

Table 7.5: AC-parameter extraction procedure for a MOSFET. Here it is assumed that $C_{GSO} = C_{GDO}$. In the first instance flat-band voltage V_{FBov} is not optimised, although it may be optimised during Step 1 in order to obtain more accurate results. The optimization is either performed on the absolute or relative deviation between model and measurements.

Step	Optimised Parameters	Measure-ment	Fitted On	Absolute/ Relative	Specific Conditions
1	k_{ov} , C_{GSO}	VI	C_{cg}	Relative	$V_{GS} < 0$ V
2	C_{OX}	V	C_{gg}	Relative	–
3	Repeat Steps 1 and 2				

7.3 Extraction of Temperature Scaling Parameters

For a specific device the temperature scaling parameters can be extracted after the miniset at room temperature has been extracted. In order to so, measurements I, III and IV need to be performed at various temperature values (at least two values different from room temperature, typically -40°C and 125°C). Since the reference temperature T_R has been chosen equal to room temperature, the modelled behaviour at room temperature is not affected by different values of the temperature scaling parameters. As a first-order estimation of the temperature scaling parameter values, the default values as given in Sections 8.2.1 and 8.2.2 are used. Again the parameter extraction scheme is slightly different for the long-channel and for the short-channel case.

Table 7.6: Temperature scaling parameter extraction procedure for a long-channel n-MOSFET, where measurements have been performed at various temperature values. For p-type transistors all voltages and currents have to be multiplied by -1. The optimization is either performed on the absolute or relative deviation between model and measurements. Parameter I_{tst} is 2.5 μA for NMOS and 0.8 μA for PMOS.

Step	Optimised Parameters	Measure-ment	Fitted On	Absolute/ Relative	Specific Conditions
1	$S_{T;\phi_B}$	I	I_D	Relative	$I_D < W/L \cdot I_{tst}$
2	η_β , η_{sr} , η_{ph} , ν_{exp} , $S_{T;\eta_{mob}}$	I	I_D	Relative	$I_D > W/L \cdot I_{tst}$
3	η_{sat}	III	I_D	Absolute	–
4	$S_{T;a_1}$	IV	I_B	Absolute	$V_{GS} \geq 0$ V
5	$S_{T;B_{GIDL}}$	IV	I_B	Absolute	$V_{GS} < 0$ V

For an accurate extraction, the temperature scaling parameters for a long-channel device have to be determined first. In the long-channel case the carrier mobility parameters (i.e. η_{sr}, η_{ph}, ν_{exp} and $S_{T;\eta_{mob}}$) can be determined, and they can subsequently be fixed for the short-channel devices. In Table 7.6 the extraction procedure for long-channel transistors is given. In Step 1 the subthreshold temperature dependence is optimised, followed by the optimization of mobility reduction parameters in Step 2. Next the temperature dependence of velocity saturation is optimised in Step 3. In Step 4,

 ©Koninklijke Philips Electronics N.V. 2004

the temperature dependence of impact ionization is determined, and finally in Step 5, the temperature dependence of the gate-induced drain leakage is optimised.

Table 7.7: Temperature scaling parameter extraction procedure for a short-channel n-MOSFET, where measurements have been performed at various temperature values. For p-type transistors all voltages and currents have to be multiplied by -1. The optimization is either performed on the absolute or relative deviation between model and measurements. Parameter I_{tst} is 2.5 μA for NMOS and 0.8 μA for PMOS.

Step	Optimised Parameters	Measurement	Fitted On	Absolute/ Relative	Specific Conditions
1	$S_{T;\phi_B}$	I	I_D	Relative	$I_D < W/L \cdot I_{tst}$
2	η_β , η_R	I	I_D	Relative	$I_D > W/L \cdot I_{tst}$
3	η_{sat}	III	I_D	Absolute	–
4	$S_{T;a_1}$	IV	I_B	Absolute	$V_{GS} \geq 0$ V
5	$S_{T;B_{GIDL}}$	IV	I_B	Absolute	$V_{GS} < 0$ V

For short-channel devices the values of the mobility reduction temperature scaling parameters (i.e. η_{sr}, η_{ph}, ν_{exp} and $S_{T;\eta_{mob}}$) of the long-channel device are copied, and next the extraction procedure as given in Table 7.7 is executed. In contrast to the long-channel case, the extraction procedure for short-channel devices optimises the parameter for series-resistance.

7.4 Extraction of Geometry Scaling Parameters

In general the most important part of the geometry scaling scheme is the determination of ΔL and ΔW, see eqs. (5.1) and (5.2), since it affects the DC-, the AC- as well as the noise model. Traditionally ΔW can be determined from the extrapolated zero-crossing in the gain factor β versus mask width W. In a similar way ΔL can be determined from the inverse gain factor $1/\beta$ versus mask length L. For modern MOS devices with pocket implants, however, it has been found that the above ΔL extraction method is no longer valid [23],[25]. Another, more accurate method is to measure the gate-to-bulk capacitance C_{GB} in accumulation for different channel lengths [24],[25]. In this case the extrapolated zero-crossing in the C_{GB} versus mask length L curve will give ΔL. Unfortunately for CMOS technologies in which gate current is non-negligible, capacitance measurements may be hampered by gate current [10]. In this case either gate current parameter I_{GINV} or I_{GACC} plotted as a function of channel length L may be used to extract ΔL [10].

In MM11, Level 1102, one can use either physical or binning geometry scaling rules. When using the binning rules of Section 5.2.2, the scaling parameters for one bin can be directly calculated from the minisets of the four corner devices of the bin. The binning scheme ensures that the minisets are exactly reproduced in the bin corners, and that no humps occur in parameter values across bin borders. The exact way to calculate binning parameters from minisets is described in AppendixB.

When using the physical scaling relations of Section 5.2.1 it is possible to calculate a parameter set for a process, given the parameter set of typical transistors of this process. To accomplish this, transistors of different lengths, widths and at different temperatures have to be measured. Using these measurements the sensitivities of the parameters on length, width and temperature can be found. For the determination of a geometry-scaled parameter set a three-step procedure is recommended:

1. determine minisets (ϕ_B, k_0, β, $\ldots$) for all measured devices, as explained in Sections 7.2 and 7.3.
2. the width and length sensitivity coefficients are optimised by fitting the appropriate geometry scaling rules to these miniset parameters.
3. finally the width and length sensitivity coefficients are optimised by fitting the result of the scaling rules and current equations to the measured currents of all devices simultaneously.

Parameter sets have been determined for several processes using this parameter extraction strategy and taking care of not exceeding the supply voltage. For all processes good results have been obtained.

©Koninklijke Philips Electronics N.V. 2004

8 Parameter Clipping and Default Values

8.1 Introduction

For the clipping of a parameter the lower bound B_L and/or the upper bound B_U are specified for the value range of that parameter. If both bounds are given the value range is the closed interval $[B_L, B_U]$ and in the case of one bound it is either the half–open interval $[B_L, \infty)$ or $(-\infty, B_U]$. If the value of a parameter exceeds its bound it has to be replaced by that particular bound. In the Sections8.2.1 and 8.2.2 default values and clipping values for the parameters of the electrical MOS Model 11 are given for n-channels and p-channels, respectively. In the Sections 8.3.1 and 8.3.2 default values and clipping values for the parameters of the physical geometrical scaling rules of MOS Model 11 are given for n-channels and p-channels, respectively. Finally, in the Sections 8.4.1 and 8.4.2 default values and clipping values for the parameters of the binning geometry scaling rules of MOS Model 11 are given for n-channels and p-channels, respectively.

Note: Once the parameters have been calculated from the physical geometrical scaling rules (see Section 5.2.1) or from the binning geometrical scaling rules (see Section 5.2.2), the clipping values of the electrical model (see Sections 8.2.1 and 8.2.2) have to be applied!

8.2 Parameter Clipping and Default Values for the Electrical Model

8.2.1 Parameter Clipping and Default Values for the Electrical N-channel Model

The default values and clipping values for the parameters of the electrical MOS Model 11 (**n-channel**) are listed below.

No.	Parameter	Units	Default	Clip low	Clip high
0	LEVEL	-	1102	-	-
1	TR	°C	21.0	-273.15	-
2	VFB	V	-1.0500	-	-
3	STVFB	VK^{-1}	0.5×10^{-3}	-	-
4	KO	$V^{1/2}$	0.5000	1.0×10^{-12}	-
5	KPINV	$V^{-1/2}$	0.0000	0.000	-
6	PHIB	V	0.9500	1.0×10^{-12}	-
7	STPHIB	VK^{-1}	-8.5×10^{-4}	-	-
8	BET	AV^{-2}	1.9215×10^{-3}	0.000	-
9	ETABET	-	1.300	-	-
10	THESR	V^{-1}	0.3562	1.0×10^{-12}	-
11	ETASR	-	0.650	-	-
12	THEPH	V^{-1}	1.29×10^{-2}	1.0×10^{-12}	-
13	ETAPH	-	1.350	-	-
14	ETAMOB	-	1.4000	0.000	-
15	STETAMOB	K^{-1}	0.000	-	-
16	NU	-	2.0000	1.000	-
17	NUEXP	-	5.250	-	-
18	THER	V^{-1}	8.12×10^{-2}	0.000	-
19	ETAR	-	0.950	-	-
20	THER1	V	0.0000	0.000	-
21	THER2	V	1.0000	0.000	-
22	THESAT	V^{-1}	0.2513	0.000	-
23	ETASAT	-	1.040	-	-
24	THETH	V^{-3}	1.0×10^{-5}	0.000	-
25	SDIBL	$V^{-1/2}$	8.53×10^{-4}	1.0×10^{-12}	-

©Koninklijke Philips Electronics N.V. 2004

26	MO	V	0.0000	0.000	0.500
27	SSF	$V^{-1/2}$	0.0120	1.0×10^{-12}	-
28	ALP	-	0.0250	0.000	-
29	VP	V	0.0500	1.0×10^{-12}	-
30	MEXP	-	5.0000	1.000	-
31	A1	-	6.0221	0.000	-
32	STA1	K^{-1}	0.000	-	-
33	A2	V	38.017	1.0×10^{-12}	-
34	A3	-	0.6407	0.000	-
35	IGINV	AV^{-2}	0.0000	0.000	-
36	BINV	V	48.000	0.000	-
37	IGACC	AV^{-2}	0.0000	0.000	-
38	BACC	V	48.000	0.000	-
39	VFBOV	V	0.0000	-	-
40	KOV	$V^{1/2}$	2.5000	1.0×10^{-12}	-
41	IGOV	AV^{-2}	0.0000	0.000	-
42	AGIDL	AV^{-3}	0.0000	0.000	-
43	BGIDL	V	41.000	0.000	-
44	STBGIDL	VK^{-1}	-3.638×10^{-4}	-	-
45	CGIDL	-	0.000	0.000	-
46	COX	F	2.98×10^{-14}	0.000	-
47	CGDO	F	6.392×10^{-15}	0.000	-
48	CGSO	F	6.392×10^{-15}	0.000	-
49	GATENOISE	-	0.0000	0.000	1.000
50	NT	J	1.624×10^{-20}	0.000	-
51	NFA	$V^{-1}m^{-4}$	8.323×10^{22}	0.000	-
52	NFB	$V^{-1}m^{-2}$	2.514×10^{7}	-	-
53	NFC	V^{-1}	0.0000	-	-
54	TOX	m	3.2×10^{-9}	1.0×10^{-12}	-
55	DTA	K	0.000	-	-

©Koninklijke Philips Electronics N.V. 2004

56	MULT	-	1.0000	0.000	-

The default values and clipping values of the additional parameters for the (**n-channel**) model including self-heating (see Section 4.2) are listed in the table below.

No.	**Parameter**	**Units**	**Default**	**Clip low**	**Clip high**
57	RTH	K/W	300.0	0.000	-
58	CTH	J/K	3.0×10^{-9}	0.000	-
59	ATH	-	0.000	-	-

 ©Koninklijke Philips Electronics N.V. 2004

8.2.2 Parameter Clipping and Default Values for the Electrical P-channel Model

The default values and clipping values for the parameters of the electrical MOS Model 11 (**p-channel**) are listed below.

No.	Parameter	Units	Default	Clip low	Clip high
0	LEVEL	-	1102	-	-
1	TR	^{o}C	21.0	-273.15	-
2	VFB	V	-1.0500	-	-
3	STVFB	VK^{-1}	0.5×10^{-3}	-	-
4	KO	$V^{1/2}$	0.5000	1.0×10^{-12}	-
5	KPINV	$V^{-1/2}$	0.0000	0.000	-
6	PHIB	V	0.9500	1.0×10^{-12}	-
7	STPHIB	VK^{-1}	-8.5×10^{-4}	-	-
8	BET	AV^{-2}	3.8140×10^{-4}	0.000	-
9	ETABET	-	0.500	-	-
10	THESR	V^{-1}	0.7300	1.0×10^{-12}	-
11	ETASR	-	0.500	-	-
12	THEPH	V^{-1}	0.0010	1.0×10^{-12}	-
13	ETAPH	-	3.750	-	-
14	ETAMOB	-	3.0000	0.000	-
15	STETAMOB	K^{-1}	0.000	-	-
16	NU	-	2.0000	1.000	-
17	NUEXP	-	3.230	-	-
18	THER	V^{-1}	7.90×10^{-2}	0.000	-
19	ETAR	-	0.400	-	-
20	THER1	V	0.0000	0.000	-
21	THER2	V	1.0000	0.000	-
22	THESAT	V^{-1}	0.1728	0.000	-
23	ETASAT	-	0.860	-	-
24	THETH	V^{-3}	0.000	0.000	-
25	SDIBL	$V^{-1/2}$	3.551×10^{-5}	1.0×10^{-12}	-
26	MO	V	0.0000	0.000	0.500

©Koninklijke Philips Electronics N.V. 2004

27	SSF	$V^{-1/2}$	0.0100	1.0×10^{-12}	-
28	ALP	-	0.0250	0.000	-
29	VP	V	0.0500	1.0×10^{-12}	-
30	MEXP	-	5.0000	1.000	-
31	A1	-	6.8583	0.000	-
32	STA1	K^{-1}	0.000	-	-
33	A2	V	57.324	1.0×10^{-12}	-
34	A3	-	0.4254	0.000	-
35	IGINV	AV^{-2}	0.0000	0.000	-
36	BINV	V	87.500	0.000	-
37	IGACC	AV^{-2}	0.0000	0.000	-
38	BACC	V	48.000	0.000	-
39	VFBOV	V	0.0000	-	-
40	KOV	$V^{1/2}$	2.5000	1.0×10^{-12}	-
41	IGOV	AV^{-2}	0.0000	0.000	-
42	AGIDL	AV^{-3}	0.0000	0.000	-
43	BGIDL	V	41.000	0.000	-
44	STBGIDL	VK^{-1}	-3.638×10^{-4}	-	-
45	CGIDL	-	0.000	0.000	-
46	COX	F	2.717×10^{-14}	0.000	-
47	CGDO	F	6.358×10^{-15}	0.000	-
48	CGSO	F	6.358×10^{-15}	0.000	-
49	GATENOISE	-	0.0000	0.000	1.000
50	NT	J	1.624×10^{-20}	0.000	-
51	NFA	$V^{-1}m^{-4}$	1.900×10^{22}	0.000	-
52	NFB	$V^{-1}m^{-2}$	5.043×10^{6}	-	-
53	NFC	V^{-1}	3.627×10^{-10}	-	-
54	TOX	m	3.2×10^{-9}	1.0×10^{-12}	-
55	DTA	K	0.000	-	-
56	MULT	-	1.0000	0.000	-

 ©Koninklijke Philips Electronics N.V. 2004

The default values and clipping values of the additional parameters for the (**p-channel**) model including self-heating (see Section 4.2) are listed in the table below.

No.	Parameter	Units	Default	Clip low	Clip high
57	RTH	K/W	300.0	0.000	-
58	CTH	J/K	3.0×10^{-9}	0.000	-
59	ATH	-	0.000	-	-

©Koninklijke Philips Electronics N.V. 2004

8.3 Parameter Clipping and Default Values for the Physical Geometrical Scaling Rules

8.3.1 Parameter Clipping and Default Values for Physical Geometrical Scaling Rules of the N-channel Model

The default values and clipping values for the parameters of the physical geometrical scaling rules of MOS Model 11 (**n-channel**) are listed below.

No.	Parameter	Units	Default	Clip low	Clip high
0	LEVEL	-	11020	-	-
1	LVAR	m	0.000	-	-
2	LAP	m	4.0×10^{-8}	-	-
3	WVAR	m	0.000	-	-
4	WOT	m	0.000	-	-
5	TR	^{o}C	21.0	-273.15	-
6	VFB	V	-1.050	-	-
7	STVFB	VK^{-1}	0.5×10^{-3}	-	-
8	KOR	$V^{1/2}$	0.500	-	-
9	SLKO	-	0.000	-	-
10	SL2KO	-	0.000	-	-
11	SWKO	-	0.000	-	-
12	KPINV	$V^{-1/2}$	0.000	-	-
13	PHIBR	V	0.950	-	-
14	STPHIB	VK^{-1}	-8.5×10^{-4}	-	-
15	SLPHIB	-	0.000	-	-
16	SL2PHIB	-	0.000	-	-
17	SWPHIB	-	0.000	-	-
18	BETSQ	AV^{-2}	3.709×10^{-4}	-	-
19	ETABETR	-	1.300	-	-
20	SLETABET	-	0.000	-	-
21	FBET1	-	0.000	-	-
22	LP1	m	0.8×10^{-6}	1.0×10^{-10}	-
23	FBET2	-	0.000	-	-
24	LP2	m	0.8×10^{-6}	1.0×10^{-10}	-

 ©Koninklijke Philips Electronics N.V. 2004

25	THESRR	V^{-1}	0.400	-	-
26	ETASR	-	0.650	-	-
27	SWTHESR	-	0.000	-	-
28	THEPHR	V^{-1}	1.29×10^{-2}	-	-
29	ETAPH	-	1.350	-	-
30	SWTHEPH	-	0.000	-	-
31	ETAMOBR	-	1.40	-	-
32	STETAMOB	K^{-1}	0.000	-	-
33	SWETAMOB	-	0.000	-	-
34	NU	-	2.000	1.000	-
35	NUEXP	-	5.250	-	-
36	THERR	V^{-1}	0.155	1.0×10^{-10}	-
37	ETAR	-	0.950	-	-
38	SWTHER	-	0.000	-	-
39	THER1	V	0.000	-	-
40	THER2	V	1.000	-	-
41	THESATR	V^{-1}	0.500	-	-
42	ETASAT	-	1.040	-	-
43	SLTHESAT	-	1.000	-	-
44	THESATEXP	-	1.000	0.000	-
45	SWTHESAT	-	0.000	-	-
46	THETHR	V^{-3}	1.0×10^{-3}	-	-
47	THETHEXP	-	1.000	0.000	-
48	SWTHETH	-	0.000	-	-
49	SDIBLO	$V^{-1/2}$	1.0×10^{-4}	-	-
50	SDIBLEXP	-	1.350	-	-
51	MOO	-	0.000	-	-
52	MOR	-	0.000	-	-
53	MOEXP	-	1.340	-	-
54	SSFR	$V^{-1/2}$	6.25×10^{-3}	-	-

©Koninklijke Philips Electronics N.V. 2004

55	SLSSF	-	1.000	-	-
56	SWSSF	-	0.000	-	-
57	ALPR	-	1.0×10^{-2}	-	-
58	SLALP	-	1.000	-	-
59	ALPEXP	-	1.000	0.000	-
60	SWALP	-	0.000	-	-
61	VP	V	5.0×10^{-2}	-	-
62	LMIN	m	1.5×10^{-7}	1.0×10^{-10}	2.5×10^{-6}
63	A1R	-	6.000	-	-
64	STA1	K^{-1}	0.000	-	-
65	SLA1	-	0.000	-	-
66	SWA1	-	0.000	-	-
67	A2R	V	38.00	-	-
68	SLA2	-	0.000	-	-
69	SWA2	-	0.000	-	-
70	A3R	-	1.000	-	-
71	SLA3	-	0.000	-	-
72	SWA3	-	0.000	-	-
73	IGINVR	AV^{-2}	0.000	0.000	-
74	BINV	V	48.00	0.000	-
75	IGACCR	AV^{-2}	0.000	0.000	-
76	BACC	V	48.00	0.000	-
77	VFBOV	V	0.000	-	-
78	KOV	$V^{1/2}$	2.500	1.0×10^{-12}	-
79	IGOVR	AV^{-2}	0.000	0.000	-
80	AGIDLR	AV^{-3}	0.000	0.000	-
81	BGIDL	V	41.00	0.000	-
82	STBGIDL	VK^{-1}	-3.638×10^{-4}	-	-
83	CGIDL	-	0.000	0.000	-
84	TOX	m	3.2×10^{-9}	1.0×10^{-12}	-

©Koninklijke Philips Electronics N.V. 2004

85	COL	F	3.2×10^{-16}	-	-
86	GATENOISE	-	0.000	0.000	1.000
87	NT	J	1.624×10^{-20}	0.000	-
88	NFAR	$V^{-1}m^{-4}$	1.573×10^{23}	-	-
89	NFBR	$V^{-1}m^{-2}$	4.752×10^{9}	-	-
90	NFCR	V^{-1}	0.000	-	-
91	L	m	2.000×10^{-6}	-	-
92	W	m	1.000×10^{-5}	-	-
93	DTA	K	0.000	-	-
94	MULT	-	1.000	0.000	-

Remark: The parameters L, W and DTA are used to calculate the electrical parameters of the actual transistor as specified in the section on parameter preprocessing.
The default values and clipping values of the additional parameters for the (**n-channel**) model including self-heating (see Section 4.2) are listed in the table below.

No.	**Parameter**	**Units**	**Default**	**Clip low**	**Clip high**
95	RTH	K/W	300.0	0.000	-
96	CTH	J/K	3.0×10^{-9}	0.000	-
97	ATH	-	0.000	-	-

©Koninklijke Philips Electronics N.V. 2004

8.3.2 Parameter Clipping and Default Values for Physical Geometrical Scaling Rules of the P-channel Model

The default values and clipping values for the parameters of the physical geometrical scaling rules of MOS Model 11 (**p-channel**) are listed below.

No.	**Parameter**	**Units**	**Default**	**Clip low**	**Clip high**
0	LEVEL	-	11020	-	-
1	LVAR	m	0.000	-	-
2	LAP	m	4.0×10^{-8}	-	-
3	WVAR	m	0.000	-	-
4	WOT	m	0.000	-	-
5	TR	^{o}C	21.0	-273.15	-
6	VFB	V	-1.050	-	-
7	STVFB	VK^{-1}	0.5×10^{-3}	-	-
8	KOR	$V^{1/2}$	0.500	-	-
9	SLKO	-	0.000	-	-
10	SL2KO	-	0.000	-	-
11	SWKO	-	0.000	-	-
12	KPINV	$V^{-1/2}$	0.000	-	-
13	PHIBR	V	0.950	-	-
14	STPHIB	VK^{-1}	-8.5×10^{-4}	-	-
15	SLPHIB	-	0.000	-	-
16	SL2PHIB	-	0.000	-	-
17	SWPHIB	-	0.000	-	-
18	BETSQ	AV^{-2}	1.150×10^{-4}	-	-
19	ETABETR	-	0.500	-	-
20	SLETABET	-	0.000	-	-
21	FBET1	-	0.000	-	-
22	LP1	m	0.8×10^{-6}	1.0×10^{-10}	-
23	FBET2	-	0.000	-	-
24	LP2	m	0.8×10^{-6}	1.0×10^{-10}	-
25	THESRR	V^{-1}	0.730	-	-

 ©Koninklijke Philips Electronics N.V. 2004

26	ETASR	-	0.500	-	-
27	SWTHESR	-	0.000	-	-
28	THEPHR	V^{-1}	1.0×10^{-3}	-	-
29	ETAPH	-	3.750	-	-
30	SWTHEPH	-	0.000	-	-
31	ETAMOBR	-	3.000	-	-
32	STETAMOB	K^{-1}	0.000	-	-
33	SWETAMOB	-	0.000	-	-
34	NU	-	2.000	1.000	-
35	NUEXP	-	3.230	-	-
36	THERR	V^{-1}	0.080	1.0×10^{-10}	-
37	ETAR	-	0.400	-	-
38	SWTHER	-	0.000	-	-
39	THER1	V	0.000	-	-
40	THER2	V	1.000	-	-
41	THESATR	V^{-1}	0.200	-	-
42	ETASAT	-	0.860	-	-
43	SLTHESAT	-	1.000	-	-
44	THESATEXP	-	1.000	0.000	-
45	SWTHESAT	-	0.000	-	-
46	THETHR	V^{-3}	0.5×10^{-3}	-	-
47	THETHEXP	-	1.000	0.000	-
48	SWTHETH	-	0.000	-	-
49	SDIBLO	$V^{-1/2}$	1.0×10^{-4}	-	-
50	SDIBLEXP	-	1.350	-	-
51	MOO	-	0.000	-	-
52	MOR	-	0.000	-	-
53	MOEXP	-	1.340	-	-
54	SSFR	$V^{-1/2}$	6.25×10^{-3}	-	-
55	SLSSF	-	1.0000	-	-

©Koninklijke Philips Electronics N.V. 2004

56	SWSSF	-	0.000	-	-
57	ALPR	-	1.0×10^{-2}	-	-
58	SLALP	-	1.000	-	-
59	ALPEXP	-	1.000	0.000	-
60	SWALP	-	0.000	-	-
61	VP	V	5.0×10^{-2}	-	-
62	LMIN	m	1.5×10^{-7}	1.0×10^{-10}	2.5×10^{-6}
63	A1R	-	6.000	-	-
64	STA1	K^{-1}	0.000	-	-
65	SLA1	-	0.000	-	-
66	SWA1	-	0.000	-	-
67	A2R	V	38.00	-	-
68	SLA2	-	0.000	-	-
69	SWA2	-	0.000	-	-
70	A3R	-	1.000	-	-
71	SLA3	-	0.000	-	-
72	SWA3	-	0.000	-	-
73	IGINVR	AV^{-2}	0.000	0.000	-
74	BINV	V	87.50	0.000	-
75	IGACCR	AV^{-2}	0.000	0.000	-
76	BACC	V	48.00	0.000	-
77	VFBOV	V	0.000	-	-
78	KOV	$V^{1/2}$	2.500	1.0×10^{-12}	-
79	IGOVR	AV^{-2}	0.000	0.000	-
80	AGIDLR	AV^{-3}	0.000	0.000	-
81	BGIDL	V	41.00	0.000	-
82	STBGIDL	VK^{-1}	-3.638×10^{-4}	-	-
83	CGIDL	-	0.000	0.000	-
84	TOX	m	3.2×10^{-9}	1.0×10^{-12}	-
85	COL	F	3.2×10^{-16}	-	-

 ©Koninklijke Philips Electronics N.V. 2004

86	GATENOISE	-	0.000	0.000	1.000
87	NT	J	1.624×10^{-20}	0.000	-
88	NFAR	$V^{-1}m^{-4}$	3.825×10^{24}	-	-
89	NFBR	$V^{-1}m^{-2}$	1.015×10^{9}	-	-
90	NFCR	V^{-1}	7.300×10^{-8}	-	-
91	L	m	2.000×10^{-6}	-	-
92	W	m	1.000×10^{-5}	-	-
93	DTA	K	0.000	-	-
94	MULT	-	1.000	0.000	-

Remark: The parameters L, W and DTA are used to calculate the electrical parameters of the actual transistor as specified in the section on parameter preprocessing.
The default values and clipping values of the additional parameters for the (**p-channel**) model including self-heating (see Section 4.2) are listed in the table below.

No.	Parameter	Units	Default	Clip low	Clip high
95	RTH	K/W	300.0	0.000	-
96	CTH	J/K	3.0×10^{-9}	0.000	-
97	ATH	-	0.000	-	-

©Koninklijke Philips Electronics N.V. 2004

8.4 Parameter Clipping and Default Values for the Binning Geometrical Scaling Rules

8.4.1 Parameter Clipping and Default Values for Binning Geometrical Scaling Rules of the N-channel Model

The default values and clipping values for the parameters of the binning geometrical scaling rules of MOS Model 11 (**n-channel**) are listed below.

No.	Parameter	Units	Default	Clip low	Clip high
0	LEVEL	-	11021	-	-
1	LVAR	m	0.000	-	-
2	LAP	m	4.000×10^{-8}	-	-
3	WVAR	m	0.000	-	-
4	WOT	m	0.000	-	-
5	TR	^{o}C	21.0	-273.15	-
6	VFB	V	-1.050	-	-
7	POKO	$V^{1/2}$	0.500	-	-
8	PLKO	$V^{1/2}$	0.000	-	-
9	PWKO	$V^{1/2}$	0.000	-	-
10	PLWKO	$V^{1/2}$	0.000	-	-
11	KPINV	$V^{-1/2}$	0.000	-	-
12	POPHIB	V	0.950	-	-
13	PLPHIB	V	0.000	-	-
14	PWPHIB	V	0.000	-	-
15	PLWPHIB	V	0.000	-	-
16	POBET	AV^{-2}	1.922×10^{-3}	-	-
17	PLBET	AV^{-2}	0.000	-	-
18	PWBET	AV^{-2}	0.000	-	-
19	PLWBET	AV^{-2}	0.000	-	-
20	POTHESR	V^{-1}	3.562×10^{-1}	-	-
21	PLTHESR	V^{-1}	0.000	-	-
22	PWTHESR	V^{-1}	0.000	-	-
23	PLWTHESR	V^{-1}	0.000	-	-
24	POTHEPH	V^{-1}	1.290×10^{-2}	-	-

©Koninklijke Philips Electronics N.V. 2004

25	PLTHEPH	V^{-1}	0.000	-	-
26	PWTHEPH	V^{-1}	0.000	-	-
27	PLWTHEPH	V^{-1}	0.000	-	-
28	POETAMOB	-	1.400	-	-
29	PLETAMOB	-	0.000	-	-
30	PWETAMOB	-	0.000	-	-
31	PLWETAMOB	-	0.000	-	-
32	POTHER	V^{-1}	8.120×10^{-2}	-	-
33	PLTHER	V^{-1}	0.000	-	-
34	PWTHER	V^{-1}	0.000	-	-
35	PLWTHER	V^{-1}	0.000	-	-
36	THER1	V	0.000	-	-
37	THER2	V	1.000	-	-
38	POTHESAT	V^{-1}	2.513×10^{-1}	-	-
39	PLTHESAT	V^{-1}	0.000	-	-
40	PWTHESAT	V^{-1}	0.000	-	-
41	PLWTHESAT	V^{-1}	0.000	-	-
42	POTHETH	V^{-3}	1.0×10^{-5}	-	-
43	PLTHETH	V^{-3}	0.000	-	-
44	PWTHETH	V^{-3}	0.000	-	-
45	PLWTHETH	V^{-3}	0.000	-	-
46	POSDIBL	$V^{-1/2}$	8.530×10^{-4}	-	-
47	PLSDIBL	$V^{-1/2}$	0.000	-	-
48	PWSDIBL	$V^{-1/2}$	0.000	-	-
49	PLWSDIBL	$V^{-1/2}$	0.000	-	-
50	POMO	-	0.000	-	-
51	PLMO	-	0.000	-	-
52	PWMO	-	0.000	-	-
53	PLWMO	-	0.000	-	-
54	POSSF	$V^{-1/2}$	1.200×10^{-2}	-	-

©Koninklijke Philips Electronics N.V. 2004

55	PLSSF	$V^{-1/2}$	0.000	-	-
56	PWSSF	$V^{-1/2}$	0.000	-	-
57	PLWSSF	$V^{-1/2}$	0.000	-	-
58	POALP	-	2.500×10^{-2}	-	-
59	PLALP	-	0.000	-	-
60	PWALP	-	0.000	-	-
61	PLWALP	-	0.000	-	-
62	VP	V	5.000×10^{-2}	-	-
63	POMEXP	-	0.200	-	-
64	PLMEXP	-	0.000	-	-
65	PWMEXP	-	0.000	-	-
66	PLWMEXP	-	0.000	-	-
67	POA1	-	6.022	-	-
68	PLA1	-	0.000	-	-
69	PWA1	-	0.000	-	-
70	PLWA1	-	0.000	-	-
71	POA2	V	$3.802\times10^{+1}$	-	-
72	PLA2	V	0.000	-	-
73	PWA2	V	0.000	-	-
74	PLWA2	V	0.000	-	-
75	POA3	-	6.407×10^{-1}	-	-
76	PLA3	-	0.000	-	-
77	PWA3	-	0.000	-	-
78	PLWA3	-	0.000	-	-
79	POIGINV	AV^{-2}	0.000	-	-
80	PLIGINV	AV^{-2}	0.000	-	-
81	PWIGINV	AV^{-2}	0.000	-	-
82	PLWIGINV	AV^{-2}	0.000	-	-
83	POBINV	V	$4.800\times10^{+1}$	-	-
84	PLBINV	V	0.000	-	-

©Koninklijke Philips Electronics N.V. 2004

85	PWBINV	V	0.000	-	-
86	PLWBINV	V	0.000	-	-
87	POIGACC	AV^{-2}	0.000	-	-
88	PLIGACC	AV^{-2}	0.000	-	-
89	PWIGACC	AV^{-2}	0.000	-	-
90	PLWIGACC	AV^{-2}	0.000	-	-
91	POBACC	V	$4.800\times10^{+1}$	-	-
92	PLBACC	V	0.000	-	-
93	PWBACC	V	0.000	-	-
94	PLWBACC	V	0.000	-	-
95	VFBOV	V	0.000	-	-
96	KOV	$V^{1/2}$	2.500	1.0×10^{-12}	-
97	POIGOV	AV^{-2}	0.000	-	-
98	PLIGOV	AV^{-2}	0.000	-	-
99	PWIGOV	AV^{-2}	0.000	-	-
100	PLWIGOV	AV^{-2}	0.000	-	-
101	POAGIDL	AV^{-3}	0.000	-	-
102	PLAGIDL	AV^{-3}	0.000	-	-
103	PWAGIDL	AV^{-3}	0.000	-	-
104	PLWAGIDL	AV^{-3}	0.000	-	-
105	POBGIDL	V	$4.100\times10^{+1}$	-	-
106	PLBGIDL	V	0.000	-	-
107	PWBGIDL	V	0.000	-	-
108	PLWBGIDL	V	0.000	-	-
109	POCGIDL	-	0.000	-	-
110	PLCGIDL	-	0.000	-	-
111	PWCGIDL	-	0.000	-	-
112	PLWCGIDL	-	0.000	-	-
113	TOX	m	3.200×10^{-9}	1.0×10^{-12}	-
114	POCOX	F	2.980×10^{-14}	-	-

©Koninklijke Philips Electronics N.V. 2004

115	PLCOX	F	0.000	-	-
116	PWCOX	F	0.000	-	-
117	PLWCOX	F	0.000	-	-
118	POCGDO	F	6.392×10^{-15}	-	-
119	PLCGDO	F	0.000	-	-
120	PWCGDO	F	0.000	-	-
121	PLWCGDO	F	0.000	-	-
122	POCGSO	F	6.392×10^{-15}	-	-
123	PLCGSO	F	0.000	-	-
124	PWCGSO	F	0.000	-	-
125	PLWCGSO	F	0.000	-	-
126	GATENOISE	-	0.000	0.000	1.000
127	NT	J	1.624×10^{-20}	0.000	-
128	PONFA	$V^{-1}m^{-4}$	8.323×10^{22}	-	-
129	PLNFA	$V^{-1}m^{-4}$	0.000	-	-
130	PWNFA	$V^{-1}m^{-4}$	0.000	-	-
131	PLWNFA	$V^{-1}m^{-4}$	0.000	-	-
132	PONFB	$V^{-1}m^{-2}$	$2.514\times10^{+7}$	-	-
133	PLNFB	$V^{-1}m^{-2}$	0.000	-	-
134	PWNFB	$V^{-1}m^{-2}$	0.000	-	-
135	PLWNFB	$V^{-1}m^{-2}$	0.000	-	-
136	PONFC	V^{-1}	0.000	-	-
137	PLNFC	V^{-1}	0.000	-	-
138	PWNFC	V^{-1}	0.000	-	-
139	PLWNFC	V^{-1}	0.000	-	-
140	POTVFB	VK^{-1}	5.000×10^{-4}	-	-
141	PLTVFB	VK^{-1}	0.000	-	-
142	PWTVFB	VK^{-1}	0.000	-	-
143	PLWTVFB	VK^{-1}	0.000	-	-
144	POTPHIB	VK^{-1}	-8.500×10^{-4}	-	-

 ©Koninklijke Philips Electronics N.V. 2004

145	PLTPHIB	VK^{-1}	0.000	-	-
146	PWTPHIB	VK^{-1}	0.000	-	-
147	PLWTPHIB	VK^{-1}	0.000	-	-
148	POTETABET	-	1.300	-	-
149	PLTETABET	-	0.000	-	-
150	PWTETABET	-	0.000	-	-
151	PLWTETABET	-	0.000	-	-
152	POTETASR	-	0.650	-	-
153	PLTETASR	-	0.000	-	-
154	PWTETASR	-	0.000	-	-
155	PLWETASR	-	0.000	-	-
156	POTETAPH	-	1.350	-	-
157	PLTETAPH	-	0.000	-	-
158	PWTETAPH	-	0.000	-	-
159	PLWETAPH	-	0.000	-	-
160	POTETAMOB	K^{-1}	0.000	-	-
161	PLTETAMOB	K^{-1}	0.000	-	-
162	PWTETAMOB	K^{-1}	0.000	-	-
163	PLWTETAMOB	K^{-1}	0.000	-	-
164	NU	-	2.000	1.000	-
165	POTNUEXP	-	5.250	-	-
166	PLTNUEXP	-	0.000	-	-
167	PWTNUEXP	-	0.000	-	-
168	PLWTNUEXP	-	0.000	-	-
169	POTETAR	-	0.950	-	-
170	PLTETAR	-	0.000	-	-
171	PWTETAR	-	0.000	-	-
172	PLWTETAR	-	0.000	-	-
173	POTETASAT	-	1.040	-	-
174	PLTETASAT	-	0.000	-	-

©Koninklijke Philips Electronics N.V. 2004

175	PWTETASAT	-	0.000	-	-
176	PLWTETASAT	-	0.000	-	-
177	POTA1	K^{-1}	0.000	-	-
178	PLTA1	K^{-1}	0.000	-	-
179	PWTA1	K^{-1}	0.000	-	-
180	PLWTA1	K^{-1}	0.000	-	-
181	POTBGIDL	VK^{-1}	-3.638×10^{-4}	-	-
182	PLTBGIDL	VK^{-1}	0.000	-	-
183	PWTBGIDL	VK^{-1}	0.000	-	-
184	PLWTBGIDL	VK^{-1}	0.000	-	-
185	L	m	2.000×10^{-6}	-	-
186	W	m	1.000×10^{-5}	-	-
187	DTA	K	0.000	-	-
188	MULT	-	1.000	0.000	-

Remark: The parameters L, W and DTA are used to calculate the electrical parameters of the actual transistor as specified in the section on parameter preprocessing.
The default values and clipping values of the additional parameters for the (**n-channel**) model including self-heating (see Section 4.2) are listed in the table below.

No.	**Parameter**	**Units**	**Default**	**Clip low**	**Clip high**
189	RTH	K/W	300.0	0.000	-
190	CTH	J/K	3.0×10^{-9}	0.000	-
191	ATH	-	0.000	-	-

 ©Koninklijke Philips Electronics N.V. 2004

8.4.2 Parameter Clipping and Default Values for Binning Geometrical Scaling Rules of the P-channel Model

The default values and clipping values for the parameters of the binning geometrical scaling rules of MOS Model 11 (**p-channel**) are listed below.

No.	Parameter	Units	Default	Clip low	Clip high
0	LEVEL	-	11021	-	-
1	LVAR	m	0.000	-	-
2	LAP	m	4.000×10^{-8}	-	-
3	WVAR	m	0.000	-	-
4	WOT	m	0.000	-	-
5	TR	ºC	21.0	-273.15	-
6	VFB	V	-1.050	-	-
7	POKO	$V^{1/2}$	0.500	-	-
8	PLKO	$V^{1/2}$	0.000	-	-
9	PWKO	$V^{1/2}$	0.000	-	-
10	PLWKO	$V^{1/2}$	0.000	-	-
11	KPINV	$V^{-1/2}$	0.000	-	-
12	POPHIB	V	0.950	-	-
13	PLPHIB	V	0.000	-	-
14	PWPHIB	V	0.000	-	-
15	PLWPHIB	V	0.000	-	-
16	POBET	AV^{-2}	3.814×10^{-4}	-	-
17	PLBET	AV^{-2}	0.000	-	-
18	PWBET	AV^{-2}	0.000	-	-
19	PLWBET	AV^{-2}	0.000	-	-
20	POTHESR	V^{-1}	7.300×10^{-1}	-	-
21	PLTHESR	V^{-1}	0.000	-	-
22	PWTHESR	V^{-1}	0.000	-	-
23	PLWTHESR	V^{-1}	0.000	-	-
24	POTHEPH	V^{-1}	1.000×10^{-3}	-	-
25	PLTHEPH	V^{-1}	0.000	-	-

©Koninklijke Philips Electronics N.V. 2004

26	PWTHEPH	V^{-1}	0.000	-	-
27	PLWTHEPH	V^{-1}	0.000	-	-
28	POETAMOB	-	3.000	-	-
29	PLETAMOB	-	0.000	-	-
30	PWETAMOB	-	0.000	-	-
31	PLWETAMOB	-	0.000	-	-
32	POTHER	V^{-1}	7.900×10^{-2}	-	-
33	PLTHER	V^{-1}	0.000	-	-
34	PWTHER	V^{-1}	0.000	-	-
35	PLWTHER	V^{-1}	0.000	-	-
36	THER1	V	0.000	-	-
37	THER2	V	1.000	-	-
38	POTHESAT	V^{-1}	1.728×10^{-1}	-	-
39	PLTHESAT	V^{-1}	0.000	-	-
40	PWTHESAT	V^{-1}	0.000	-	-
41	PLWTHESAT	V^{-1}	0.000	-	-
42	POTHETH	V^{-3}	0.000	-	-
43	PLTHETH	V^{-3}	0.000	-	-
44	PWTHETH	V^{-3}	0.000	-	-
45	PLWTHETH	V^{-3}	0.000	-	-
46	POSDIBL	$V^{-1/2}$	3.551×10^{-5}	-	-
47	PLSDIBL	$V^{-1/2}$	0.000	-	-
48	PWSDIBL	$V^{-1/2}$	0.000	-	-
49	PLWSDIBL	$V^{-1/2}$	0.000	-	-
50	POMO	-	0.000	-	-
51	PLMO	-	0.000	-	-
52	PWMO	-	0.000	-	-
53	PLWMO	-	0.000	-	-
54	POSSF	$V^{-1/2}$	1.000×10^{-2}	-	-
55	PLSSF	$V^{-1/2}$	0.000	-	-

©Koninklijke Philips Electronics N.V. 2004

56	PWSSF	$V^{-1/2}$	0.000	-	-
57	PLWSSF	$V^{-1/2}$	0.000	-	-
58	POALP	-	2.500×10^{-2}	-	-
59	PLALP	-	0.000	-	-
60	PWALP	-	0.000	-	-
61	PLWALP	-	0.000	-	-
62	VP	V	5.000×10^{-2}	-	-
63	POMEXP	-	0.200	-	-
64	PLMEXP	-	0.000	-	-
65	PWMEXP	-	0.000	-	-
66	PLWMEXP	-	0.000	-	-
67	POA1	-	6.858	-	-
68	PLA1	-	0.000	-	-
69	PWA1	-	0.000	-	-
70	PLWA1	-	0.000	-	-
71	POA2	V	$5.732\times10^{+1}$	-	-
72	PLA2	V	0.000	-	-
73	PWA2	V	0.000	-	-
74	PLWA2	V	0.000	-	-
75	POA3	-	4.254×10^{-1}	-	-
76	PLA3	-	0.000	-	-
77	PWA3	-	0.000	-	-
78	PLWA3	-	0.000	-	-
79	POIGINV	AV^{-2}	0.000	-	-
80	PLIGINV	AV^{-2}	0.000	-	-
81	PWIGINV	AV^{-2}	0.000	-	-
82	PLWIGINV	AV^{-2}	0.000	-	-
83	POBINV	V	87.50	-	-
84	PLBINV	V	0.000	-	-
85	PWBINV	V	0.000	-	-

©Koninklijke Philips Electronics N.V. 2004

86	PLWBINV	V	0.000	-	-
87	POIGACC	AV^{-2}	0.000	-	-
88	PLIGACC	AV^{-2}	0.000	-	-
89	PWIGACC	AV^{-2}	0.000	-	-
90	PLWIGACC	AV^{-2}	0.000	-	-
91	POBACC	V	48.00	-	-
92	PLBACC	V	0.000	-	-
93	PWBACC	V	0.000	-	-
94	PLWBACC	V	0.000	-	-
95	VFBOV	V	0.000	-	-
96	KOV	$V^{1/2}$	2.500	-	-
97	POIGOV	AV^{-2}	0.000	-	-
98	PLIGOV	AV^{-2}	0.000	-	-
99	PWIGOV	AV^{-2}	0.000	-	-
100	PLWIGOV	AV^{-2}	0.000	-	-
101	POAGIDL	AV^{-3}	0.000	-	-
102	PLAGIDL	AV^{-3}	0.000	-	-
103	PWAGIDL	AV^{-3}	0.000	-	-
104	PLWAGIDL	AV^{-3}	0.000	-	-
105	POBGIDL	V	$4.100\times10^{+1}$	-	-
106	PLBGIDL	V	0.000	-	-
107	PWBGIDL	V	0.000	-	-
108	PLWBGIDL	V	0.000	-	-
109	POCGIDL	-	0.000	-	-
110	PLCGIDL	-	0.000	-	-
111	PWCGIDL	-	0.000	-	-
112	PLWCGIDL	-	0.000	-	-
113	TOX	m	3.2×10^{-9}	-	-
114	POCOX	F	2.717×10^{-14}	-	-
115	PLCOX	F	0.000	-	-

 ©Koninklijke Philips Electronics N.V. 2004

116	PWCOX	F	0.000	-	-
117	PLWCOX	F	0.000	-	-
118	POCGDO	F	6.358×10^{-15}	-	-
119	PLCGDO	F	0.000	-	-
120	PWCGDO	F	0.000	-	-
121	PLWCGDO	F	0.000	-	-
122	POCGSO	F	6.358×10^{-15}	-	-
123	PLCGSO	F	0.000	-	-
124	PWCGSO	F	0.000	-	-
125	PLWCGSO	F	0.000	-	-
126	GATENOISE	-	0.000	0.000	1.000
127	NT	J	1.624×10^{-20}	-	-
128	PONFA	$V^{-1}m^{-4}$	1.900×10^{22}	-	-
129	PLNFA	$V^{-1}m^{-4}$	0.000	-	-
130	PWNFA	$V^{-1}m^{-4}$	0.000	-	-
131	PLWNFA	$V^{-1}m^{-4}$	0.000	-	-
132	PONFB	$V^{-1}m^{-2}$	5.043×10^{6}	-	-
133	PLNFB	$V^{-1}m^{-2}$	0.000	-	-
134	PWNFB	$V^{-1}m^{-2}$	0.000	-	-
135	PLWNFB	$V^{-1}m^{-2}$	0.000	-	-
136	PONFC	V^{-1}	3.627×10^{-10}	-	-
137	PLNFC	V^{-1}	0.000	-	-
138	PWNFC	V^{-1}	0.000	-	-
139	PLWNFC	V^{-1}	0.000	-	-
140	POTVFB	VK^{-1}	0.5×10^{-3}	-	-
141	PLTVFB	VK^{-1}	0.000	-	-
142	PWTVFB	VK^{-1}	0.000	-	-
143	PLWTVFB	VK^{-1}	0.000	-	-
144	POTPHIB	VK^{-1}	-8.5×10^{-4}	-	-
145	PLTPHIB	VK^{-1}	0.000	-	-

©Koninklijke Philips Electronics N.V. 2004

146	PWTPHIB	VK^{-1}	0.000	-	-
147	PLWTPHIB	VK^{-1}	0.000	-	-
148	POTETABET	-	0.500	-	-
149	PLTETABET	-	0.000	-	-
150	PWTETABET	-	0.000	-	-
151	PLWTETABET	-	0.000	-	-
152	POTETASR	-	0.500	-	-
153	PLTETASR	-	0.000	-	-
154	PWTETASR	-	0.000	-	-
155	PLWETASR	-	0.000	-	-
156	POTETAPH	-	3.750	-	-
157	PLTETAPH	-	0.000	-	-
158	PWTETAPH	-	0.000	-	-
159	PLWETAPH	-	0.000	-	-
160	POTETAMOB	K^{-1}	0.000	-	-
161	PLTETAMOB	K^{-1}	0.000	-	-
162	PWTETAMOB	K^{-1}	0.000	-	-
163	PLWTETAMOB	K^{-1}	0.000	-	-
164	NU	-	2.000	-	-
165	POTNUEXP	-	3.230	-	-
166	PLTNUEXP	-	0.000	-	-
167	PWTNUEXP	-	0.000	-	-
168	PLWTNUEXP	-	0.000	-	-
169	POTETAR	-	0.400	-	-
170	PLTETAR	-	0.000	-	-
171	PWTETAR	-	0.000	-	-
172	PLWTETAR	-	0.000	-	-
173	POTETASAT	-	0.860	-	-
174	PLTETASAT	-	0.000	-	-
175	PWTETASAT	-	0.000	-	-

©Koninklijke Philips Electronics N.V. 2004

No.	Parameter	Units	Default	Clip low	Clip high
176	PLWTETASAT	-	0.000	-	-
177	POTA1	K^{-1}	0.000	-	-
178	PLTA1	K^{-1}	0.000	-	-
179	PWTA1	K^{-1}	0.000	-	-
180	PLWTA1	K^{-1}	0.000	-	-
181	POTBGIDL	VK^{-1}	-3.638×10^{-4}	-	-
182	PLTBGIDL	VK^{-1}	0.000	-	-
183	PWTBGIDL	VK^{-1}	0.000	-	-
184	PLWTBGIDL	VK^{-1}	0.000	-	-
185	L	m	2.000×10^{-6}	-	-
186	W	m	1.000×10^{-5}	-	-
187	DTA	K	0.000	-	-
188	MULT	-	1.000	0.000	-

Remark: The parameters L, W and DTA are used to calculate the electrical parameters of the actual transistor as specified in the section on parameter preprocessing.
The default values and clipping values of the additional parameters for the (**p-channel**) model including self-heating (see Section 4.2) are listed in the table below.

No.	**Parameter**	**Units**	**Default**	**Clip low**	**Clip high**
189	RTH	K/W	300.0	0.000	-
190	CTH	J/K	3.0×10^{-9}	0.000	-
191	ATH	-	0.000	-	-

©Koninklijke Philips Electronics N.V. 2004

©Koninklijke Philips Electronics N.V. 2004

9 Pstar Specific Items

9.1 Syntax

n-channel geometrical model	:	MN_n (D,G,S,B)	<parameters>
p-channel geometrical model	:	MP_n (D,G,S,B)	<parameters>
n-channel electrical model	:	MNE_n (D,G,S,B)	<parameters>
p-channel electrical model	:	MPE_n (D,G,S,B)	<parameters>

n	:	occurrence indicator
<parameters>	:	list of model parameters

D, G, S and B are drain, gate, source and bulk terminals respectively.

©Koninklijke Philips Electronics N.V. 2004

9.2 DC Operating Point Output

The DC operating point output facility gives information on the state of a device at its operation point. Besides terminal currents and voltages, the magnitudes of linearized internal elements are given. In some cases meaningful quantities can be derived which are then also given (e.g. f_T). The objective of the DC operating point facility is twofold:

- Calculate small-signal equivalent circuit element values
- Open a window on the internal bias conditions of the device and its basic capabilities.

Below the printed items are described. Here $C_{x(y)}$ indicates the derivative of the charge Q at terminal x to the voltage at terminal y, when all other terminals remain constant.

No.	Symbol	Program Name	Units	Description
0	I_{DS}	IDS	A	Drain current, excl. avalanche and tunnel currents
1	I_{avl}	IAVL	A	Substrate current due to weak-avalanche
2	I_{GS}	IGS	A	Gate-to-source current due to direct tunnelling
3	I_{GD}	IGD	A	Gate-to-drain current due to direct tunnelling
4	I_{GB}	IGB	A	Gate-to-bulk current due to direct tunnelling
5	V_{DS}	VDS	V	Drain-source voltage
6	V_{GS}	VGS	V	Gate-source voltage
7	V_{SB}	VSB	V	Source-bulk voltage
8	V_{TO}	VTO	V	Zero-bias threshold voltage: $V_{TO} = V_{FB} + P_D \cdot (\phi_B + 2 \cdot \phi_T) + k_0 \cdot \sqrt{\phi_B + 2 \cdot \phi_T}$
9	V_{TS}	VTS	V	Threshold voltage including back-bias effects: $V_{TS} = V_{FB} + P_D \cdot \left(V_{SB_t} + 2 \cdot \phi_T\right) - \left(V_{SB_t} - \phi_B\right) + k_0 \cdot \sqrt{V_{SB_t} + 2 \cdot \phi_T}$
10	V_{TH}	VTH	V	Threshold voltage including back-bias and drain-bias effects: $V_{TH} = V_{FB} + P_D \cdot \left(V_{SB_t} + 2 \cdot \phi_T\right) - \left(V_{SB_t} - \phi_B\right) + k_0 \cdot \sqrt{V_{SB_t} + 2 \cdot \phi_T} - \Delta V_G$
11	V_{GT}	VGT	V	Effective gate drive voltage including back-bias and drain voltage effects: $V_{GT} = V_{inv_0}$
12	V_{DSAT}	VDSS	V	Drain saturation voltage at actual bias
13	$V_{DS_{eff}}$	VSAT	V	Saturation limit: $V_{DS_{eff}} = V_{DS} - V_{DSAT}$
14	g_m	GM	A/V	Transconductance (assumed $V_{DS} > 0$): $g_m = \partial I_{DS} / \partial V_{GS}$
15	g_{mb}	GMB	A/V	Substrate-transconductance (assumed $V_{DS} > 0$): $g_{mb} = \partial I_{DS} / \partial V_{BS}$
16	g_{ds}	GDS	A/V	Output conductance: $g_{ds} = \partial I_{DS} / \partial V_{DS}$
17	$C_{D(D)}$	CDD	F	$C_{D(D)} = \partial Q_D / \partial V_{DS}$

 ©Koninklijke Philips Electronics N.V. 2004

No.	Symbol	Program Name	Unit	Description
18	$C_{D(G)}$	CDG	F	$C_{D(G)} = -\partial Q_D / \partial V_{GS}$
19	$C_{D(S)}$	CDS	F	$C_{D(S)} = C_{D(D)} - C_{D(G)} - C_{D(B)}$
20	$C_{D(B)}$	CDB	F	$C_{D(B)} = \partial Q_D / \partial V_{SB}$
21	$C_{G(D)}$	CGD	F	$C_{G(D)} = -\partial Q_G / \partial V_{DS}$
22	$C_{G(G)}$	CGG	F	$C_{G(G)} = \partial Q_G / \partial V_{GS}$
23	$C_{G(S)}$	CGS	F	$C_{G(S)} = C_{G(G)} - C_{G(D)} - C_{G(B)}$
24	$C_{G(B)}$	CGB	F	$C_{G(B)} = \partial Q_G / \partial V_{SB}$
25	$C_{S(D)}$	CSD	F	$C_{S(D)} = -\partial Q_S / \partial V_{DS}$
26	$C_{S(G)}$	CSG	F	$C_{S(G)} = -\partial Q_S / \partial V_{GS}$
27	$C_{S(S)}$	CSS	F	$C_{S(S)} = C_{S(G)} + C_{S(D)} + C_{S(B)}$
28	$C_{S(B)}$	CSB	F	$C_{S(B)} = \partial Q_S / \partial V_{SB}$
29	$C_{B(D)}$	CBD	F	$C_{B(D)} = -\partial Q_B / \partial V_{DS}$
30	$C_{B(G)}$	CBG	F	$C_{B(G)} = -\partial Q_B / \partial V_{GS}$
31	$C_{B(S)}$	CBS	F	$C_{B(S)} = C_{B(B)} - C_{B(D)} - C_{B(G)}$
32	$C_{B(B)}$	CBB	F	$C_{B(B)} = -\partial Q_B / \partial V_{SB}$
33	$C_{GD_{ov}}$	CGDOL	F	Gate-drain overlap capacitance of the actual transistor: $C_{GD_{ov}} = -\partial Q_{ov_L} / \partial V_{DS}$
34	$C_{GS_{ov}}$	CGSOL	F	Gate-source overlap capacitance of the actual transistor: $C_{GS_{ov}} = \partial Q_{ov_0} / \partial V_{GS}$
35	W_E	WEFF	m	Effective channel width for geometrical models
36	L_E	LEFF	m	Effective channel length for geometrical models
37	u	U	-	Transistor gain: $u = g_m / g_{ds}$
38	R_{out}	ROUT	Ω	Small-signal output resistance: $R_{out} = 1 / g_{ds}$
39	V_{Early}	VEARLY	V	Equivalent Early voltage: $V_{Early} = \lvert I_{DS} \rvert / g_{ds}$
40	k_{eff}	KEFF	$\sqrt{V}$	Body effect parameter: $k_{eff} = k_0$
41	β_{eff}	BEFF	A/V^2	Gain factor: $\beta_{eff} = 2 \cdot \lvert I_{DS} \rvert / {V_{inv_0}}^2$
42	f_T	FUG	Hz	Unity gain frequency at actual bias: $f_T = \frac{g_m}{2\pi\left(C_{G(G)}+C_{GS_{ov}}+C_{GD_{ov}}\right)}$
43	$\sqrt{S_{V_{G\,th}}}$	SQRTSFW	$V/\sqrt{Hz}$	Input-referred RMS white noise voltage density: $\sqrt{S_{V_{G\,th}}} = \sqrt{S_{th}} / g_m$
44	$\sqrt{S_{V_{G\,fl}}}$	SQRTSFF	$V/\sqrt{Hz}$	Input-referred RMS white noise voltage density at 1 kHz: $\sqrt{S_{V_{G\,fl}}} = \sqrt{S_{fl}(1kHz)} / g_m$
45	f_{knee}	FKNEE	Hz	Cross-over frequency above which white noise is dominant: $f_{knee} = 1Hz \cdot S_{fl}(1Hz) / S_{th}$

References

[1] R. van Langevelde, *MOS Model 11, Level 1100* NL-UR 2001/813, 2001.
internet: `http://www.semiconductors.philips.com/Philips_Models`.

[2] R. van Langevelde, A.J. Scholten and D.B.M. Klaassen, *MOS Model 11, Level 1101* NL-UR 2002/802, 2002.
internet: `http://www.semiconductors.philips.com/Philips_Models`.

[3] R. van Langevelde, A.J. Scholten and D.B.M. Klaassen, *Physical Background of MOS Model 11, Level 1101* NL-TN 2003/00239, 2003.
internet: `http://www.semiconductors.philips.com/Philips_Models`.

[4] R. van Langevelde, "A Compact MOSFET Model for Distortion Analysis in Analog Circuit Design," *PhD Thesis*, TU Eindhoven, Eindhoven 1998.
Available on request. Write to: Ronald.van.Langevelde@philips.com

[5] R. van Langevelde and F.M. Klaassen, "An Explicit Surface-Potential Based MOSFET Model for Circuit Simulation," *Solid-State Electron.*, Vol. 44, pp. 409-418, 2000.

[6] R.M.D.A. Velghe, D.B.M. Klaassen, F.M. Klaassen, *MOS Model 9,* NL-UR 003/94, 1994.
internet: `http://www.semiconductors.philips.com/Philips_Models`.

[7] R. van Langevelde and F.M. Klaassen, "Influence of Mobility Degradation on Distortion Analysis in MOSFETs," *in Proceedings ESSDERC 1996*, pp. 667-670, 1996.

[8] R. van Langevelde and F.M. Klaassen, "Effect of Gate-Field Dependent Mobility Degradation on Distortion Analysis in MOSFET's," *IEEE Trans. Electron Devices*, Vol. ED-44, No. 11, pp. 2044-2052, 1997.

[9] R. van Langevelde and F.M. Klaassen, "Accurate Drain Conductance Modeling for Distortion Analysis in MOSFETs," *IEDM 1997 Tech. Digest*, pp. 313-316, 1997.

[10] R. van Langevelde *et al.*, "Gate Current: Modeling, ΔL Extraction and Impact on RF Performance," *IEDM 2001 Tech. Digest*, pp. 289-292, 2001.

[11] R. van Langevelde *et al.*, "New Compact Model for Induced Gate Current Noise," *IEDM 2003 Tech. Digest*, pp. 867-870, 2003.

[12] A.R. Boothroyd, S.W. Tarasewicz and C. Slaby, "MISNAN A Physically Based Continuous MOSFET Model for CAD Applications," *IEEE Trans. Computer-Aided Design*, Vol. CAD-10, No. 12, pp. 1512-1529, 1991.

[13] K. Joardar, K.K. Gullapulli, C.C. McAndrew, M.E. Burnham and A. Wild, "An Improved MOSFET Model for Circuit Simulation," *IEEE Trans. Electron Devices*, Vol. ED-45, No. 1, pp. 134-148, 1998.

[14] Z.A. Weinberg, "On Tunneling in Metal-Oxide-Silicon Structures," *J. Appl. Phys.*, Vol. 53, pp. 5052-56, 1982.

[15] F. Stern, "Quantum Properties of Surface Space-Charge Layers," *CRC Crit. Rev. Solid State Sci.*, pp. 499-514, 1974.

[16] S.-Y. Oh, D.E. Ward and R.W. Dutton, "Transient Analysis of MOS Transistors," *IEEE J. Solid-State Circ.*, Vol. 15, pp. 636-643, 1980.

 ©Koninklijke Philips Electronics N.V. 2004

[17] R. Rios and N.D. Arora, ”Determination of Ultra-Thin Gate Oxide Thicknesses for CMOS Structures Using Quantum Effects,” *IEDM 1994 Tech. Digest*, pp. 613-316, 1994.

[18] A.J. Scholten, L.F. Tiemeijer, P.W.H. de Vreede and D.B.M. Klaassen, ”A Large Signal Non-Quasi-Static MOS Model for RF Circuit Simulation,” *IEDM 1999 Tech. Digest*, pp. 163-166, 1999.

[19] K.K. Hung, P.K. Ko, C. Hu and Y.C. Cheng, ”A Unified Model for the Flicker Noise in Metal-Oxide-Semiconductor Field-Effect Transistors,” *IEEE Trans. Electron Devices*, Vol. ED-37, No. 3, pp. 654-665, 1990.

[20] K.K. Hung, P.K. Ko, C. Hu and Y.C. Cheng, ”A Physics-Based MOSFET Noise Model for Circuit Simulators,” *IEEE Trans. Electron Devices*, Vol. ED-37, No. 5, pp. 1323-1333, 1990.

[21] A.J. Scholten and D.B.M. Klaassen, ”New 1/f Noise Model in MOS Model 9, Level 903,” *NL-UR 816/98*, 1998.

[22] H.C. de Graaff and F.M. Klaassen, *Compact transistor modelling for circuit design.* Vienna/New York: Springer-Verlag, 1990.

[23] M. Minondo, G. Gouget and A. Juge, ”New Length Scaling of Current Gain Factor and Characterization Method for Pocket Implanted MOSFET's,” *Proc. ICMTS 2001*, pp. 263-267, 2001.

[24] T.S. Hsieh, Y.W. Chang, W.J. Tsai and T.C. Lu, ”A New Leff Extraction Approach for Devices with Pocket Implants,” *Proc. ICMTS 2001*, pp. 15-18, 2001.

[25] A.J. Scholten, R. Duffy, R. van Langevelde and D.B.M. Klaassen, ”Compact Modelling of Pocket-Implanted MOSFETs,” *in Proceedings ESSDERC 2001*, pp. 311-314, 2001.

©Koninklijke Philips Electronics N.V. 2004

 ©Koninklijke Philips Electronics N.V. 2004

A Auxiliary Equations

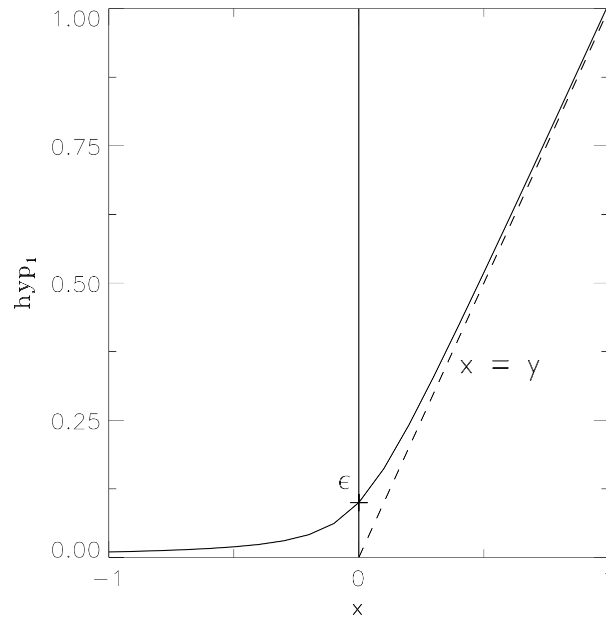

$$\text{hyp}_1\{x,\epsilon\} = \frac{1}{2}\cdot\left(x+\sqrt{x^2+4\cdot\epsilon^2}\right) \tag{A.1}$$

$$\frac{\partial\text{hyp}_1\{x,\epsilon\}}{\partial x} = \frac{\text{hyp}_1\{x,\epsilon\}}{\sqrt{x^2+4\cdot\epsilon^2}} \tag{A.2}$$

$$\frac{\partial^2\text{hyp}_1\{x,\epsilon\}}{\partial x^2} = \frac{2\cdot\epsilon}{\left(x^2+4\cdot\epsilon^2\right)^{3/2}} \tag{A.3}$$

©Koninklijke Philips Electronics N.V. 2004

©Koninklijke Philips Electronics N.V. 2004

B Coefficients in the binning rules for geometry scaling

In this Appendix we will derive expressions for the coefficients in the binning scaling rules, P_0, P_L, P_W, and P_{LW}, as given in Sections 5.2 and 5.2.2. These coefficients will be expressed in terms of parameter values at the corners of bin (L_{min}, W_{min}), (L_{min}, W_{max}), (L_{max}, W_{max}), and (L_{max}, W_{min}) (see Fig. B.1).

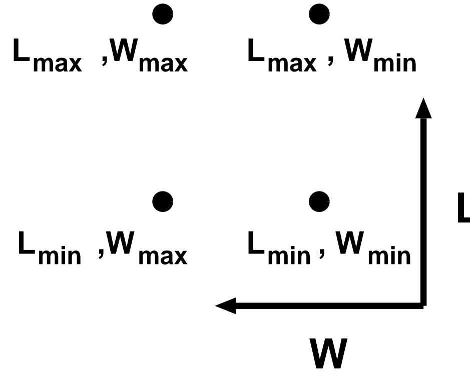

Figure B.1: Schematic view of a bin, showing the four corners (L_{min}, W_{min}), (L_{min}, W_{max}), (L_{max}, W_{max}), and (L_{max}, W_{min}).

B.1 Coefficients for type I scaling

$$\begin{aligned} P_0 = & \frac{L_{E,\,min} \cdot W_{E,\,min}}{(L_{E,\,max} - L_{E,\,min}) \cdot (W_{E,\,max} - W_{E,\,min})} \cdot P(L_{E,\,min},\ W_{E,\,min}) \\ & - \frac{L_{E,\,min} \cdot W_{E,\,max}}{(L_{E,\,max} - L_{E,\,min}) \cdot (W_{E,\,max} - W_{E,\,min})} \cdot P(L_{E,\,min},\ W_{E,\,max}) \\ & + \frac{L_{E,\,max} \cdot W_{E,\,max}}{(L_{E,\,max} - L_{E,\,min}) \cdot (W_{E,\,max} - W_{E,\,min})} \cdot P(L_{E,\,max},\ W_{E,\,max}) \\ & - \frac{L_{E,\,max} \cdot W_{E,\,min}}{(L_{E,\,max} - L_{E,\,min}) \cdot (W_{E,\,max} - W_{E,\,min})} \cdot P(L_{E,\,max},\ W_{E,\,min}) \end{aligned} \tag{B.1}$$

$$\begin{aligned} P_L = & - \frac{L_{E,\,max} \cdot L_{E,\,min} \cdot W_{E,\,min}}{(L_{E,\,max} - L_{E,\,min}) \cdot (W_{E,\,max} - W_{E,\,min})} \cdot P(L_{E,\,min},\ W_{E,\,min}) \\ & + \frac{L_{E,\,max} \cdot L_{E,\,min} \cdot W_{E,\,max}}{(L_{E,\,max} - L_{E,\,min}) \cdot (W_{E,\,max} - W_{E,\,min})} \cdot P(L_{E,\,min},\ W_{E,\,max}) \\ & - \frac{L_{E,\,max} \cdot L_{E,\,min} \cdot W_{E,\,max}}{(L_{E,\,max} - L_{E,\,min}) \cdot (W_{E,\,max} - W_{E,\,min})} \cdot P(L_{E,\,max},\ W_{E,\,max}) \\ & + \frac{L_{E,\,max} \cdot L_{E,\,min} \cdot W_{E,\,min}}{(L_{E,\,max} - L_{E,\,min}) \cdot (W_{E,\,max} - W_{E,\,min})} \cdot P(L_{E,\,max},\ W_{E,\,min}) \end{aligned} \tag{B.2}$$

$$\begin{aligned} P_W = & - \frac{L_{E,\,min} \cdot W_{E,\,max} \cdot W_{E,\,min}}{(L_{E,\,max} - L_{E,\,min}) \cdot (W_{E,\,max} - W_{E,\,min})} \cdot P(L_{E,\,min},\ W_{E,\,min}) \\ & + \frac{L_{E,\,min} \cdot W_{E,\,max} \cdot W_{E,\,min}}{(L_{E,\,max} - L_{E,\,min}) \cdot (W_{E,\,max} - W_{E,\,min})} \cdot P(L_{E,\,min},\ W_{E,\,max}) \end{aligned}$$

©Koninklijke Philips Electronics N.V. 2004

$$
\begin{aligned}
&- \frac{L_{\text{E, max}} \cdot W_{\text{E, max}} \cdot W_{\text{E, min}}}{(L_{\text{E, max}} - L_{\text{E, min}}) \cdot (W_{\text{E, max}} - W_{\text{E, min}})} \cdot P(L_{\text{E, max}},\ W_{\text{E, max}}) \\
&+ \frac{L_{\text{E, max}} \cdot W_{\text{E, max}} \cdot W_{\text{E, min}}}{(L_{\text{E, max}} - L_{\text{E, min}}) \cdot (W_{\text{E, max}} - W_{\text{E, min}})} \cdot P(L_{\text{E, max}},\ W_{\text{E, min}})
\end{aligned} \tag{B.3}
$$

$$
\begin{aligned}
P_{\text{LW}} = &\frac{L_{\text{E, max}} \cdot L_{\text{E, min}} \cdot W_{\text{E, max}} \cdot W_{\text{E, min}}}{(L_{\text{E, max}} - L_{\text{E, min}}) \cdot (W_{\text{E, max}} - W_{\text{E, min}})} \cdot P(L_{\text{E, min}},\ W_{\text{E, min}}) \\
&- \frac{L_{\text{E, max}} \cdot L_{\text{E, min}} \cdot W_{\text{E, max}} \cdot W_{\text{E, min}}}{(L_{\text{E, max}} - L_{\text{E, min}}) \cdot (W_{\text{E, max}} - W_{\text{E, min}})} \cdot P(L_{\text{E, min}},\ W_{\text{E, max}}) \\
&+ \frac{L_{\text{E, max}} \cdot L_{\text{E, min}} \cdot W_{\text{E, max}} \cdot W_{\text{E, min}}}{(L_{\text{E, max}} - L_{\text{E, min}}) \cdot (W_{\text{E, max}} - W_{\text{E, min}})} \cdot P(L_{\text{E, max}},\ W_{\text{E, max}}) \\
&- \frac{L_{\text{E, max}} \cdot L_{\text{E, min}} \cdot W_{\text{E, max}} \cdot W_{\text{E, min}}}{(L_{\text{E, max}} - L_{\text{E, min}}) \cdot (W_{\text{E, max}} - W_{\text{E, min}})} \cdot P(L_{\text{E, max}},\ W_{\text{E, min}})
\end{aligned} \tag{B.4}
$$

B.2 Coefficients for type II scaling

$$
\begin{aligned}
P_0 = &\frac{L_{\text{E, max}} \cdot W_{\text{E, max}}}{(L_{\text{E, max}} - L_{\text{E, min}}) \cdot (W_{\text{E, max}} - W_{\text{E, min}})} \cdot P(L_{\text{E, min}},\ W_{\text{E, min}}) \\
&- \frac{L_{\text{E, max}} \cdot W_{\text{E, min}}}{(L_{\text{E, max}} - L_{\text{E, min}}) \cdot (W_{\text{E, max}} - W_{\text{E, min}})} \cdot P(L_{\text{E, min}},\ W_{\text{E, max}}) \\
&+ \frac{L_{\text{E, min}} \cdot W_{\text{E, min}}}{(L_{\text{E, max}} - L_{\text{E, min}}) \cdot (W_{\text{E, max}} - W_{\text{E, min}})} \cdot P(L_{\text{E, max}},\ W_{\text{E, max}}) \\
&- \frac{L_{\text{E, min}} \cdot W_{\text{E, max}}}{(L_{\text{E, max}} - L_{\text{E, min}}) \cdot (W_{\text{E, max}} - W_{\text{E, min}})} \cdot P(L_{\text{E, max}},\ W_{\text{E, min}})
\end{aligned} \tag{B.5}
$$

$$
\begin{aligned}
P_{\text{L}} = &- \frac{W_{\text{E, max}}}{(L_{\text{E, max}} - L_{\text{E, min}}) \cdot (W_{\text{E, max}} - W_{\text{E, min}})} \cdot P(L_{\text{E, min}},\ W_{\text{E, min}}) \\
&+ \frac{W_{\text{E, min}}}{(L_{\text{E, max}} - L_{\text{E, min}}) \cdot (W_{\text{E, max}} - W_{\text{E, min}})} \cdot P(L_{\text{E, min}},\ W_{\text{E, max}}) \\
&- \frac{W_{\text{E, min}}}{(L_{\text{E, max}} - L_{\text{E, min}}) \cdot (W_{\text{E, max}} - W_{\text{E, min}})} \cdot P(L_{\text{E, max}},\ W_{\text{E, max}}) \\
&+ \frac{W_{\text{E, max}}}{(L_{\text{E, max}} - L_{\text{E, min}}) \cdot (W_{\text{E, max}} - W_{\text{E, min}})} \cdot P(L_{\text{E, max}},\ W_{\text{E, min}})
\end{aligned} \tag{B.6}
$$

$$
\begin{aligned}
P_{\text{W}} = &- \frac{L_{\text{E, max}}}{(L_{\text{E, max}} - L_{\text{E, min}}) \cdot (W_{\text{E, max}} - W_{\text{E, min}})} \cdot P(L_{\text{E, min}},\ W_{\text{E, min}}) \\
&+ \frac{L_{\text{E, max}}}{(L_{\text{E, max}} - L_{\text{E, min}}) \cdot (W_{\text{E, max}} - W_{\text{E, min}})} \cdot P(L_{\text{E, min}},\ W_{\text{E, max}}) \\
&- \frac{L_{\text{E, min}}}{(L_{\text{E, max}} - L_{\text{E, min}}) \cdot (W_{\text{E, max}} - W_{\text{E, min}})} \cdot P(L_{\text{E, max}},\ W_{\text{E, max}}) \\
&+ \frac{L_{\text{E, min}}}{(L_{\text{E, max}} - L_{\text{E, min}}) \cdot (W_{\text{E, max}} - W_{\text{E, min}})} \cdot P(L_{\text{E, max}},\ W_{\text{E, min}})
\end{aligned} \tag{B.7}
$$

$$
\begin{aligned}
P_{\text{LW}} = &\frac{1}{(L_{\text{E, max}} - L_{\text{E, min}}) \cdot (W_{\text{E, max}} - W_{\text{E, min}})} \cdot P(L_{\text{E, min}},\ W_{\text{E, min}}) \\
&- \frac{1}{(L_{\text{E, max}} - L_{\text{E, min}}) \cdot (W_{\text{E, max}} - W_{\text{E, min}})} \cdot P(L_{\text{E, min}},\ W_{\text{E, max}})
\end{aligned}
$$

 ©Koninklijke Philips Electronics N.V. 2004

$$
\begin{aligned}
&+ \frac{1}{(L_{\text{E, max}} - L_{\text{E, min}}) \cdot (W_{\text{E, max}} - W_{\text{E, min}})} \cdot P(L_{\text{E, max}},\ W_{\text{E, max}}) \\
&- \frac{1}{(L_{\text{E, max}} - L_{\text{E, min}}) \cdot (W_{\text{E, max}} - W_{\text{E, min}})} \cdot P(L_{\text{E, max}},\ W_{\text{E, min}})
\end{aligned}
\qquad \text{(B.8)}
$$

B.3 Coefficients for type III scaling

$$
\begin{aligned}
P_0 \;=\; &- \frac{L_{\text{E, min}} \cdot W_{\text{E, max}}}{(L_{\text{E, max}} - L_{\text{E, min}}) \cdot (W_{\text{E, max}} - W_{\text{E, min}})} \cdot P(L_{\text{E, min}},\ W_{\text{E, min}}) \\
&+ \frac{L_{\text{E, min}} \cdot W_{\text{E, min}}}{(L_{\text{E, max}} - L_{\text{E, min}}) \cdot (W_{\text{E, max}} - W_{\text{E, min}})} \cdot P(L_{\text{E, min}},\ W_{\text{E, max}}) \\
&- \frac{L_{\text{E, max}} \cdot W_{\text{E, min}}}{(L_{\text{E, max}} - L_{\text{E, min}}) \cdot (W_{\text{E, max}} - W_{\text{E, min}})} \cdot P(L_{\text{E, max}},\ W_{\text{E, max}}) \\
&+ \frac{L_{\text{E, max}} \cdot W_{\text{E, max}}}{(L_{\text{E, max}} - L_{\text{E, min}}) \cdot (W_{\text{E, max}} - W_{\text{E, min}})} \cdot P(L_{\text{E, max}},\ W_{\text{E, min}})
\end{aligned}
\qquad \text{(B.9)}
$$

$$
\begin{aligned}
P_{\text{L}} \;=\; &\frac{L_{\text{E, max}} \cdot L_{\text{E, min}} \cdot W_{\text{E, max}}}{(L_{\text{E, max}} - L_{\text{E, min}}) \cdot (W_{\text{E, max}} - W_{\text{E, min}})} \cdot P(L_{\text{E, min}},\ W_{\text{E, min}}) \\
&- \frac{L_{\text{E, max}} \cdot L_{\text{E, min}} \cdot W_{\text{E, min}}}{(L_{\text{E, max}} - L_{\text{E, min}}) \cdot (W_{\text{E, max}} - W_{\text{E, min}})} \cdot P(L_{\text{E, min}},\ W_{\text{E, max}}) \\
&+ \frac{L_{\text{E, max}} \cdot L_{\text{E, min}} \cdot W_{\text{E, min}}}{(L_{\text{E, max}} - L_{\text{E, min}}) \cdot (W_{\text{E, max}} - W_{\text{E, min}})} \cdot P(L_{\text{E, max}},\ W_{\text{E, max}}) \\
&- \frac{L_{\text{E, max}} \cdot L_{\text{E, min}} \cdot W_{\text{E, max}}}{(L_{\text{E, max}} - L_{\text{E, min}}) \cdot (W_{\text{E, max}} - W_{\text{E, min}})} \cdot P(L_{\text{E, max}},\ W_{\text{E, min}})
\end{aligned}
\qquad \text{(B.10)}
$$

$$
\begin{aligned}
P_{\text{W}} \;=\; &\frac{L_{\text{E, min}}}{(L_{\text{E, max}} - L_{\text{E, min}}) \cdot (W_{\text{E, max}} - W_{\text{E, min}})} \cdot P(L_{\text{E, min}},\ W_{\text{E, min}}) \\
&- \frac{L_{\text{E, min}}}{(L_{\text{E, max}} - L_{\text{E, min}}) \cdot (W_{\text{E, max}} - W_{\text{E, min}})} \cdot P(L_{\text{E, min}},\ W_{\text{E, max}}) \\
&+ \frac{L_{\text{E, max}}}{(L_{\text{E, max}} - L_{\text{E, min}}) \cdot (W_{\text{E, max}} - W_{\text{E, min}})} \cdot P(L_{\text{E, max}},\ W_{\text{E, max}}) \\
&- \frac{L_{\text{E, max}}}{(L_{\text{E, max}} - L_{\text{E, min}}) \cdot (W_{\text{E, max}} - W_{\text{E, min}})} \cdot P(L_{\text{E, max}},\ W_{\text{E, min}})
\end{aligned}
\qquad \text{(B.11)}
$$

$$
\begin{aligned}
P_{\text{LW}} \;=\; &- \frac{L_{\text{E, max}} \cdot L_{\text{E, min}}}{(L_{\text{E, max}} - L_{\text{E, min}}) \cdot (W_{\text{E, max}} - W_{\text{E, min}})} \cdot P(L_{\text{E, min}},\ W_{\text{E, min}}) \\
&+ \frac{L_{\text{E, max}} \cdot L_{\text{E, min}}}{(L_{\text{E, max}} - L_{\text{E, min}}) \cdot (W_{\text{E, max}} - W_{\text{E, min}})} \cdot P(L_{\text{E, min}},\ W_{\text{E, max}}) \\
&- \frac{L_{\text{E, max}} \cdot L_{\text{E, min}}}{(L_{\text{E, max}} - L_{\text{E, min}}) \cdot (W_{\text{E, max}} - W_{\text{E, min}})} \cdot P(L_{\text{E, max}},\ W_{\text{E, max}}) \\
&+ \frac{L_{\text{E, max}} \cdot L_{\text{E, min}}}{(L_{\text{E, max}} - L_{\text{E, min}}) \cdot (W_{\text{E, max}} - W_{\text{E, min}})} \cdot P(L_{\text{E, max}},\ W_{\text{E, min}})
\end{aligned}
\qquad \text{(B.12)}
$$

©Koninklijke Philips Electronics N.V. 2004

 ©Koninklijke Philips Electronics N.V. 2004